Application of the Differential Method to Diffraction Gratings That Utilize Total Internal Reflection Facets

By

Michael Sean Dyck Smith

A Thesis Submitted to the Faculty of Graduate Studies
In Partial Fulfillment of the Requirements
for the Degree of

MASTER OF SCIENCE

Department of Physics
University of Manitoba
Winnipeg, Manitoba

THE UNIVERSITY OF MANITOBA

FACULTY OF GRADUATE STUDIES

*****

COPYRIGHT PERMISSION PAGE

APPLICATION OF THE DIFFERENTIAL METHOD TO DIFFRACTION GRATINGS THAT UTILIZE TOTAL INTERNAL REFLECTION FACETS

BY

MICHAEL SEAN DYCK SMITH

A Thesis/Practicum submitted to the Faculty of Graduate Studies of The University of Manitoba in partial fulfillment of the requirements of the degree

of

MASTER OF SCIENCE

ABSTRACT

Integrated optical grating devices with facets designed to take advantage of total internal reflection have recently been demonstrated. To date, analysis of these total internal reflection (TIR) gratings has been limited to an elementary ray optics approach. This thesis presents the first analysis of these gratings based on the full electromagnetic theory of light. The validity of designing diffraction gratings with total internal reflection facets is demonstrated. Results indicate that the efficiency of the retro-reflected order of 20^{th} order gratings etched in silica glass is enhanced by more than 11 dB for the TE mode when the TIR grating design is used in place of a similar echelle grating without facet metalization. Comparisons are made between results found using the full electromagnetic theory of light and simple scalar wave approximations, qualitative agreement is found for the retro-reflected order, particularly for grating orders 15-25.

ACKNOWLEDGEMENTS

I wish to thank my advisor Dr. Ken McGreer and TR*Labs* for the opportunity to do research in the exciting field of fiber optics. I appreciate Dr. McGreer's help in choosing a thesis topic and reading this thesis. I am grateful for the excellent facilities TR*Labs* has provided as well as the financial assistance of TR*Labs* and NSERC.

I thank Dr. Sergey Sadov for sharing his knowledge of diffraction grating theory and for his assistance debugging my computer programs. I also thank fellow graduate students Heather Hnatiuk, Dan Jackson, and Dr. Zhijian Sun for their help and discussions related to course work and my thesis.

I wish to thank my family and friends for their interest and encouragement over the course of my studies. I am particularly grateful for my wife Valerie's understanding and constant support. My sister Alison has also been very encouraging.

CONTENTS

LIST OF FIGURES

LIST OF TABLES

1 INTRODUCTION

1.1 BACKGROUND

A diffraction grating consists of an array of repeating optical elements whose effects, when summed together, act to alter (or "diffract") incoming electromagnetic (EM) waves. The elements of the grating direct light of a particular wavelength into discrete orders, each order corresponding to a different direction of travel away from the grating. Diffraction gratings are primarily used to produce spatial separation of light according to wavelength[1]. This spatial separation is known as dispersion and occurs because diffraction varies depending on the wavelength of the light. Different wavelengths of light have maxima and minima of intensity at different angles. For example, an incident beam of white light is separated into its constituent colors much like what happens with a prism. This occurs for each of the diffracted orders so you will have, for the case of incident white light, a number of spectra of light diffracted off the grating.

Grating elements can be arranged in different ways. In unchirped planar diffraction gratings the elements (lines of the grating) are equally spaced along a plane and are designed to diffract incident plane waves to out-going plane waves. In concave diffraction gratings the elements are placed along a concave surface (such as a section of a sphere, cylinder, or toroid) and are designed to diffract incident diverging waves to out-going converging waves. Concave diffraction gratings provide the dual functions of focusing and diffraction. The configuration in which a grating is used is known as its mount. Planar gratings in the Littrow mount and concave gratings in the Eagle mount are

designed and arranged so that the diffraction order of interest is the retro-reflection* order which is directed back towards the incoming wave[2].

Diffraction gratings come in a wide variety of shapes; some of the more common grating profiles are depicted in figure 1-1. Incident light would travel in the same plane as the page and the gratings would actually extend perpendicular to the page. Diffraction gratings are often referred to by their method of production. The traditional method of manufacturing gratings was to rule a series of grooves on an optical surface[3]. Master ruled gratings are now produced using a diamond tool, known as a ruling engine, on a thin coating of metal that has been evaporated onto a planar or concave surface. Ruled gratings generally have a triangular profile. Interference gratings, or holographic gratings (this is actually a misnomer, as their production and use have nothing to do with holography[1]), are produced by the photographic recording of an interference field. Sinusoidal gratings are a good example of gratings that can be produced in this manner. Recently, the microfabrication techniques of integrated semiconductor devices have been used to produce gratings of many different shapes.

---

* In this thesis the term retro-reflection order is used, as this particular order of diffraction is one of the "reflected" orders. The term retro-diffraction order could also have been used. Note that "reflected" orders and "transmitted" orders are not simply reflected or transmitted. Rather, they are diffracted off the grating. Reflected orders are simply diffracted to the same side of the grating as the incident light while transmitted orders are diffracted to the opposite side of the grating as the incident light.

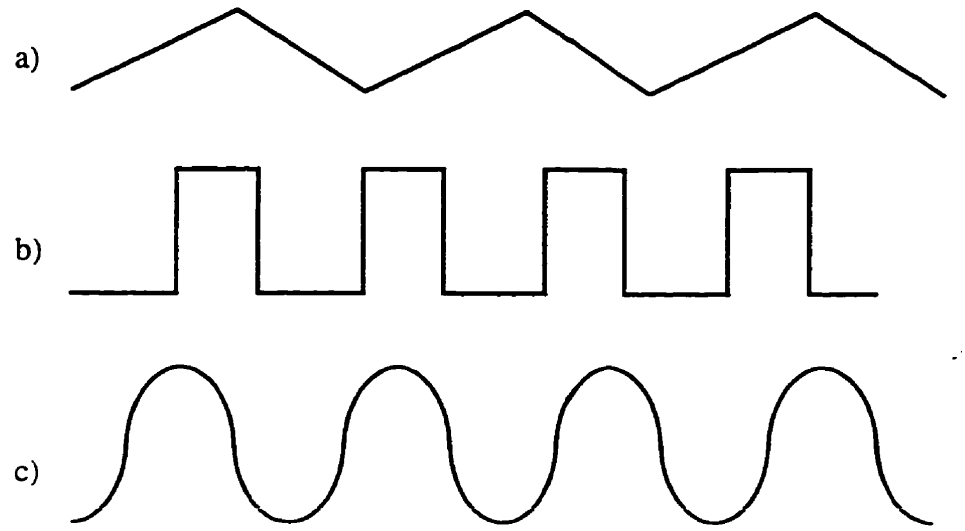

Figure 1-1: Profiles of a) triangular, b) lamellar, and c) sinusoidal gratings

1.2 APPLICATION

Diffraction gratings have been commercially available for spectroscopic applications for over 50 years[1]. They have recently been applied in wavelength division multiplexing (WDM) and dense wavelength division multiplexing (DWDM) optical fiber communication systems as demultiplexers and add/drop multiplexers. In WDM systems several wavelengths of light are used to carry signals along a single fiber. Multiplexers splice the different signal wavelengths together at the input to the system and demultiplexers split apart the different signal wavelengths at the output of the system. Present systems commonly make use of demultiplexers constructed with thin film interference filters[4] or fiber Bragg gratings[5]. The ever-increasing demand for bandwidth is pushing the industry to increase the number of channels a system can support. Filtering techniques quickly become expensive and difficult to manage as the number of channels increases[6]. Planar integrated circuits are more practical for a large number of

channels. These devices include arrayed-waveguide gratings[7] and integrated diffraction gratings[8].

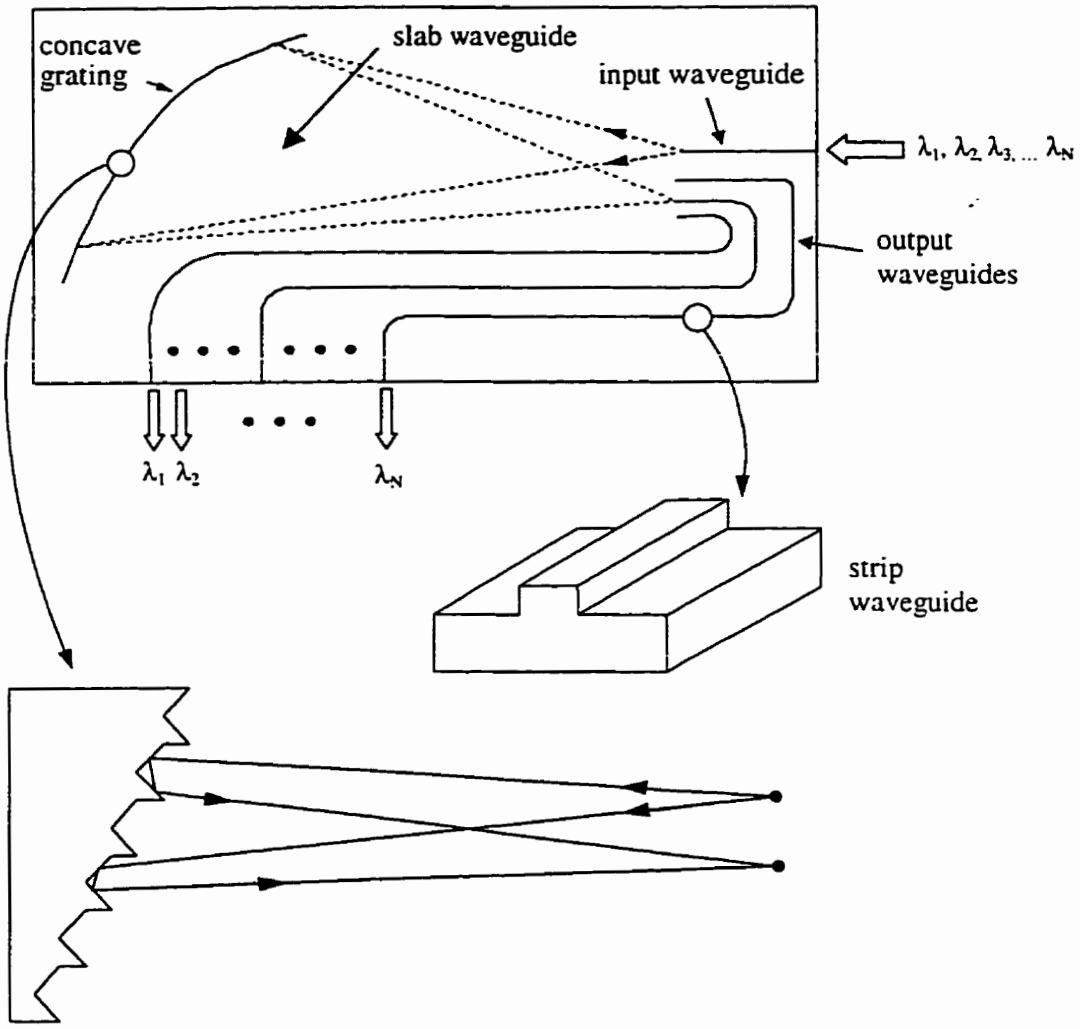

Figure 1-2: Integrated concave diffraction grating demultiplexer

Planar integrated circuits use optical waveguides to confine the direction in which light may travel. Slab waveguides allow light to travel freely in horizontal directions while confining it in the vertical direction. Strip waveguides channel light along in one direction. Integrated diffraction grating demultiplexers (see figure 1-2) consist of a strip waveguide, which directs light towards the diffraction grating. Light comes out of the

strip waveguide into a slab waveguide where it is allowed to spread out horizontally on its way to the grating. Etching away part of the slab waveguide creates the grating. This dielectric grating is formed by the boundary between two dielectrics – the slab waveguide and air. The light diffracts off the grating and is focussed to an output strip waveguide. Depending on the wavelength of light, the angle of diffraction will vary and the light will be directed towards a different output strip waveguide.

1.3 STATEMENT OF PROBLEM

Until recently, integrated optical diffraction gratings primarily used a groove shape copied from ruled gratings. More specifically they used the concave grating equivalent of echelle gratings in the Littrow mount[8,9]. Taking their name from the French word for staircase, echelle gratings consist of "steps" formed by two facets with a 90° angle between them. An echelle grating in the Littrow mount is oriented as in figure 1-3a) so that each groove of the grating has one "illuminated" facet, which the incident light strikes at normal incidence, and one "shaded" facet, which the incident light does not strike. In an elementary view of the grating, the illuminated facet acts like a mirror reflecting the light back towards its point of origin. Initially, integrated gratings were simply dielectric gratings formed by an interface between the slab waveguide and air[8]. Since the reflection coefficient for normal incidence on such an interface is low, this interface has been coated with metal in many applications to enhance the reflectance of the grating[10].

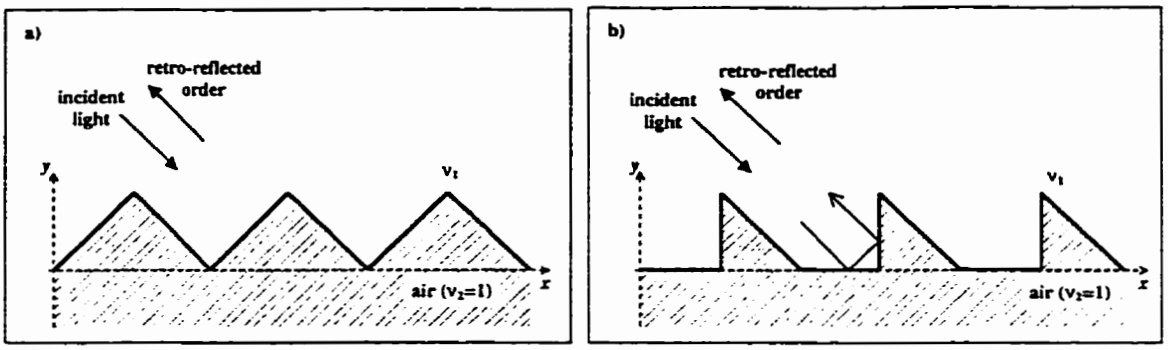

Figure 1-3: Profiles of a) Echelle and b) Total Internal Reflection (TIR) gratings

Using the echelle groove shape for integrated optical devices does not take advantage of the increased control and flexibility which the microfabrication process affords. It is no longer necessary to use groove shapes that may be easily fabricated with a ruling engine. By changing the groove shape design, high diffraction efficiency can be achieved without metal coatings. McGreer proposed a groove shape based on replacing the illuminated facet in an echelle grating with two facets designed to exhibit total internal reflection[11]. This total internal reflection (TIR) grating is shown in figure 1-3b). Taking an elementary approach to this grating, the light should strike each of the facets at an angle smaller than 90° as illustrated by the arrows in the figure. If the refractive index difference is large enough, light should undergo total internal reflection (*i.e.* 100% reflection) off each facet, hence coating the gratings would no longer be necessary.

Recently devices based on Eagle mounted concave gratings designed to use total internal reflection at the dielectric/air interface have been demonstrated[12-14]. Up until now, theoretical discussion of the reflection of light from these grooves has been limited to an elementary ray optics approach. This thesis presents the first rigorous treatment (using the full electromagnetic theory of light) of bulk-optic gratings with grooves that utilize total internal reflection. Strictly speaking, the results are not valid for integrated

diffraction gratings because guided modes will diffract differently than plane waves. Nevertheless, validation of the principle of using total internal reflection for a bulk-optic grating strengthens the qualitative argument that total internal reflection can be used to enhance the efficiency of the retro-diffracted order for integrated gratings.

1.4 OBJECTIVE

The objective of this thesis is to characterize theoretical predictions of the diffraction from Littrow mounted total internal reflection (TIR) gratings. Comparisons will be made to the diffraction from echelle gratings in the Littrow mount. Given the probable applications (wavelength division multiplexing), the gratings will be designed for a central wavelength of 1.550 μm and assessed for relevant optical materials. In order to simplify calculations, this study will be restricted to planar bulk-optic gratings perpendicular to the plane of incidence and with an angle of incidence of 45°.

1.5 OUTLINE OF THESIS

- In chapter 2 modeling of diffraction gratings is discussed. First some basic grating theory is discussed, then a simple model based on scalar wave approximations is introduced followed by a discussion of full electromagnetic wave theory. The differential method for analyzing gratings is described in detail.
- In chapter 3 results from the differential method algorithm are compared with previously published results in order to verify the algorithm's correctness. A method of determining the accuracy of results produced by the algorithm is also developed.
- In chapter 4 results from the differential method algorithm for Littrow mounted bulk-optic echelle and TIR gratings are presented and discussed. The responses of these

two types of gratings are characterized and compared with one another. Comparisons are also made with results from the scalar wave approximation and with previously published experimental results.

- In chapter 5 conclusions and recommendations for future work are discussed.

2 MODELING GRATINGS

2.1 BASIC GRATING THEORY

As mentioned in the introduction, a diffraction grating consists of an array of repeating elements. For basic grating theory the nature of the elements is irrelevant; the periodicity of the elements is important. Consider a plane wave incident on a planar grating of period d at an angle $\theta^{(inc)}$ from the grating normal. Now consider two rays from that plane wave which strike adjacent elements of the grating as in figure 2-1. If we know the wavelength of the light, λ it is now easy to determine at which directions the diffracted rays will add constructively based on the fact that a path length difference equal to an integer number of wavelengths will produce constructive interference. Constructive interference will occur at the angles given by the Bragg or grating equation,

$$\frac{n\lambda}{d} = \sin\theta_n^{(1)} - \sin\theta^{(inc)}, \text{ for } y>0 \qquad (2.1)$$

$$\frac{n\lambda}{d} = \sin\theta_n^{(2)} - \sin\theta^{(inc)}, \text{ for } y<0 \qquad (2.2)$$

where n is an integer known as the diffraction order and the angles $\theta_n^{(1)}$ and $\theta_n^{(2)}$ are defined along with their sign conventions in figure 2-1. Equation (2.1) defines the reflected orders (which travel in positive y directions) and (2.2) defines the transmitted orders (which travel in negative y directions). It should be noted that λ is the wavelength of light in the medium in which the grating is placed. If the medium below the grating has a different refractive index than the medium above the grating (2.2) should be

replaced with $\frac{n\lambda}{d} = \sin\theta_n^{(2)} - \frac{v_1}{v_2}\sin\theta^{(inc)}$, where v_1 is the refractive index* above the grating, v_2 is the refractive index below the grating, and λ is the wavelength of light in v_2.

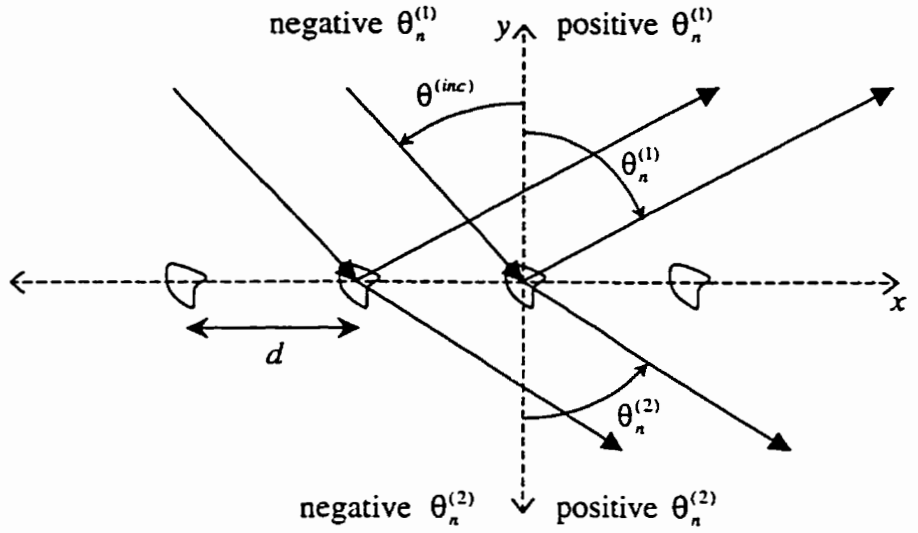

Figure 2-1: Parallel rays incident on grating elements

The total number of diffracted orders depends on the angle of incidence as well as the ratio λ/d (if the refractive index below the grating is different from that above, the number of transmitted orders also depends on the refractive index values). The zeroth reflected order corresponds to waves that are reflected directly off the grating (just as would happen with a planar mirror). The zeroth transmitted order corresponds to waves that travel straight through the grating (just as would happen with no grating). It can be seen in equations (2.1) and (2.2) that changing the wavelength changes the angles of all the orders except the zeroth (*i.e.* dispersion affects all but the zeroth reflected and zeroth

* v is often used in grating theory to represent refractive index rather than the traditional *n* in order to avoid confusion with grating orders and subscripts of Fourier transforms

transmitted orders). For higher orders it is easy to see that the dispersion will be larger; therefore, when using a grating to separate out different wavelengths of light, higher orders are often preferable. The free spectral range (FSR) of a grating is defined as the range over which the wavelength can be varied for a particular order without overlapping with different wavelengths of light from adjacent orders[15]. The FSR will decrease with increasing order so there is a trade-off between FSR and dispersion. Since the zeroth order (reflected or transmitted) does not exhibit dispersion, it is of no use to have light diffracted into this order. If a grating is designed to operate in a particular order, it is desirable to have the majority of light diffracted into that order.

To use a grating in the Littrow mount it must be designed so that one of the orders is travelling in the opposite direction as the incoming wave (*i.e.* $\theta_n^{(1)} = -\theta^{(inc)}$ for some value of n). For the retro-reflected order to correspond to the $-m^{th}$ reflected order, where m is defined as the "grating order," equation (2.1) implies that the grating spacing needs to satisfy

$$d = \frac{m\lambda}{2\sin\theta^{(inc)}}, \tag{2.3}$$

where λ is the wavelength of light in the medium above the grating. Figure 2-2 illustrates the reflected orders for echelle and TIR gratings in the –3 order Littrow mount. These are third order gratings.

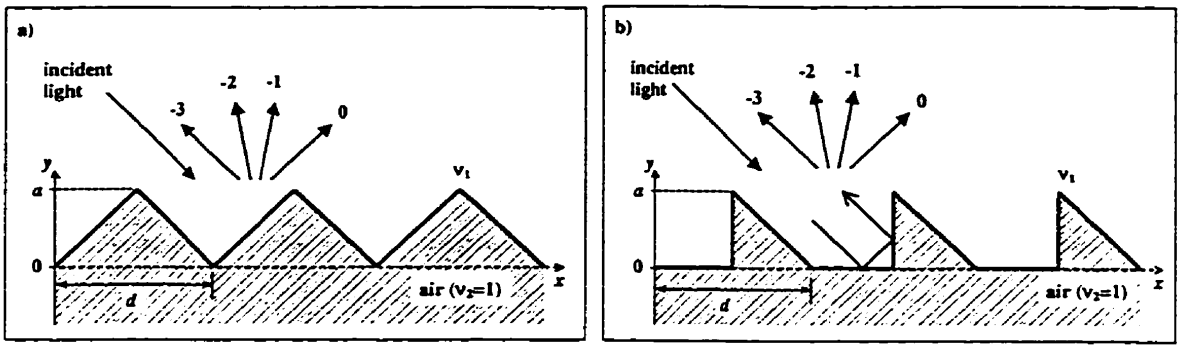

Figure 2-2: 3rd order a) Echelle and b) TIR gratings in the Littrow mount

2.2 SCALAR WAVE THEORY

2.2.1 Ray Optics

The simplest model of the echelle and TIR gratings uses a ray optics approach. The law of reflection states that for a ray of light incident on the boundary between two dielectrics, the angle of incidence equals the angle of reflection ($\theta_i = \theta_r$). The law of refraction (Snell's law) states that $v_1 \sin\theta_i = v_2 \sin\theta_t$. These angles and indices of refraction are defined in figure 2-3.

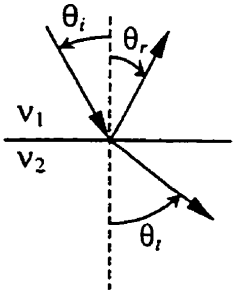

Figure 2-3: Geometry for Snell's Law

Rays strike facets of the echelle grating at normal incidence ($\theta_i = 0$). Using Snell's law, a portion of the light is transmitted straight through as if there were no boundary ($\theta_t = 0$) and using the law of reflection a portion of the light is reflected

directly back the way it came ($\theta_r = 0$). Rays strike the boundaries of the TIR grating twice and according to the law of reflection end up travelling back in the retro-reflected direction. Using Snell's law we can calculate the angles of the transmitted rays from each of the two boundaries and we notice that these angles depend on the ratio of the two refractive indices. Looking at Snell's law it can be seen that if the ratio between the indices of refraction is large enough (i.e. $\nu_1 \sin\theta_i / \nu_2 > 1$) the transmitted ray does not exist and all light is reflected. This condition is known as total internal reflection. If the dielectric below the grating is assumed to be air (ν_2=1) and we assume an angle of incidence of 45°, then the condition for total internal reflection is ν_1>1.414. The ray optics approach tells us what is required for total internal reflection but tells us nothing about the reflectance in other cases.

2.2.2 The Fresnel Equations

Taking the approximation a little further, we can use the Fresnel equations to determine more accurately just how much light is reflected or transmitted at each boundary. Although the Fresnel equations are derived from electromagnetic optics of plane waves they are easily calculated and make for a quick first approximation for the gratings. The Fresnel equations are polarization dependent. When the component of the electric field perpendicular to the direction of travel is parallel to the boundary between the two dielectrics the light is in the TE (transverse electric) polarization. When the component of the magnetic field perpendicular to the direction of travel is parallel to the boundary between the two dielectrics the light is in the TM (transverse magnetic) polarization. The portion of the light intensity reflected at a boundary between two dielectrics is given by the Fresnel equations[16]:

$$R = \left| \frac{v_1 \cos\theta_1 - v_2 \cos\theta_2}{v_1 \cos\theta_1 + v_2 \cos\theta_2} \right|^2, \text{ for TE polarization and} \tag{2.4}$$

$$R = \left| \frac{v_1 \cos\theta_1 - v_2 \cos\theta_2}{v_1 \cos\theta_1 + v_2 \cos\theta_2} \right|^2, \text{ for TM polarization} \tag{2.5}$$

where $\cos\theta_2 = \left(1 - \frac{v_1}{v_2}\sin^2\theta_1\right)^{1/2}$ and θ_1=angle of incidence (θ_i).

For the echelle grating, θ_1=0° and R is polarization independent

$$R = \left(\frac{v_1 - v_2}{v_1 + v_2} \right)^2. \tag{2.6}$$

For the TIR grating when θ_1=45° as long as v_1>1.414 (this is the total internal reflection condition) R is again polarization independent and equal to 1.

2.2.3 Fraunhofer Diffraction

The approximations so far have taken into account reflection off only one grating element. The next step in furthering the model is to take into account the wave nature of light and determine the interference pattern for waves reflected off of all the elements. Two-dimensional Fraunhofer diffraction can be used to approximate the interference between the light reflected off of each element. For the echelle grating the approximation is obvious - we can treat each of the illuminated facets as a single slit emitting light, ignoring the diffraction effects of the shaded facets. For the TIR grating, tracing the path of rays reflecting off of the two facets, reflected rays are in phase at the same position as the illuminated echelle facet would be. So the Fraunhofer diffraction pattern for the echelle and TIR gratings will be identical. It turns out that since adjacent facets differ by an integer multiple of wavelengths, we may treat the sum of reflections off of all the

facets as multiple slit diffraction with no spaces between the slits which is a common problem in optics. The solution takes the form[17]

$$I(\theta) = I_0 \operatorname{sinc}^2\left(\frac{k_1 D}{2}\sin\theta\right), \tag{2.7}$$

where θ is the angle measured from the direction the slits (facets) are facing, D is the width of the slits (facets), and k_1 is the wavevector, $k_1 = \nu_1 2\pi/\lambda_0$ (we use λ_0 for the free-space wavelength of the light). We can now make the approximation that the relative intensity of light diffracted into each of the orders is given by the value from (2.7) evaluated at the angle of that particular order.

Our full scalar wave approximation for the reflected orders will be the product of the reflectance R and the relative intensity of light diffracted into that order, which can be calculated with Fraunhofer diffraction theory. The portion of light diffracted into the n^{th} reflected order is known as the reflected efficiency, e_m and will be given by

$$e_m = R\frac{\operatorname{sinc}^2\left(\frac{k_1 D}{2}\sin\theta_n'\right)}{\sum_{l\in U_1}\operatorname{sinc}^2\left(\frac{k_1 D}{2}\sin\theta_l'\right)} \tag{2.8}$$

where U_1 includes all reflected orders, θ_n' is the angle of the n^{th} reflected order measured from the normal to the facets, and $\operatorname{sinc}\theta = \sin\theta/\theta$. For a grating in the $-m$ order Littrow mount with an angle of incidence of 45° we can use (2.3) to show that for light with a free space wavelength λ_0 to exactly retro-reflect the grating spacing must be such that $D = m\lambda_0/2\nu_1$. For this specific case we can then write (2.8) as

$$e_m = R\frac{\operatorname{sinc}^2\left(m\pi\sin\left(45° - \theta_n^{(1)}\right)\right)}{\sum_{l\in U_1}\operatorname{sinc}^2\left(m\pi\sin\left(45° - \theta_l^{(1)}\right)\right)}. \tag{2.9}$$

2.3 ELECTROMAGNETIC THEORY OF GRATINGS

The scalar wave approximation does not ensure that the boundary conditions are satisfied on the shaded facets and neglects the effect that the shaded facets have on the diffraction of the light. The effect of the shaded facets may be viewed as introducing a new source of electromagnetic radiation. The magnitude and phase of this source would then be determined by requirements of the boundary matching conditions. This view effectively illustrates the physical nature of the corrections to the simple model, but does not lead to a practical method for calculating the diffracted waves. To accurately take into account the effects of the shaded facets, we turn to the full electromagnetic theory of gratings.

2.3.1 Notation

Vectors will be represented by bold characters, for example $\mathbf{u}$. A unit vector will be indicated with a hat, like this $\hat{\mathbf{u}}$. Throughout this discussion, we will be working in a rectangular coordinate system so we denote three unit vectors in the directions of the primary axes as $\hat{\mathbf{x}}$, $\hat{\mathbf{y}}$, $\hat{\mathbf{z}}$. O represents the origin (x=0, y=0, z=0) and $\mathbf{r}$ represents a vector from O to some point within the coordinate system.

In this discussion we only consider monochromatic electromagnetic fields of angular frequency ω so their time dependence can be represented by $\exp(-i\omega t)$. Consequently, any vector function $\mathbf{a}(\mathbf{r},t)$ can be represented by its associated complex vector function $\mathbf{A}(\mathbf{r})$, where

$$\mathbf{a}(\mathbf{r},t) = \mathrm{Re}\big(\mathbf{A}(\mathbf{r})\exp(-i\omega t)\big). \qquad (2.10)$$

We will be making use of the vector differential operator, or del operator, ∇ which is defined as

$$\nabla \equiv \frac{\partial}{\partial x}\hat{\mathbf{x}} + \frac{\partial}{\partial y}\hat{\mathbf{y}} + \frac{\partial}{\partial z}\hat{\mathbf{z}}. \tag{2.11}$$

The del operator defines the following common operations:[18]

- The gradiant of a scalar $C \equiv \nabla C$.
- The divergence of a vector $\mathbf{A} \equiv \nabla \cdot \mathbf{A}$.
- The curl of a vector $\mathbf{A} \equiv \nabla \times \mathbf{A}$.
- The Laplacian of a scalar $C \equiv \nabla^2 C$, where $\nabla^2 = \frac{\partial^2}{\partial x^2} + \frac{\partial^2}{\partial y^2} + \frac{\partial^2}{\partial z^2}$.

2.3.2 Maxwell's Equations

In any medium where the dielectric permittivity $\varepsilon(\mathbf{r})$ and the magnetic permeability $\mu(\mathbf{r})$ are continuous the time-harmonic Maxwell equations are given by[19]

$$\nabla \times \mathbf{E} = i\omega\mathbf{B}, \tag{2.12}$$

$$\nabla \times \mathbf{H} = \mathbf{J} - i\omega\mathbf{D}, \tag{2.13}$$

$$\nabla \cdot \mathbf{D} = \rho, \tag{2.14}$$

$$\nabla \cdot \mathbf{B} = 0, \tag{2.15}$$

where $\mathbf{E}(\mathbf{r})$ and $\mathbf{D}(\mathbf{r})$ represent the electric field, $\mathbf{B}(\mathbf{r})$ and $\mathbf{H}(\mathbf{r})$ represent the magnetic field, $\rho(\mathbf{r})$ is the charge density, and $\mathbf{J}(\mathbf{r})$ the current density.

The following relationships may be used to eliminate $\mathbf{D}$ and $\mathbf{B}$ from Maxwell's equations:

$$\mathbf{D} = \varepsilon\mathbf{E} \tag{2.16}$$

$$\mathbf{B} = \mu\mathbf{H}. \tag{2.17}$$

As we will only deal with dielectric gratings, ε will have only real values and the permeability μ will be equal to that of vacuum, μ_0.

2.3.3 The Helmholtz Equation

Consider a region of constant ε which has neither charge nor current (ρ=0, **J**=0). Substituting $\mu_0\mathbf{H}$ for **B** and taking the curl of both sides of (2.12) gives

$$\nabla\times\nabla\times\mathbf{E} = i\omega\mu_0\nabla\times\mathbf{H}.$$

Applying the vector identity $\nabla\times\nabla\times\mathbf{A} = \nabla(\nabla\cdot\mathbf{A}) - \nabla^2\mathbf{A}$ to the left hand side, substituting from (2.13) into the right hand side and replacing **D** with ε**E** gives

$$\nabla(\nabla\cdot\mathbf{E}) - \nabla^2\mathbf{E} = i\omega\mu_0(-i\omega\varepsilon\mathbf{E}).$$

From (2.14) and (2.16) $(\nabla\cdot\mathbf{E})$ must be equal to zero leaving us with the Helmholtz equation

$$\nabla^2\mathbf{E} + k^2\mathbf{E} = 0, \tag{2.18}$$

where

$$k^2 = \varepsilon\mu_0\omega^2. \tag{2.19}$$

Starting from (2.13) and following similar steps, it can be shown that **H** must also satisfy the Helmholtz equation

$$\nabla^2\mathbf{H} + k^2\mathbf{H} = 0. \tag{2.20}$$

In a dielectric ε, μ=μ_0, and ω are all real and positive so we can write

$$k = (\varepsilon\mu_0)^{1/2}\omega. \tag{2.21}$$

Since the refractive index ν for a dielectric may be defined as[16]

$$\nu \equiv \left(\frac{\varepsilon}{\varepsilon_0}\right)^{1/2} \tag{2.22}$$

we can write

$$k = k_0\nu, \tag{2.23}$$

where

$$k_0 = (\varepsilon_0 \mu_0)^{1/2} \omega \tag{2.24}$$

would characterize the same wave in vacuum.

A simple solution of the Helmholtz equation is the plane wave

$$\mathbf{E} = \mathbf{E}_0 \exp(\frac{2\pi}{\lambda} \hat{\mathbf{u}} \cdot \mathbf{r}), \tag{2.25}$$

where $\hat{\mathbf{u}}$ is a unit vector in any direction, and provided

$$\lambda = \frac{2\pi}{k}. \tag{2.26}$$

Looking at (2.25) $\hat{\mathbf{u}}$ must be in the direction that the wave is travelling and λ must be the wavelength in the medium. Notice that if $\mathbf{r}$ is in direction $\hat{\mathbf{u}}$, increasing the value of r by λ makes $\mathbf{E}$ progress through a full cycle. Combining (2.23, 2.26) we can relate the wavelength in the medium λ and the free space wavelength λ_0.

$$\lambda = \frac{\lambda_0}{\nu}. \tag{2.27}$$

2.3.4 Boundary Conditions

Wherever there is a discontinuity in the medium, the electric and magnetic fields must satisfy certain boundary conditions. Define $\hat{\mathbf{n}}_{21}$ as a unit vector normal to the boundary between two continuous regions pointing from region 2 to region 1. Define the field $\mathbf{A}_j$ as the field $\mathbf{A}$ evaluated in region j at a point approaching the point where a vector in the direction of $\hat{\mathbf{n}}_{21}$ crosses the boundary between regions 2 and 1. We can then write the boundary conditions as[19]

$$\hat{\mathbf{n}}_{21} \times (\mathbf{E}_1 - \mathbf{E}_2) = 0, \tag{2.28}$$

$$\hat{\mathbf{n}}_{21} \times (\mathbf{H}_1 - \mathbf{H}_2) = \mathbf{J}_s, \tag{2.29}$$

$$\hat{\mathbf{n}}_{21} \cdot (\mathbf{D}_1 - \mathbf{D}_2) = \rho_s, \tag{2.30}$$

$$\hat{\mathbf{n}}_{21} \cdot (\mathbf{B}_1 - \mathbf{B}_2) = 0, \tag{2.31}$$

where $\mathbf{J}_s$ is the surface current density and ρ_s is the surface charge density. For a dielectric grating $\mathbf{J}_s$ and ρ_s will both be equal to zero.

2.3.5 General Dielectric Grating

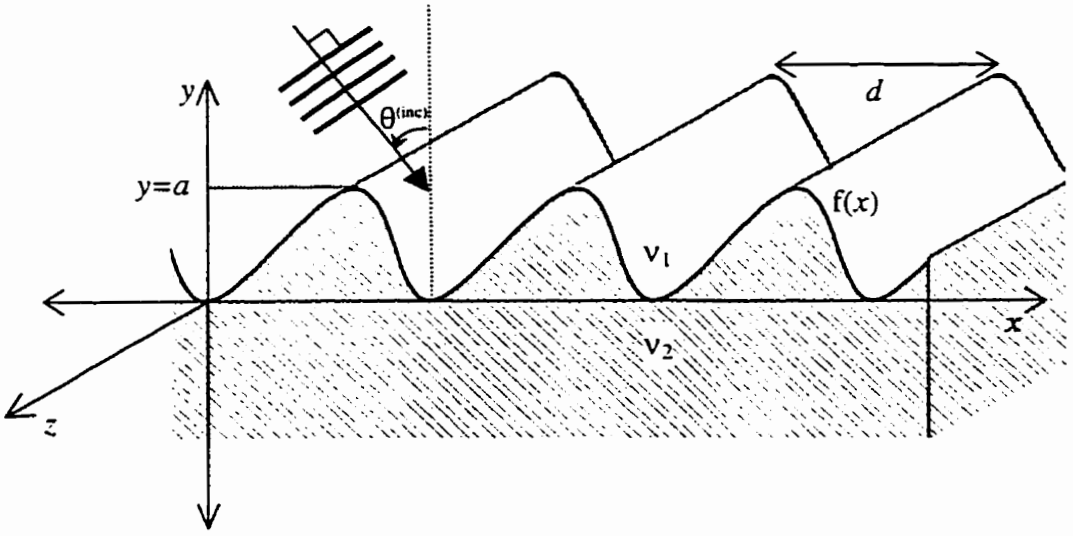

Figure 2-4: General dielectric grating

A general dielectric grating is shown in figure 2-4. The grating boundary is defined by the surface y=f(x) which is infinite and periodic in the x direction with period d. The grating is unchanging in the z direction. f(x) is piecewise continuous and lies between the planes y=0 and y=a. The grating is composed of two different dielectric regions with refractive indices ν_1 above f(x) and ν_2 below f(x).

Assume we have a plane wave incident in the z=0 plane from above the dielectric grating at an angle $\theta^{(inc)}$ as shown in figure 2-4. The incident wave vector $\mathbf{k}^{(inc)}=k_1 \hat{\mathbf{u}}$ ($\hat{\mathbf{u}}$

indicates the direction the wave is travelling) has components in the x and y directions, represented by α and $-\beta$ respectively, where

$$\alpha = k_1 \sin\theta^{(inc)} \text{ and} \tag{2.32}$$

$$\beta = k_1 \cos\theta^{(inc)}. \tag{2.33}$$

Assume that the incoming wave is in one of two fundamental modes of polarization, transverse electric (TE) or transverse magnetic (TM). In TE polarization (also known as P polarization) the component of the electric field perpendicular to the direction of travel (*i.e.* the transverse electric field) points in a direction along the grooves of the grating. In TM polarization (also known as S polarization) the transverse magnetic field points in a direction along the grooves of the grating. In order to treat the two polarizations simultaneously we introduce a new scalar function $u(x,y)$ which represents E_z in TE polarization and H_z in TM polarization. A different Helmholtz equation must be satisfied in each region:

$$\nabla^2 u + k_1^2 u = 0, \quad \text{if } y > f(x) \tag{2.34}$$

$$\nabla^2 u + k_2^2 u = 0, \quad \text{if } y < f(x). \tag{2.35}$$

Now we can determine boundary conditions for the general dielectric grating. First from (2.28), taking the limit as you approach $f(x)$ from either side of the boundary along a path normal to $f(x)$ leads to the result for TE mode that

$$u_1(x, f(x)) = u_2(x, f(x)).$$

Since $\mathbf{J}_s$=0, (2.29) gives the same result for TM mode which leads to the conclusion that u is continuous for both polarizations.

From (2.12) and (2.17) we have for TE mode

$$\nabla \times (u\,\hat{z}) = i\omega\mu\mathbf{H},$$

which gives us

$$\mathbf{H}_1 = \frac{-i}{\omega\mu_1}\nabla\times(u_1\,\hat{z}), \text{ and } \mathbf{H}_2 = \frac{-i}{\omega\mu_2}\nabla\times(u_2\,\hat{z}).$$

Using the identity $\nabla\times\mathbf{A}+\nabla\times\mathbf{B}=\nabla\times(\mathbf{A}+\mathbf{B})$ we can write

$$\mathbf{H}_1-\mathbf{H}_2 = \frac{-i}{\omega}\nabla\times\left(\frac{u_1}{\mu_1}\hat{z}-\frac{u_2}{\mu_2}\hat{z}\right).$$

Substituting this into (2.29) and recalling that $\mathbf{J}_s$=0

$$\frac{-i}{\omega}\hat{\mathbf{n}}_{21}\times\left(\nabla\times\left(\frac{u_1}{\mu_1}\hat{z}-\frac{u_2}{\mu_2}\hat{z}\right)\right)=0.$$

Using the identity $\mathbf{A}\times(\mathbf{B}\times\mathbf{C})=\mathbf{B}(\mathbf{A}\cdot\mathbf{C})-\mathbf{C}(\mathbf{A}\cdot\mathbf{B})$ gives

$$\frac{-i}{\omega}\left(\nabla\left[\hat{\mathbf{n}}_{21}\cdot\left(\frac{u_1}{\mu_1}\hat{z}-\frac{u_2}{\mu_2}\hat{z}\right)\right]-\left(\frac{u_1}{\mu_1}\hat{z}-\frac{u_2}{\mu_2}\hat{z}\right)\left[\hat{\mathbf{n}}_{21}\cdot\nabla\right]\right)=0.$$

($\hat{\mathbf{n}}_{21}\cdot\nabla$ operating on the bracketed term is 0.)

Taking *d/dn* to be the derivative with respect to the direction of the normal, $\hat{\mathbf{n}}_{21}$ we get

$$\frac{1}{\mu_1}\frac{du_1}{dn}=\frac{1}{\mu_2}\frac{du_2}{dn}. \tag{2.36}$$

Since $\mu_1=\mu_2=\mu_0$ for dielectrics, (2.36) reduces to

$$\frac{du_1}{dn}=\frac{du_2}{dn}. \tag{2.37}$$

Using (2.16) and (2.13) and following the same process for the corresponding equations in TM mode leads to the result

$$\frac{1}{\varepsilon_1}\frac{du_1}{dn}=\frac{1}{\varepsilon_2}\frac{du_2}{dn}. \tag{2.38}$$

The boundary conditions for a dielectric grating may be summarized by saying

- u is continuous for both polarizations,

- du/dn is continuous for TE polarization,
- $\varepsilon^{-1} du/dn$ is continuous for TM polarization.

2.3.6 Rayleigh Expansions

The incoming plane wave is given by

$$u^{(inc)}(x, y) = \exp(i(\alpha x - \beta y)). \tag{2.39}$$

The total field above the grating will be the sum of the incident and reflected fields,

$$u = u^{(inc)} + u^{(ref)},\ y>f(x), \tag{2.40}$$

while the total field below the grating will be simply the transmitted field,

$$u=u^{(trans)},\ y<f(x). \tag{2.41}$$

We now introduce a radiation condition based on well known experimental results[19] - that the reflected and transmitted fields each be bounded as $|y|$ approaches infinity and that they be described by a superposition of plane waves. The problem then is to find a function that satisfies the Helmholtz equation, the boundary conditions and the radiation condition. We assume the existence and uniqueness of this solution.

From (2.39) the incident wave has the property

$$u^{(inc)}(x+nd, y) = u^{(inc)}(x, y)\exp(i\alpha nd), \tag{2.42}$$

where n is any integer. The boundary condition requiring continuity of u can be stated as

$$u^{(inc)}(x, f(x)) = u^{(trans)}(x, f(x)) - u^{(refl)}(x, f(x)). \tag{2.43}$$

Restating this boundary condition at $x+nd$, substituting from (2.42), and rearranging gives

$$\begin{aligned} u^{(inc)}(x, f(x)) = {} & u^{(trans)}(x+nd, f(x))\exp(-i\alpha nd) \\ & - u^{(refl)}(x+nd, f(x))\exp(-i\alpha nd) \end{aligned} \tag{2.44}$$

This implies that the product of the reflected or transmitted waves and the factor $\exp(-i\alpha x)$ is a periodic function of period d. Recognizing that from (2.42) the incident wave must also meet this condition we can introduce the new periodic function

$$v(x, y) \equiv u(x, y)\exp(-i\alpha x). \tag{2.45}$$

Because of this relationship u is known as a pseudo-periodic function[19]. Since u must satisfy the Helmholtz equation and the radiation condition then v must also satisfy the Helmholtz equation and radiation condition.

We can represent $v(x,y)$ using a Fourier expansion in x. Substitution into (2.45) gives the result

$$u(x, y) = \exp(i\alpha x)\sum_{n=-\infty}^{\infty} v_n(y)\exp(inKx) = \sum_{n=-\infty}^{\infty} v_n(y)\exp(i\alpha_n x), \tag{2.46}$$

where

$$K = \frac{2\pi}{d} \text{ and} \tag{2.47}$$

$$\alpha_n = k_1 \sin\theta^{(inc)} + nK. \tag{2.48}$$

Let a be the maximum value of $f(x)$. If $y>a$, $u(x,y)$ must verify the Helmholtz equation (2.34) for any x. Substituting (2.46) into (2.34) we can write

$$\sum_{n=-\infty}^{\infty}\left[\frac{d^2 v_n}{dy^2} + \left(k_1^2 - \alpha_n^2\right)v_n\right]\exp(inKx) = 0 \tag{2.49}$$

implying that, for any value of the integer n

$$\frac{d^2 v_n}{dy^2} + \left(k_1^2 - \alpha_n^2\right)v_n = 0. \tag{2.50}$$

If we define U_1 as the set of integers for which $\left(k_1^2 - \alpha_n^2\right)$ is positive and define

$$\beta_n^{(1)} = \left(k_1^2 - \alpha_n^2\right)^{1/2} \text{ if } n \in U_1, \tag{2.51}$$

$$\beta_n^{(1)} = i\left(\alpha_n^{\,2} - k_1^{\,2}\right)^{1/2} \text{ if } n \notin U_1, \tag{2.52}$$

where $i^2 = -1$, then the general solution of (2.50) is

$$v_n(y) = A_n^{(1)} \exp(-i\beta_n^{(1)} y) + B_n^{(1)} \exp(i\beta_n^{(1)} y) \text{ for } y>a. \tag{2.53}$$

Below y=0 the same equations apply, except of course replacing k_1 with k_2. Define U_2 as the set of integers for which $\left(k_2^{\,2} - \alpha_n^{\,2}\right)$ is positive and define

$$\beta_n^{(2)} = \left(k_2^{\,2} - \alpha_n^{\,2}\right)^{1/2}, \text{ if } n \in U_2 \tag{2.54}$$

$$\beta_n^{(2)} = i\left(\alpha_n^{\,2} - k_2^{\,2}\right)^{1/2}, \text{ if } n \notin U_2 \tag{2.55}$$

then the general solution of the new differential equation corresponding to (2.50) is

$$v_n(y) = A_n^{(2)} \exp(-i\beta_n^{(2)} y) + B_n^{(2)} \exp(i\beta_n^{(2)} y) \text{ for } y<0. \tag{2.56}$$

Expansions of the type given in (2.53) and (2.56) are known as Rayleigh expansions as they appear to have been introduced by Rayleigh[19]. Combining these Rayleigh expansions with (2.46) gives the following results for the transverse field of interest:

$$u(x, y) = \sum_{n=-\infty}^{\infty} A_n^{(1)} \exp(i\alpha_n x - i\beta_n^{(1)} y) + \sum_{n=-\infty}^{\infty} B_n^{(1)} \exp(i\alpha_n x + i\beta_n^{(1)} y) \text{ for } y>a, \tag{2.57}$$

$$u(x, y) = \sum_{n=-\infty}^{\infty} A_n^{(2)} \exp(i\alpha_n x - i\beta_n^{(2)} y) + \sum_{n=-\infty}^{\infty} B_n^{(2)} \exp(i\alpha_n x + i\beta_n^{(2)} y) \text{ for } y<0. \tag{2.58}$$

Looking at these equations it can be seen that if an A_n or B_n coefficient's corresponding β_n value is real, the coefficient represents a propagating plane wave while if β_n is imaginary the coefficient represents an exponentially damped or exponentially growing wave traveling along the grating. We are only concerned with the propagating waves at this point so the following discussion will only consider those cases. Since β_n must then be positive, each of the A_n coefficients represent downward propagating plane waves while

the B_n coefficients represent upward propagating plane waves (as far as the y coordinate is concerned). If the incident wave is assumed to come from above the grating then $A_n^{(1)}$ coefficients represent incoming plane waves, $B_n^{(1)}$ coefficients represent plane waves reflected off the grating, while the $A_n^{(2)}$ coefficients represent transmitted plane waves. The $B_n^{(2)}$ coefficients would represent waves propagating toward the grating from below so they must all equal zero in this case. The angles at which these plane waves are travelling can be determined from

$$\theta_n^{(inc)} = \sin^{-1}\left(\frac{\alpha_n}{k_1}\right), \tag{2.59}$$

$$\theta_n^{(1)} = \sin^{-1}\left(\frac{\alpha_n}{k_1}\right), \tag{2.60}$$

$$\theta_n^{(2)} = \sin^{-1}\left(\frac{\alpha_n}{k_2}\right), \tag{2.61}$$

where the angles of incident waves $\theta_n^{(inc)}$, reflected waves $\theta_n^{(1)}$, and transmitted waves $\theta_n^{(2)}$ are defined as shown in figure 2-5. As one would expect, the angles calculated using equations (2.60) and (2.61) are the same as those calculated using equation (2.1) and the modified version of (2.2) which takes into account the different refractive indices.

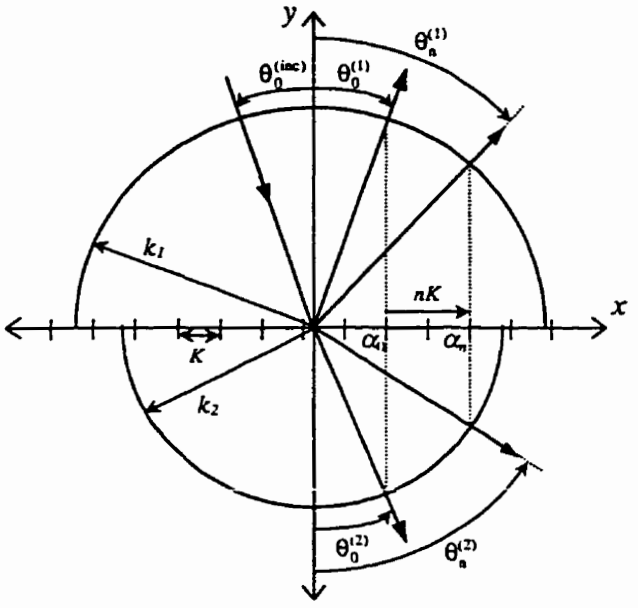

Figure 2-5: Illustration of angles of diffraction from a dielectric grating

Equation (2.59) introduces the possibility of having more than one incident wave, or an incident wave at an angle other than $\theta_0^{(inc)}$ ($\theta_0^{(inc)}$ is equal to our initial definition of the angle of incidence, $\theta^{(inc)}$). For now, assume there is only one incoming plane wave and it is at the angle $\theta_0^{(inc)}$.

2.3.7 Calculating Efficiencies

In the study of gratings it is useful to determine how much of the incident energy goes into each of the reflected and transmitted orders. Consider the situation in Figure 2-4 where we have one plane wave incident from above the dielectric grating. The $A_n^{(1)}$ coefficients represent the incoming waves, so only one will have a non-zero value. For calculation purposes assume the incoming wave has a magnitude of 1. The $B_n^{(1)}$ coefficients represent the reflected plane waves while the $A_n^{(2)}$ coefficients represent

transmitted waves. The $B_n^{(2)}$ coefficients represent waves propagating toward the grating from below so they must all equal zero. We can now write

$$u(x, y) = \exp(i\alpha x - i\beta y) + \sum_{n=-\infty}^{\infty} B_n^{(1)} \exp(i\alpha_n x + i\beta_n^{(1)} y), \text{ if } y>a \tag{2.62}$$

$$u(x, y) = \sum_{n=-\infty}^{\infty} A_n^{(2)} \exp(i\alpha_n x + i\beta_n^{(2)} y), \text{ if } y<0. \tag{2.63}$$

Define the efficiency e_{rn} of the n^{th} reflected wave as the ratio of its flux density through the plane $y=a$ to the flux density of the incident plane wave through the same plane. Similarly, define the efficiency e_{tn} of the n^{th} transmitted wave as the ratio of its flux density through the plane $y=0$ to the flux density of the incident plane wave through the plane $y=a$. The intensity of a plane wave in a dielectric is given by[16]

$$I = \frac{|E_0|^2 \nu}{2(\varepsilon/\mu_0)^{1/2}} = \frac{|H_0|^2 (\varepsilon/\mu_0)^{1/2}}{2\nu}. \tag{2.64}$$

Applying this to equations (2.62) and (2.63), recognizing that the component of the wave vector normal to the plane is the one which contributes to the flux density through the plane, it can easily be shown that if $\theta^{(inc)}$ is the angle of incidence the various reflected efficiencies are given by

$$e_{rn} = \left|B_n^{(1)}\right|^2 \frac{\cos\theta_n^{(1)}}{\cos\theta^{(inc)}} \quad \text{for } n \in U_1, \tag{2.65}$$

while the transmitted efficiencies are given by

$$e_{tn} = \left|A_n^{(2)}\right|^2 \frac{\cos\theta_n^{(2)}}{\cos\theta^{(inc)}} \frac{\nu_2}{\nu_1} \text{ for } n \in U_2 \text{ (TE polarization)}, \tag{2.66}$$

$$e_{tn} = \left|A_n^{(2)}\right|^2 \frac{\cos\theta_n^{(2)}}{\cos\theta^{(inc)}} \frac{\nu_1}{\nu_2} \text{ for } n \in U_2 \text{ (TM polarization)}. \tag{2.67}$$

Calculation of the $B_n^{(1)}$ and $A_n^{(2)}$ coefficients is thus sufficient to determine the efficiencies for a dielectric grating. Note that the energy balance criterion[19] requires that the sum of all reflected and transmitted efficiencies equal unity. This criterion simply implies that the total energy of the reflected and transmitted waves must be equivalent to the energy of the incident wave.

2.3.8 Propagation in the Grating Region

Consider the TE mode. We can replace the two Helmholtz equations (2.34, 2.35) with a single one

$$\nabla^2 \mathrm{u} + k^2(x, y)\,\mathrm{u} = 0\,, \tag{2.68}$$

where u is the z component of **E** and

$$k^2(x, y) = \begin{cases} k_1^{\,2} & \text{if } y > \mathrm{f}(x) \\ k_2^{\,2} & \text{if } y < \mathrm{f}(x) \end{cases}. \tag{2.69}$$

Since u is a pseudo-periodic function, we can say that (2.68) is valid in the sense of distributions[19]. This is a statement arising out of the distribution theory. Distribution theory describes the relationships between functionals rather than vector functions. When applying distribution theory the operations curl, divergence, gradient and Laplacian need to be redefined. These new definitions automatically take into account the boundary conditions of Maxwell's equations so boundary conditions may be ignored[19]. Since u and *du/dn* are continuous for TE mode, the Laplacian in the sense of distributions is actually going to be the same as the standard Laplacian[19]. This means we can ignore the boundary conditions and rewrite the Helmholtz equation (2.68) using the

series expansion of u (2.46) and replacing the periodic function $k^2(x,y)$ by its Fourier series $\sum_{n=-\infty}^{\infty}(k^2)_n(y)\exp(inKx)$:

$$\exp(i\alpha x)\left[\sum_{n=-\infty}^{\infty}\left(\frac{d^2 v_n}{dy^2}-\alpha_n^2 v_n\right)\exp(inKx)+\sum_{m=-\infty}^{\infty} v_m \exp(imKx)-\sum_{l=-\infty}^{\infty}(k^2)_l(y)\exp(ilKx)\right]=0 \qquad (2.70)$$

where $(k^2)_n$ can be calculated using

$$(k^2)_n(y)=\frac{1}{d}\int_{-d/2}^{d/2}k^2(x,y)\exp(inKx)dx. \qquad (2.71)$$

Making the substitution $n=l+m$ (2.70) can be rewritten as

$$\sum_{n=-\infty}^{\infty}\left(\frac{d^2 v_n(y)}{dy^2}-\alpha_n^2 v_n(y)+\sum_{m=-\infty}^{\infty}(k^2)_{n-m}(y)\,v_m(y)\right)\exp(inKx)=0,$$

which implies that for each value of n

$$\frac{d^2 v_n}{dy^2}-\alpha_n^2 v_n+\sum_{m=-\infty}^{\infty}(k^2)_{n-m}\,v_m=0. \qquad (2.72)$$

This is a straightforward second order differential equation that we can write in matrix form as

$$V''=M(y)V, \qquad (2.73)$$

where V is a column matrix composed of the functions $v_n(y)$, V'' is a column matrix composed of the second derivatives of $v_n(y)$ with respect to y, and M is a square matrix composed of the elements

$$M_{nm}=\alpha_n^2\delta_{mn}-(k^2)_{n-m}. \qquad (2.74)$$

This equation describes the field in the entire grating region ($0<y<a$) and the solution of a field propagating through this area may be found using standard numerical algorithms. This solution along with the known Rayleigh expansions outside the grating region may be used to calculate the efficiencies for any dielectric grating using the differential method.

2.4 THE DIFFERENTIAL METHOD

The differential method can be outlined as follows:

- A field is assigned below the grating and written using the Rayleigh expansion (2.56).
- A numerical integration algorithm is applied to the differential equation in the grating region (2.72) in order to calculate the propagation of the field in reverse from $y=0$ to $y=a$.
- The field above the grating is converted into incident and reflected plane waves using the Rayleigh expansions (2.53).
- By repeating the process, matrices relating the Rayleigh expansion of the incoming plane wave to those of the reflected and transmitted plane waves can be determined and from these matrices the grating efficiencies can be calculated.

2.4.1 Definitions

Outside of the grating region, we have found the general solutions to the Helmholtz equation and we can write them as

$$u(x, y) = \sum_{n=-\infty}^{\infty} v_n(y) \exp(i\alpha_n x), \tag{2.75}$$

where

$$v_n(y) = A_n^{(1)} \exp(-i\beta_n^{(1)} y) + B_n^{(1)} \exp(i\beta_n^{(1)} y), \text{ for } y>a \tag{2.76}$$

$$v_n(y) = A_n^{(2)} \exp(-i\beta_n^{(2)}), \qquad \text{for } y<0 \qquad (2.77)$$

Call $\psi_A^{(1)}$, $\psi_B^{(1)}$, and $\psi_A^{(2)}$ the column vectors built from the coefficients $A_n^{(1)}$, $B_n^{(1)}$, and $A_n^{(2)}$ respectively. Introducing the square matrices M_A, M_B, R and T we can define the following relationships:

$$\psi_A^{(1)} = M_A \psi_A^{(2)} \qquad (2.78)$$

$$\psi_B^{(1)} = M_B \psi_A^{(2)} \qquad (2.79)$$

$$\psi_B^{(1)} = R \psi_A^{(1)} \qquad (2.80)$$

$$\psi_A^{(2)} = T \psi_A^{(1)} \qquad (2.81)$$

If M_A and M_B are known we can then calculate the reflection matrix R and the transmission matrix T using the relationships

$$T = (M_A)^{-1}, \qquad (2.82)$$

$$R = M_B (M_A)^{-1} = M_B T. \qquad (2.83)$$

2.4.2 Calculation of T and R

All the Fourier series are written as sums from $-\infty$ to ∞. Since it is impossible to do numerical calculations of this scope we choose some number N, and make all summations from n=–N to n=+N. This means that all square matrices will have dimensions of N_{matrix}=2N+1 and all column vectors will have N_{matrix} rows. N should be chosen large enough that all real reflected and transmitted orders are included (i.e. all the values in the sets U_1 and U_2 are included in the range [–N, +N]). Further choosing of the size of N should be based on numerical results (this is discussed in chapter 3) or some knowledge of the Fourier components for larger N.

Start by choosing the field below the grating so that one of the values of $A_n^{(2)}=1$ and all other $A_n^{(2)}=0$. The derivative of $A_n^{(2)}$ just below the grating is straightforward from (2.53) and since the tangential electric field and its derivative are continuous in TE mode we can write

$$v_n(0) = A_n^{(2)}, \tag{2.84}$$

$$\frac{d v_n}{dy}(0) = -i\beta_n^{(2)} A_n^{(2)}. \tag{2.85}$$

The functions v_n and their first derivatives are now known at $y=0$. Applying the differential equation in the grating region (2.72) and using a standard numerical algorithm for second order differential equations, propagate the functions v_n through the grating region to $y=a$. We used the numerical integration algorithm presented in chapter 4 of "Electromagnetic Theory of Gratings"[20] which implements the Noumerov algorithm[21]. Once $v_n(a)$ and $\frac{d v_n}{dy}(a)$ have been found for all n we can determine what plane waves must exist above the grating. The continuity of the tangential electric field and its derivative means we can use equations (2.53) and (2.56) along with their derivatives to get

$$A_n^{(1)} = \frac{1}{2}\left(v_n(a) - \frac{1}{i\beta_n^{(1)}} \frac{d v_n}{dy}(a) \right) \exp\left(i\beta_n^{(1)} a\right) \tag{2.86}$$

$$B_n^{(1)} = \frac{1}{2}\left(v_n(a) + \frac{1}{i\beta_n^{(1)}} \frac{d v_n}{dy}(a) \right) \exp\left(-i\beta_n^{(1)} a\right) \tag{2.87}$$

The resulting values of $\psi_A^{(1)}$ and $\psi_B^{(1)}$ are then the values of the n^{th} (where n was the value that we chose $A_n^{(2)}=1$) columns of M_A and M_B respectively (this is obvious if you look at

equations (2.78) and (2.79)). By repeating this process N_{matrix} times, setting a different $A_n^{(2)}$ equal to 1 each time the complete matrices M_A and M_B may be calculated. From M_A and M_B equations (2.82) and (2.83) can then be used to calculate T and R. T and R describe everything we need to know about the system.

2.4.3 Calculation of Efficiencies

The matrices T and R allow us to calculate the coefficients $B_n^{(1)}$ and $A_n^{(2)}$ from the coefficients $A_n^{(1)}$. T and R are independent of which of the coefficients $A_n^{(1)}$ have non-zero values. This means that any or all of the values of $A_n^{(1)}$ may be assigned as incoming plane waves and the corresponding reflected and transmitted plane waves calculated using T and R. To be consistent with our definition of $\theta^{(inc)}$ and for n to be equal to the correct diffracted order numbers we choose $A_0^{(1)}$ as the incident plane wave (corresponding to the input angle $\theta_0^{(inc)} = \theta^{(inc)}$) and assign it a value of 1. All other $A_n^{(1)}$ are assigned values of zero. The reflected plane waves ($B_n^{(1)}$ coefficients) and transmitted plane waves ($A_n^{(2)}$ coefficients) are calculated with equations (2.80) and (2.81). Using equations (2.65) and (2.66) the efficiencies can then be determined:

$$e_m = \left|B_n^{(1)}\right|^2 \frac{\cos\theta_n^{(1)}}{\cos\theta^{(inc)}}, \tag{2.88}$$

$$e_m = \left|A_n^{(2)}\right|^2 \frac{\cos\theta_n^{(2)}}{\cos\theta^{(inc)}} \frac{\nu_2}{\nu_1}, \tag{2.89}$$

where $\theta_n^{(1)}$ and $\theta_n^{(2)}$, given by (2.60) and (2.61), are the angles of the reflected and transmitted plane waves respectively.

2.4.4 Centering Real Orders in the Vectors

It is desirable to center the real orders in the vectors used for calculating efficiencies. Centering reduces the size of the vectors and matrices required to include all real orders, thus making matrix inversion possible for gratings with greater numbers of orders. If the incident plane wave is described as $A_0^{(1)} = 1$, the real orders will not necessarily be centered in the matrices and vectors. For example, consider the 3rd order gratings depicted in figure 2-2. The angle of incidence $\theta^{(inc)}$ is 45°. To include all the real orders for these gratings we must take our summations from n=-3 to n=+3 even though n=1, n=2, and n=3 do not correspond to real orders. A better method is to temporarily choose $\theta^{(inc)}$ to be 13.6° (this corresponds to a wave incident along the same line but in the opposite direction as the –2 reflected order in the diagram). The angles of all incident and diffracted real orders (*i.e.* $\theta_n^{(inc)}$, $\theta_n^{(1)}$ for $n \in U_1$, and $\theta_n^{(2)}$ for $n \in U_2$) remain the same as when $\theta^{(inc)} = 45°$, only with the n coefficients all increased by 1. The coefficients of the matrices T and R relating real orders also remain the same, only shifted so that they relate the correct orders. We now need to take summations only from n=-2 to n=+2 to include all real orders. We have effectively centered all the real orders (as well as possible when there are an even number, n=+2 is still not a real order). Since we are actually interested in the case of a plane wave incident at 45°, we choose $A_1^{(1)}$ as our incident wave. With our temporary assignment of $\theta^{(inc)}$=13.6°, $A_1^{(1)}$ now corresponds to an incident plane wave at the angle $\theta_1^{(inc)} = 45°$. Efficiencies are calculated as before, the only differences being that $A_1^{(1)}$ (not $A_0^{(1)}$) is assigned the value of 1, and $\theta^{(inc)} = 45°$ in used in equations (2.88) and (2.89). Once calculations are complete, the order

numbers, n are then reassigned for the angles and efficiencies as they would have been if we had initially chosen $\theta^{(inc)} = 45°$.

This method of centering real orders by temporarily choosing $\theta^{(inc)}$ equal to the smallest of the angles $\theta_n^{(inc)}$ was used to obtain all results presented in this thesis. An equivalent process should be to take summations from n=-N+l to n=+N+l, where l is chosen so that the real orders are centered in the vectors.

2.4.5 A Brief Note on TM polarization

I have not included theoretical discussion of using the differential method for the TM polarization. In TM polarization du/dn is not continuous throughout the grating region. Consequently, the Helmholtz equation (2.68) will not necessarily be valid in the sense of distributions. The Helmholtz equation needs to be replaced by a propagation equation that will be valid in the sense of distributions in the grating region. For further discussion of using the differential method for TM polarization see chapter 4 of "Electromagnetic Theory of Gratings"[20].

3 VERIFICATION OF ALGORITHM

The differential method has been one of the most popular methods for analyzing arbitrary profile gratings[22]. Given its previous success in replicating experimental results for different gratings[23,24], we did not attempt experimental verification of the validity of the differential method. In this chapter we verify the correctness of our algorithm. First, results consistent with previously published results are obtained, then a method for determining the accuracy of further results is developed.

3.1 CONSISTENCY OF RESULTS WITH PUBLISHED RESULTS

The first step in the verification process is to show that the programmed algorithm is consistent with the algorithm developed in the literature. On page 222 of "Electromagnetic Theory of Gratings," Maystre et al present graphical results obtained using the differential method for three different dielectric gratings[25]. (Results for the zeroth order efficiencies of the grating in Fig. 6.104 in "Electromagnetic Theory of Gratings" were also reported by Knop[26] who used a different calculation method. Knop's results agree very closely with those reported by Maystre et al.) Using our diffraction method programs, TE mode efficiencies for each of the gratings reported by Maystre et al were calculated - these results are plotted in figures 3-1 to 3-3. Comparing our figures to those of Maystre et al it can be seen that there is very close agreement. There are, however, some small deviations in our plots that do not appear on theirs. For example, the dips in the zeroth order efficiency of figure 3-1 at approximately 0.72μm and 0.75μm. These small discrepancies could possibly be attributed to using a smaller wavelength spacing for calculated points. Maystre et al and Knop did not indicate what wavelength

spacing was used for their calculations so this hypothesis can not be verified. The only significant difference between our results and the corresponding published results can be found between wavelengths of 0.7μm and 0.8μm in the first diffracted order of the grating plotted in figure 3-2. It can be seen that over this range the first order efficiency in our plot rises from about 0.025 to 0.2 while Maystre et al's corresponding plot stays approximately constant at 0.025.

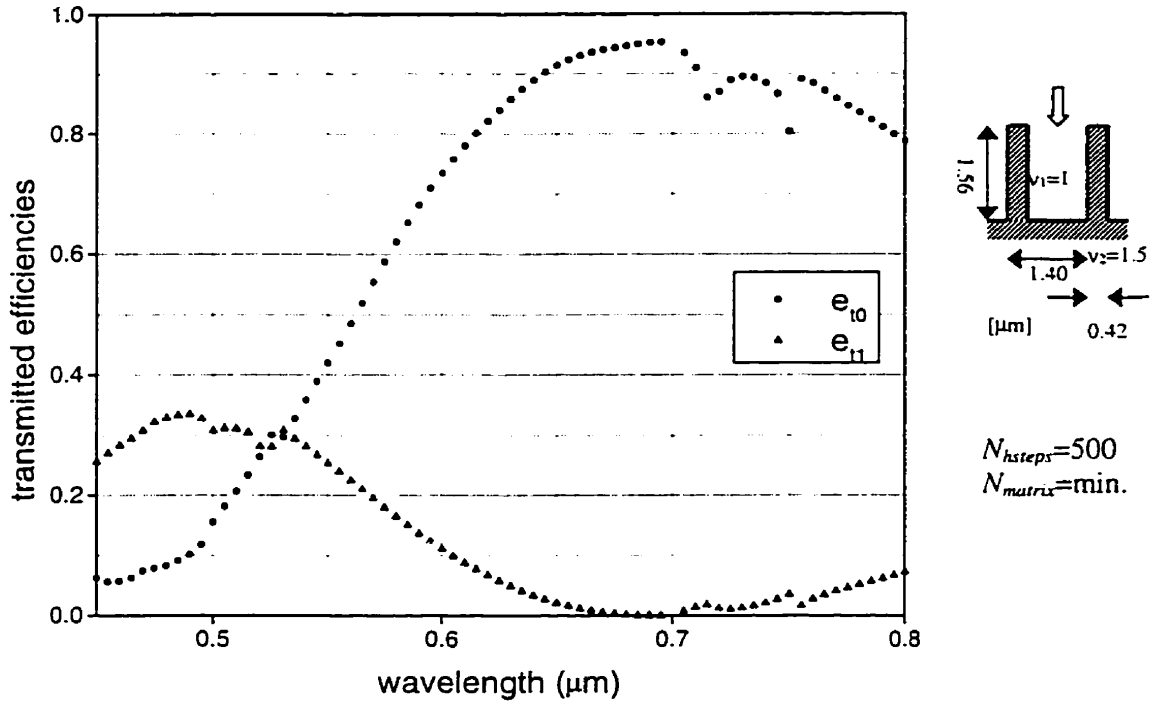

Figure 3-1: TE mode efficiency curves of dielectric lamellar grating for comparison with top graph of Fig. 6.104[25] in "Electromagnetic Theory of Gratings"

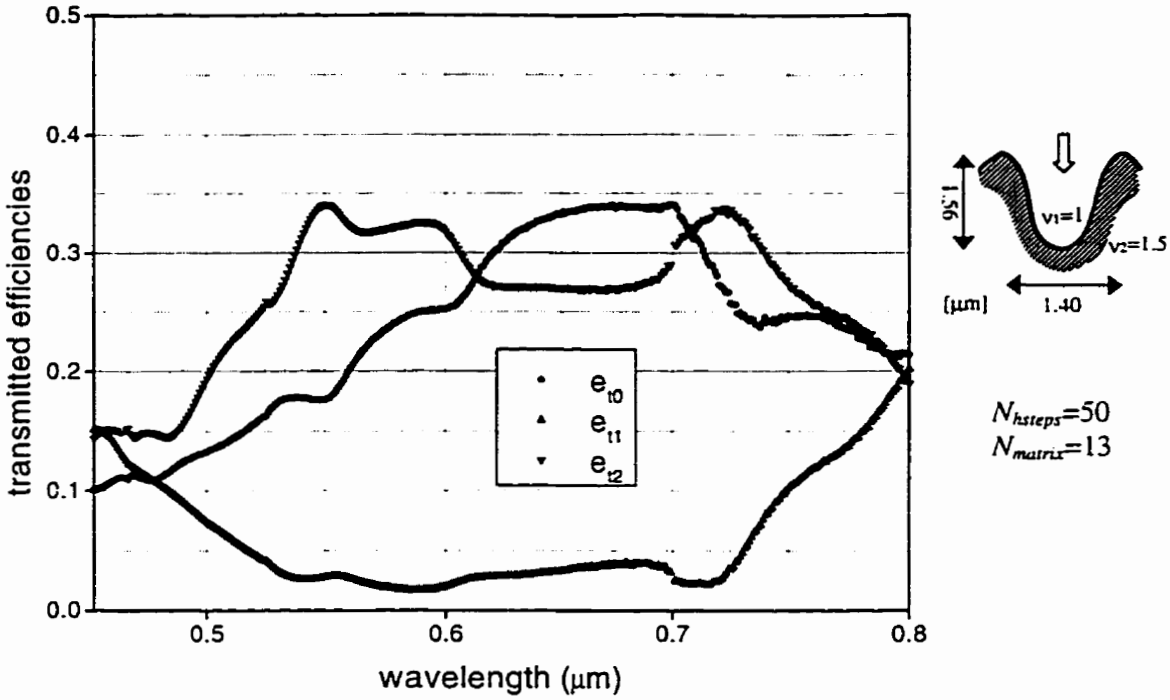

Figure 3-2: TE mode efficiency curves of dielectric lamellar grating for comparison with bottom graph of Fig. 6.104[25] in "Electromagnetic Theory of Gratings"

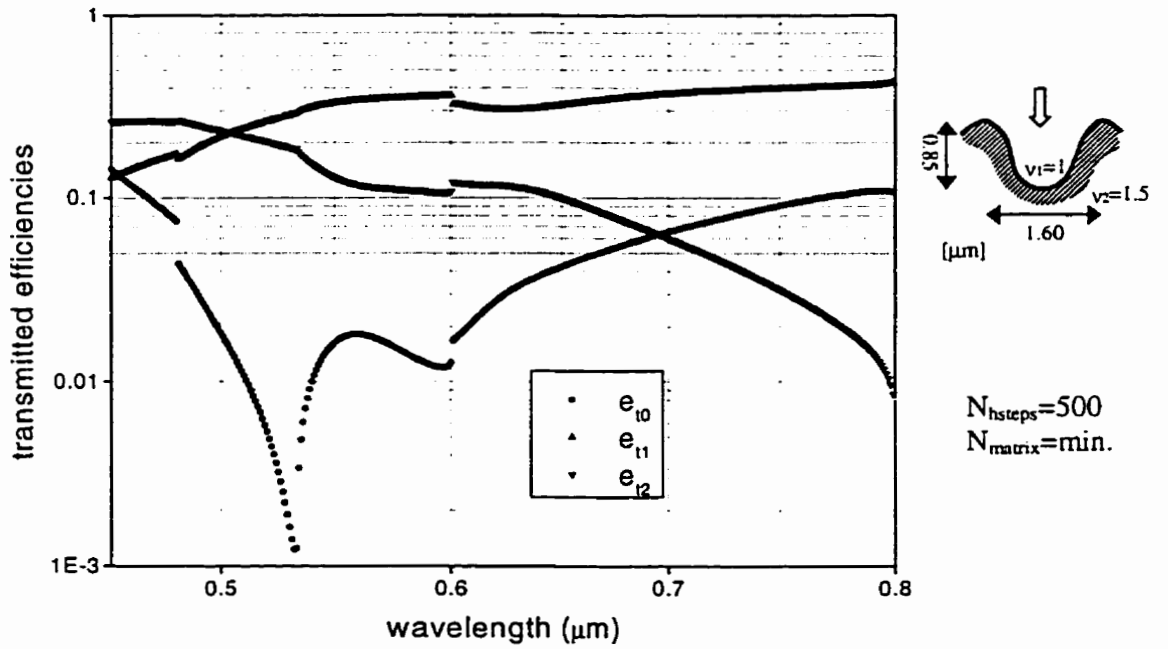

Figure 3-3: TE mode efficiency curves of dielectric lamellar grating for comparison with Fig. 6.105[25] in "Electromagnetic Theory of Gratings"

To further verify the consistency of our programmed algorithm with that presented in the literature a paper by Vincent was found containing numerical results for a lamellar transmission grating obtained using the differential method[27]. He used 19 terms in the Fourier series (N_{matrix}=19) but did not indicate how many steps he used for numerical integration. Table 3-1 presents results calculated using 19 term Fourier series and three different step sizes for numerical integration (N_{hsteps} = 50, 500, & 5000) along with Vincent's results. Looking at table 3-1 it can be seen that our results for this grating agree very closely with those of Vincent, the best agreement occurring for N_{hsteps} = 500 where all values agree to either 6 or 7 decimal places.

Table 3-1: Comparison of diffraction efficiencies calculated for lamellar transmission grating pictured on right.

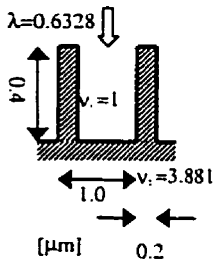

Order	Angle of Diffraction (°)	Diffraction Efficiencies			
		My calculated results			Published Results[27]
		N_{hsteps}=50	N_{hsteps}=500	N_{hsteps}=5000	
r_0	0.000	0.2680423	0.2680288	0.2680285	0.2680287
r_{-1}	39.257	0.0122900	0.0122915	0.0122915	0.0122915
t_0	0.000	0.1030229	0.1030530	0.1030519	0.1030528
t_1	9.384	0.1256445	0.1256183	0.1256187	0.1256183
t_2	19.032	0.0309303	0.0309360	0.0309361	0.0309360
t_3	29.285	0.0495860	0.0495929	0.0495933	0.0495928
t_4	40.708	0.0516288	0.0516321	0.0516327	0.0516321
t_5	54.612	0.0354150	0.0354155	0.0354160	0.0354155
t_6	78.043	0.0089727	0.0089728	0.0089729	0.0089727

3.2 DETERMINING ACCURACY OF RESULTS

There are two variables in the algorithm that may be adjusted in order to change the results for a grating with a given geometry. These variables are the number of Fourier components, N_{matrix} and the number of steps taken for numerical integration,

N_{hsteps}. A measure of the accuracy of results is obtained by varying N_{matrix} and/or N_{hsteps} and comparing the different results.

Two measures of accuracy are used. First, the sum of the efficiencies for the grating should be equal to 1. This condition is necessary but not sufficient to show that the results are valid[19]. If the sum of the efficiencies is not equal to 1 at least one of the efficiencies must be incorrect because the system is not conserving energy. Secondly we look for convergence of results as N_{matrix} and/or N_{hsteps} are increased. Looking at the overall variation in the results as a function of N_{matrix} and N_{hsteps}, appropriate values of each may be chosen.

After an appropriate choice of N_{matrix} and N_{hsteps} our validity criterion demanded only that the sum of efficiencies be within 10% of 1. The validity criterion was not satisfied for grating orders higher than 25 for TE mode and 3 for TM mode. This particular difficulty with the TM mode is inherent in the differential method[20]. Failure to satisfy the validity criterion also increases with grating depth, number of orders, and difference in refractive index values[20,25]. While our validity criterion only required 10% agreement, it should be noted that most results presented in this thesis agreed to a much greater extent.

3.2.1 Dependency of accuracy on N_{hsteps}

The first variable examined was N_{hsteps}. In order to reduce the calculation time, the minimum value of N_{matrix} that included all real grating orders was used for this part of the analysis. Grating efficiencies were calculated for echelle and TIR gratings using the following combinations:

- All calculable design orders (i.e. up to the highest order where the sum of the efficiencies was still within 10% of 1).
- 13 different values of ν_1 distributed between 1 and 3.6 (ν_2 was kept constant at 1).
- 3 values of N_{hsteps} - 50, 500, and 5000. (These numbers were selected after experimenting with various values.)

Comparisons were then made between results from the same gratings but with different values of N_{hsteps} used for calculation. The results for selected design orders are presented, for the reader's reference, in tables A-1 to A-8 of the Appendix. Based on the cost in calculation time of increasing N_{hsteps} and the small percentage difference (see tables) between results calculated with N_{hsteps} = 500 and 5000 it was decided that N_{hsteps} = 500 is a reasonable value to use for these gratings.

Typical plots of the relationship between N_{hsteps} and calculated efficiencies are presented in figure 3-4. It can be seen that the retro-reflection efficiencies for the 10^{th} order TIR gratings are very stable between N_{hsteps} = 50 and N_{hsteps} = 5000. Using a larger or smaller number of steps the results start to diverge.

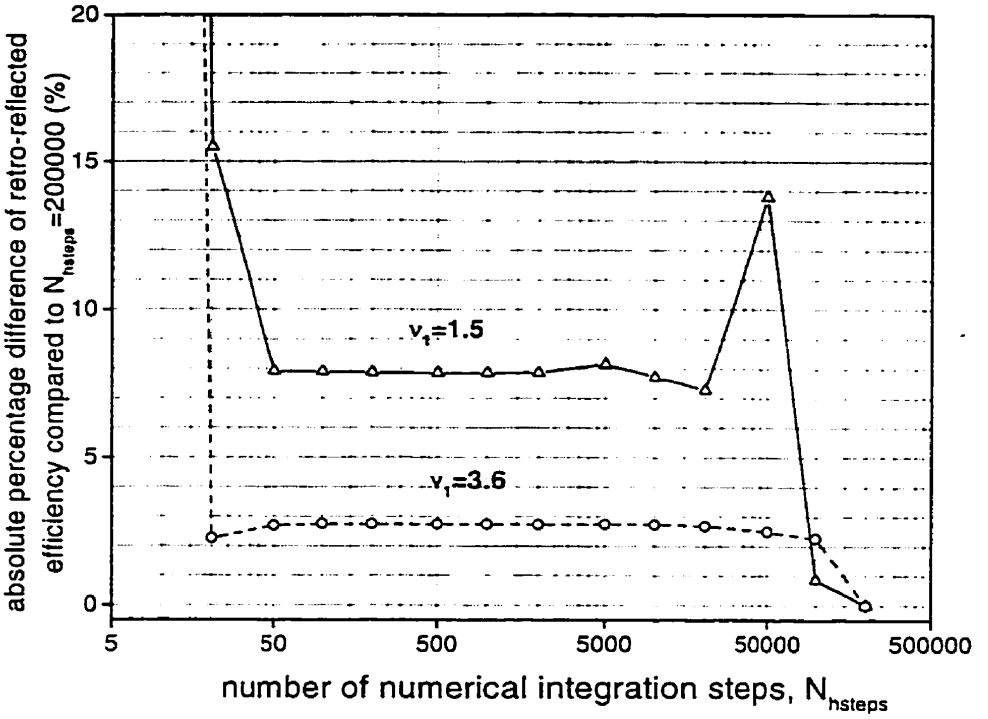

Figure 3-4: Dependence of results on number of numerical integration steps for 10th order TIR grating (for v_1=1.5, N_{matrix}=23; for v_1=3.6, N_{matrix}=19)

3.2.2 Dependency of accuracy on N_{matrix}

The second variable examined was N_{matrix}. N_{hsteps} = 500 was used for all of this part of the analysis since it was judged in the previous section to be a reasonable value for the gratings in question. Grating efficiencies were calculated for the following combinations of parameters:

- Design orders 1, 5, 10, 15, 20 (25 was about the maximum calculable order).
- 13 different values of v_1 distributed between 1 and 3.6 (v_2 was kept constant at 1).
- 7 values of N_{matrix} – 5, 11, 15, 21, 25, 31, 35 (These numbers were selected based on the minimum matrix sizes and after experimenting with various values.)

In order to reduce calculation and analysis time comparisons of these results were done only for the echelle grating. The geometry of the TIR grating is assumed to be close

enough to that of the echelle grating that only one set of values needs to be reported. Comparisons were made between results for the same gratings calculated using different values of N_{matrix}. The comparisons are presented, for the reader's reference, in tables A-9 to A-23. A plot of typical results is presented in figure 3-5 and the same plot with a different scale in figure 3-6. Looking at the tables and graphs some generalizations can be made. Using a matrix size less than the minimum size required to include all orders appears to introduce significant error in some of the efficiencies (even though the sum of the efficiencies may still be within 10% of 1). The percentage difference between results calculated for consecutive matrix sizes tends to decrease as the matrix size is increased from the minimum size. This decrease continues only to a certain point where it starts to increase again and quickly the sum of efficiencies becomes much larger than 1 and the results are obviously no longer accurate. As the order of the grating is increased this region of decreasing percentage differences becomes smaller and smaller until at the largest calculable order, only the minimum matrix size satisfies the condition that the sum of efficiencies be within 10% of 1.

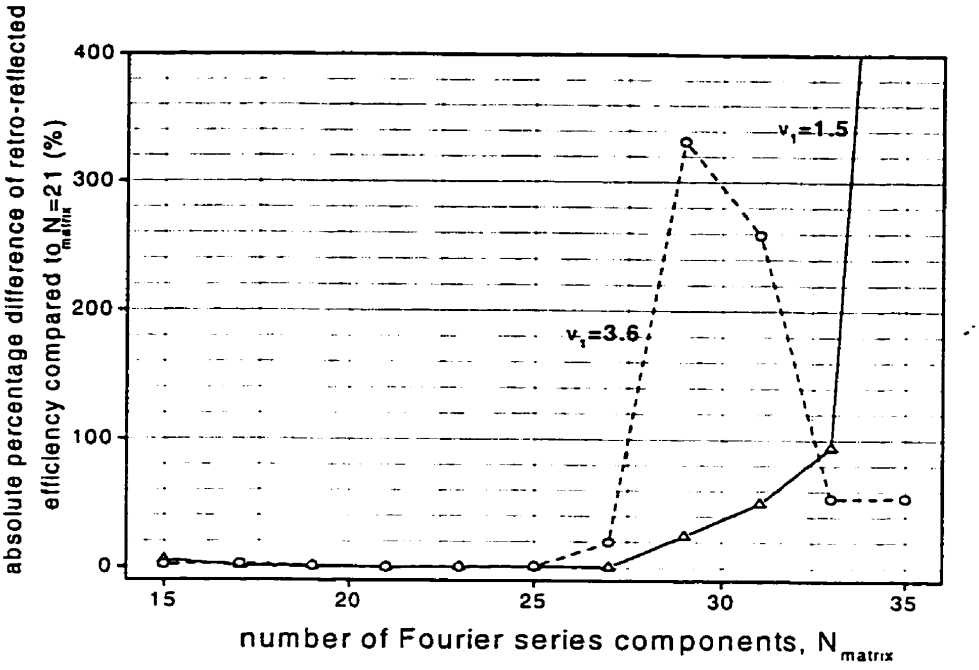

Figure 3-5: Dependence of results on number of Fourier series components, N_{matrix} for 10th order TIR gratings (N_{hsteps}=500)

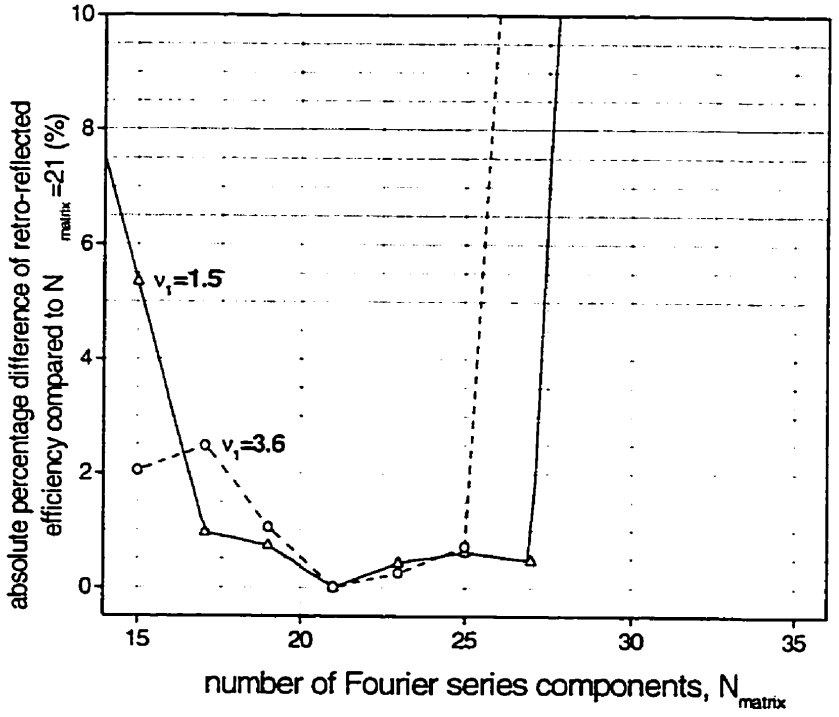

Figure 3-6: Dependence of results on number of Fourier series components, N_{matrix} for 10th order TIR gratings (N_{hsteps}=500)

It was assumed that the 'best' result occurs when the percentage difference between results calculated for consecutive matrix sizes is minimized. The reasoning behind this is that as you increase the matrix size you are increasing the number of Fourier coefficients and providing a better approximation of the actual grating shape. As you increase N_{matrix} you also increase the number of evanescent orders and the size of the matrix M_A which must be inverted. There is a large range of values in M_A and therefore it becomes difficult to invert and the results start to be less reliable the larger it is. A correlation was found between the 'best' results and the sum of the efficiencies. The largest matrix size for which the sum of efficiencies is within .001% of 1 was found to correspond to the 'best' matrix size for each of the orders that results were calculated for. This is the criterion used for choosing what matrix size to use for the results presented in this thesis.

The matrix size barely large enough to include all real orders was the minimum matrix size used to obtain the results presented in this thesis. Results presented in the following chapter were calculated using the largest matrix size for which the sum of efficiencies is within .001% of 1. In cases where this criterion could not be met, the minimum matrix size was used. Results are only presented for cases in which the sum of efficiencies is within 10% of 1. An estimation of uncertainty is not provided for any of the results. Tables presented in the Appendix may be used to estimate the calculation uncertainty in a particular data point.

4 RESULTS AND DISCUSSION

In this chapter, calculated diffraction efficiencies are presented for the echelle and TIR gratings described earlier (see figure 1-3). The gratings' responses are characterised over a range of relevant optical materials. Comparisons are made between the two gratings to test the concept of using total-internal reflection facets in grating design. Comparisons are also made between values calculated using scalar wave theory and those calculated using the differential method. Finally, theoretical results are compared with some previously reported experimental results.

4.1 SCOPE OF STUDY

To simplify the geometry we restrict our study to an incoming plane wave approaching at an angle of 45° with respect to the plane of the grating. The gratings are assumed to be two-dimensional planar bulk-optic gratings. The gratings are operated in the $-m^{th}$ order Littrow mount (*i.e.* retro-reflection corresponds to the $-m^{th}$ reflected order, for example see figure 2-2 for gratings in the –3 order Littrow mount) where m is referred to as the "grating order." Only results satisfying the validity criterion discussed in chapter 3 are reported. Since very few of the results calculated for the TM mode satisfied the validity criterion, only results for the TE mode are reported in this thesis.

Since current application of TIR gratings is for WDM components[12-14] the gratings were designed for a free-space wavelength, λ_0=1550 nm. There is a "transmission window" around 1550 nm where silica fibre exhibits its lowest loss[28] so most fibre optic telecommunications utilises light around this wavelength.

In all cases discussed, the region below the grating is air, for which the refractive index ν_2=1. The region above the grating may be any of a number of optical materials. Calculations were completed for values between ν_1=1 (air) and ν_1=3.6 (GaAs). This range includes SiO_2 (ν_1=1.45), Si_3N_4 (ν_1=2), Si (ν_1=3.5), and InP (ν_1=3.5) which are all materials commonly used in integrated optics[16,29].

4.2 THE SCALAR WAVE APPROXIMATION

The scalar wave approximation described in chapter 2 consists of two components – the Fresnel reflection component which varies with the refractive index above the grating ν_1, and the Fraunhofer diffraction component which varies with grating order *m*. The Fraunhofer component is the same for TIR and echelle gratings while the Fresnel component is different.

Figures 4-1 and 4-2 show the Fresnel reflection component as a function of ν_1. This component was calculated using equation (2.4). Figures 4-3 and 4-4 show the Fraunhofer diffraction component for retro-reflection for grating orders 1 to 30. This component was calculated using the Fraunhofer diffraction portion of equation (2.9). As indicated by equation (2.9), the scalar wave approximation of retro-reflection for a particular order grating can be found by multiplying the appropriate curve in figure 4-1 by the appropriate value from figure 4-3 (or adding the appropriate decibel values from figures 4-2 and 4-4). Looking at figures 4-3 and 4-4, it can be seen that the Fraunhofer component's effect is quite small, decreasing with increasing grating order. For grating orders larger than 6 its effect is less than 10%.

As illustrated in figures 4-1 and 4-2, the scalar wave approximation predicts that the retro-reflected efficiency for the TIR and echelle gratings will be zero for ν_1=1. This

is the limiting case where the medium becomes homogeneous and the interface (and thus the grating) vanishes. For the case $\nu_l=1$ it is clear that the incident light propagates forward without being diffracted. This means that all light should be in the zeroth transmitted order. As a check of our computer program, the limiting case of $\nu_l=1$ was calculated for all gratings reported in this thesis. In all cases, differential method and scalar wave approximation results indicate that all the light ends up in the zeroth transmitted order.

As illustrated in figures 4-1 and 4-2, the scalar wave approximation predicts that the retro-reflected efficiency for the TIR gratings will start at zero for $\nu_l=1$, increase slowly to the point where $\nu_l\cong1.3$, then increase sharply between $\nu_l\cong1.3$ and $\nu_l\cong1.45$ where it will level off for further increases in ν_l. Since the angle of incidence on the facets is 45° for the TIR grating we know that for $\nu_l>1.414$ the Fresnel reflection coefficient will be equal to 1. As illustrated in figure 4-1, the scalar wave approximation predicts that the retro-reflected efficiency for the echelle grating will increase approximately linearly with increasing ν_l. This translates into the curved plot we see in figure 4-2 when decibel units are used. Figures 4-3 and 4-4 show that the scalar wave approximation predicts retro-reflected efficiencies will generally increase with increasing grating order. It appears that the effect of increasing the order will be largest for smaller orders.

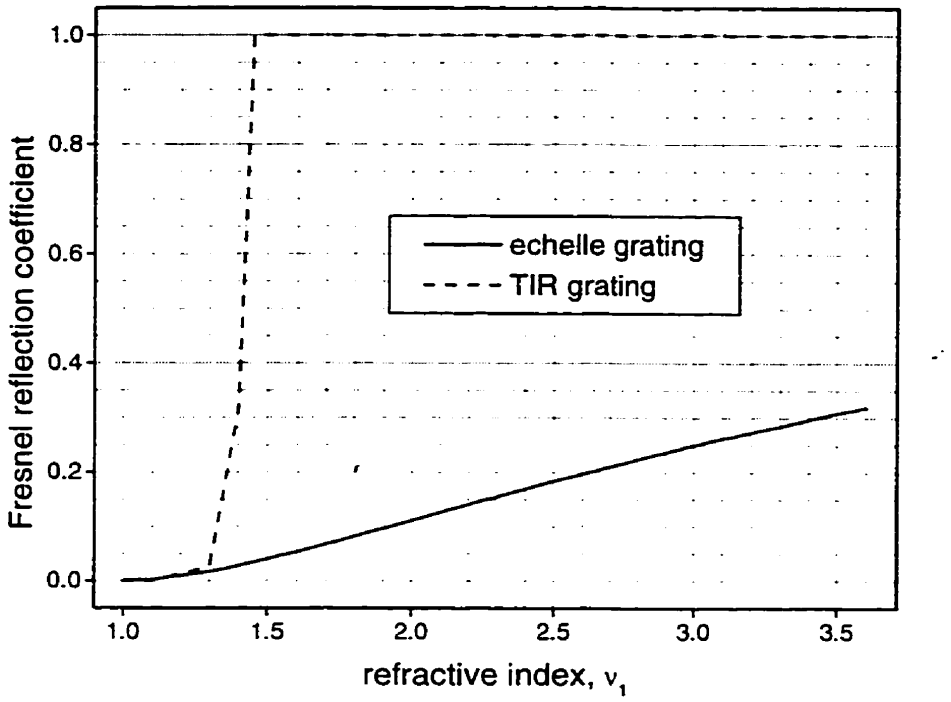

Figure 4-1: Plot of Fresnel reflection component of the scalar wave approximation according to equation (2.4) for TIR and echelle gratings

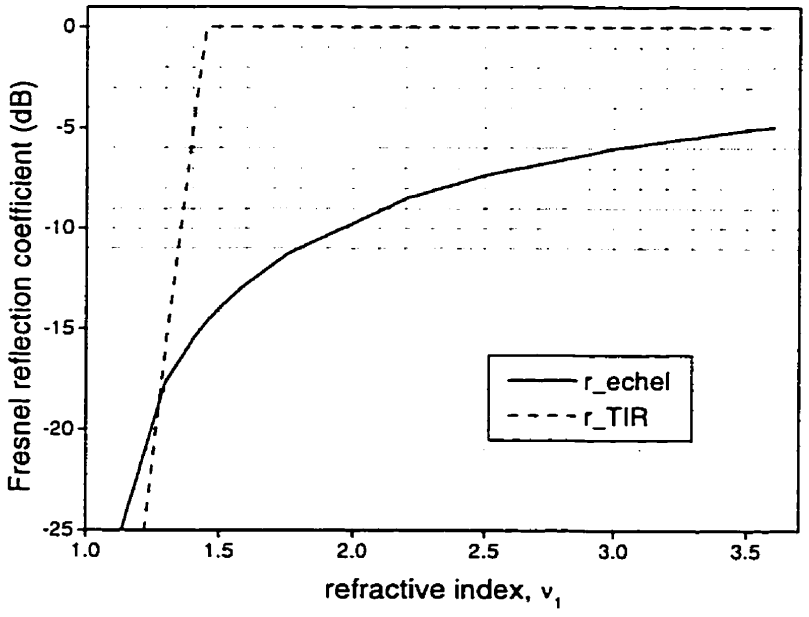

Figure 4-2: Plot of Fresnel reflection component of the scalar wave approximation according to equation (2.4) for TIR and echelle gratings in decibel units

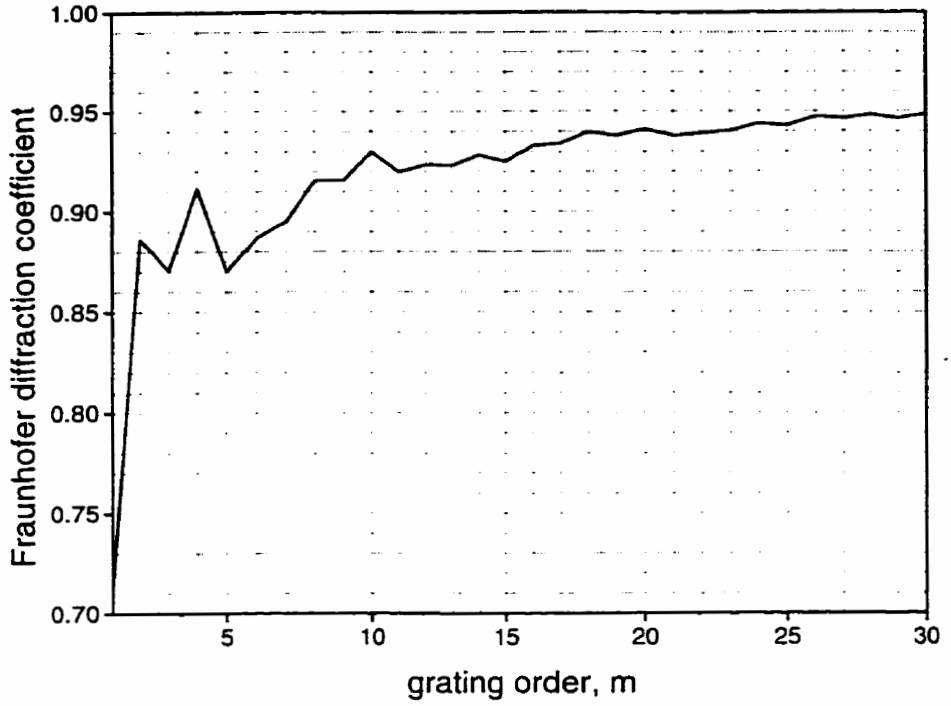

Figure 4-3: Plot of Fraunhofer diffraction component of the scalar wave approximation according to equation (2.9) for TIR and echelle gratings

Figure 4-4: Plot of Fraunhofer diffraction component of the scalar wave approximation according to equation (2.9) for TIR and echelle gratings in decibel units

4.3 COMPARISON OF SCALAR WAVE APPROXIMATION AND DIFFERENTIAL METHOD RESULTS FOR RETRO-REFLECTED EFFICIENCIES

4.3.1 Retro-Reflected Efficiencies as a Function of Refractive Index

Figures 4-5 to 4-10 show the retro-reflected efficiencies as a function of refractive index for both the echelle and TIR gratings. Differential method results are presented along with the scalar wave approximations. Graphs for grating orders 1, 2, 5, 10, 15, and 20 are given.

As illustrated by the TIR grating curves in figures 4-5 to 4-10, there is a sharp increase in the retro-reflection efficiency between $\nu_1 \cong 1.3$ and $\nu_1 \cong 1.45$. This was predicted by the scalar wave approximation as total internal reflection starts to occur in this range. The 1st, 2nd, and 5th order echelle gratings also show a sharp increase in this region which is not predicted by the scalar wave approximation since the light strikes the facets at normal incidence. According to grating theory, as the value of ν_1 is increased, there are fewer and fewer transmitted orders. With an angle of incidence of 45° to the normal of the grating, two transmitted orders always disappear as ν_1 is increased above 1.414. For a first order grating this means there are no longer any transmitted orders, all light is reflected for $\nu_1 > 1.414$ so it must go into either the retro-reflected order or zeroth reflected order. As the order of the grating is increased there are more transmitted and reflected orders so the loss of two transmitted orders becomes less significant. Perhaps this is why the sharp increase is not visible at all on the plots for 10th, 15th, and 20th order echelle gratings.

As illustrated in figure 4-5 the differential method results for the 1st order TIR and echelle gratings look very similar. Weak dependence of the efficiency on the groove

shape has been observed for 1st order Littrow mount gratings with infinite conductivity[25]. Perhaps this is because there are so few orders that the light may be diffracted into.

In figures 4-6 to 4-10 you can see the difference between the TIR and echelle gratings increasing as the grating order is increased. For each of the grating orders plotted, other than the 1st, it can be seen that the maximum difference between the TIR and echelle gratings occurs between ν_1=1.45 and ν_1=1.75.

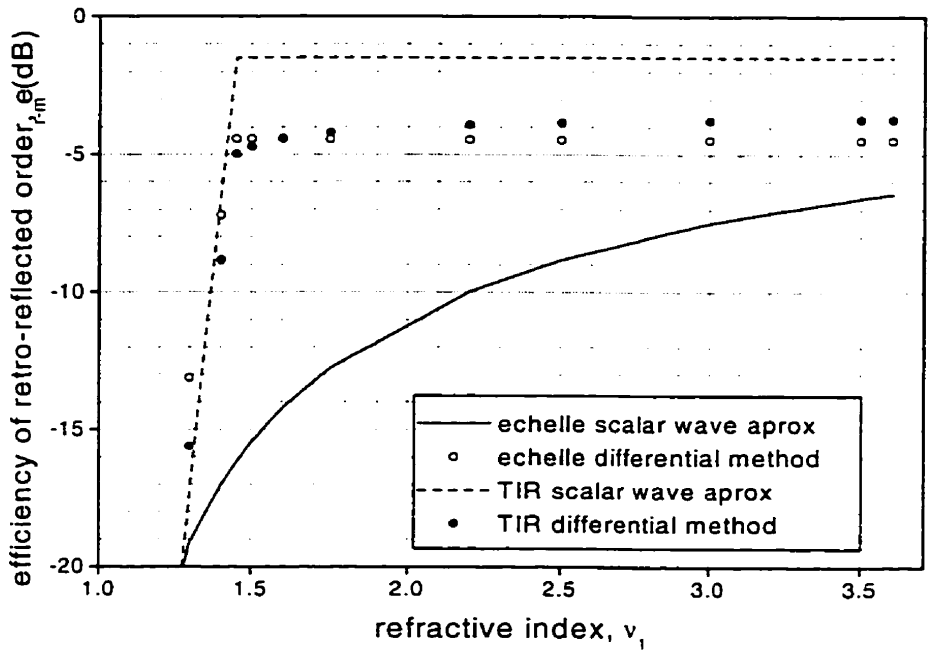

Figure 4-5: Plot of differential method results along with scalar wave approximations for retro-reflected efficiencies as a function of refractive index for 1st order echelle and TIR gratings

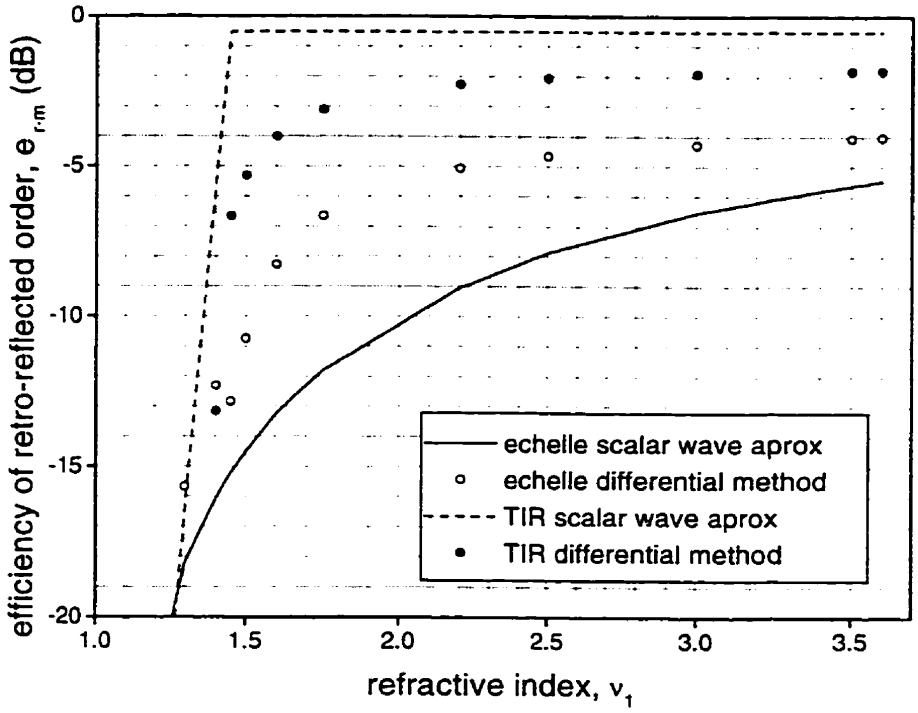

Figure 4-6: Plot of differential method results along with scalar wave approximations for retro-reflected efficiencies as a function of refractive index for 2nd order echelle and TIR gratings

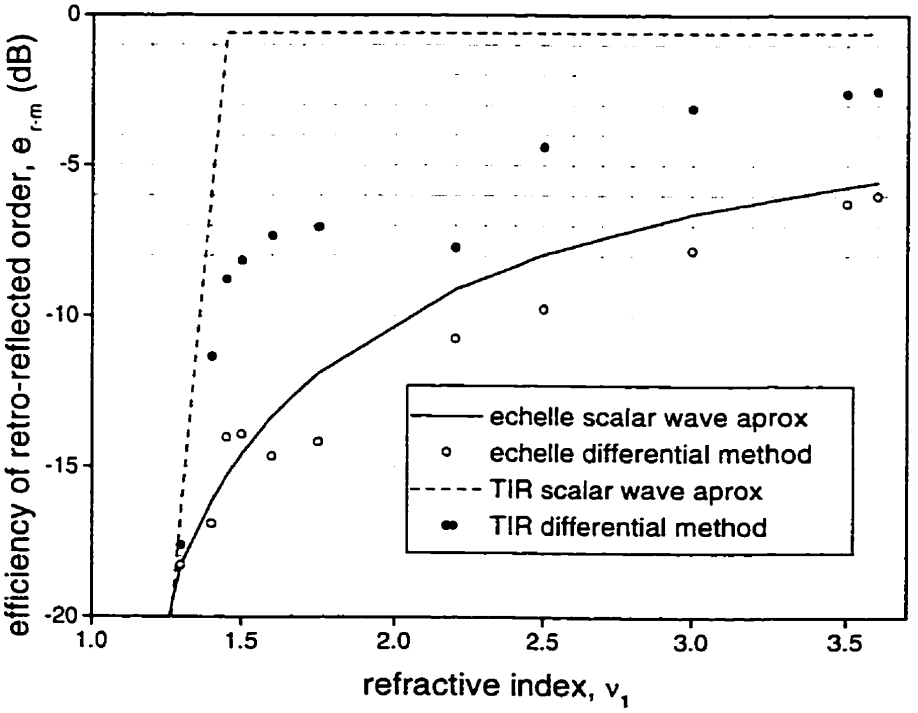

Figure 4-7: Plot of differential method results along with scalar wave approximations for retro-reflected efficiencies as a function of refractive index for 5th order echelle and TIR gratings

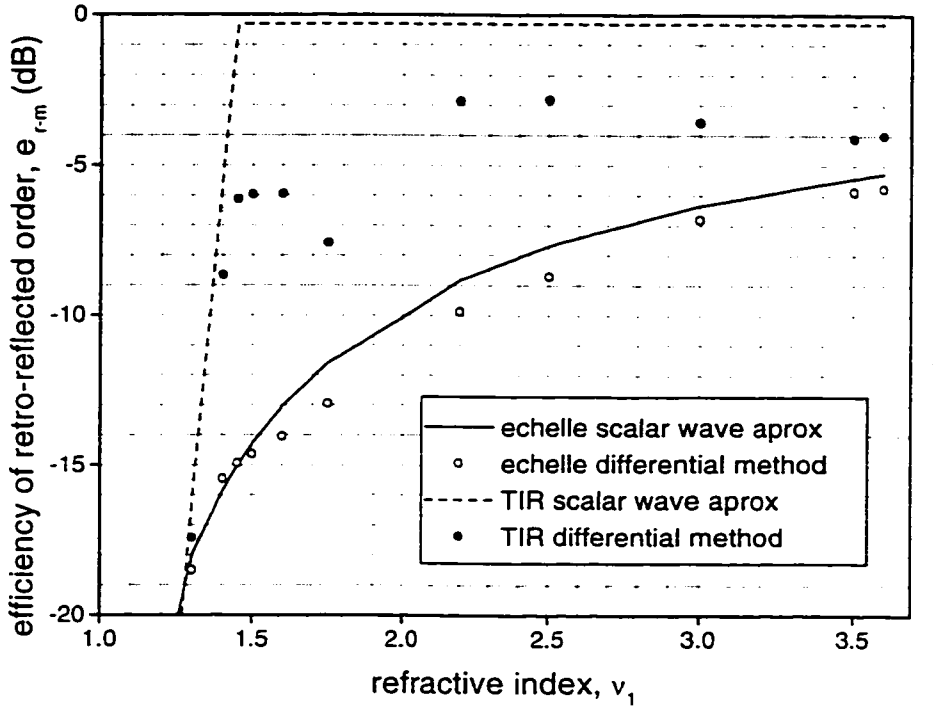

Figure 4-8: Plot of differential method results along with scalar wave predictions for retro-reflected efficiencies as a function of refractive index for 10^{th} order echelle and TIR gratings

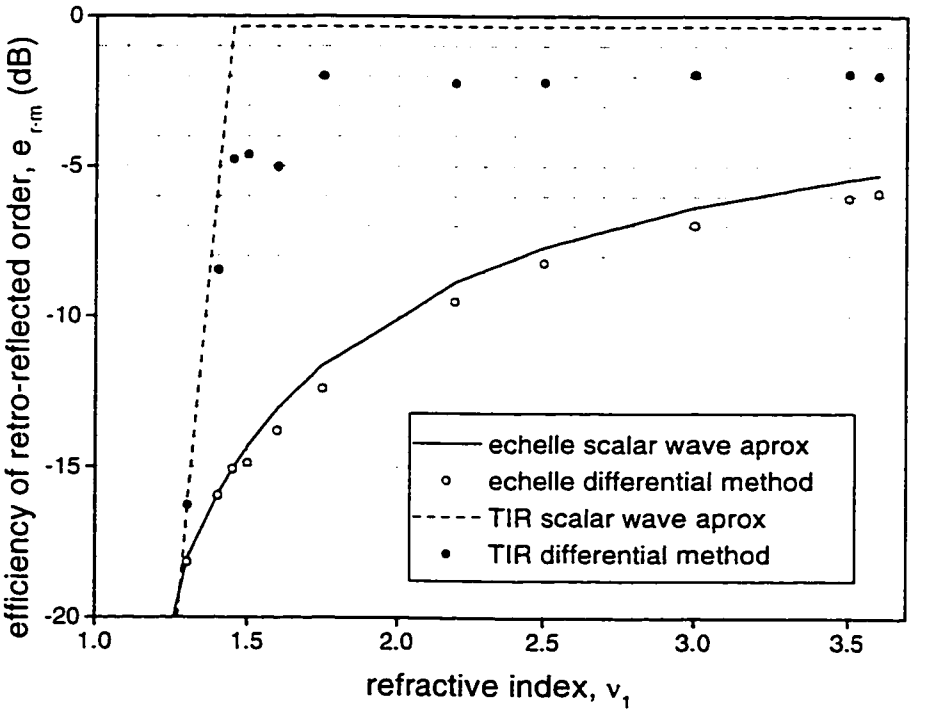

Figure 4-9: Plot of differential method results along with scalar wave approximations for retro-reflected efficiencies as a function of refractive index for 15^{th} order echelle and TIR gratings

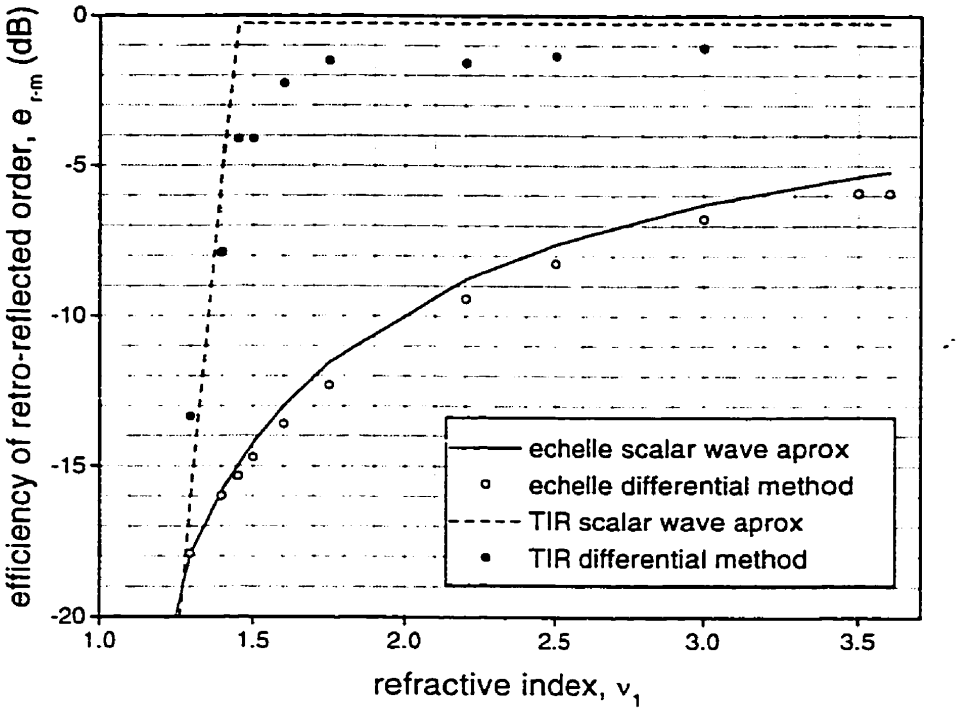

Figure 4-10: Plot of differential method results along with scalar wave approximations for retro-reflected efficiencies as a function of refractive index for 20th order echelle and TIR gratings

Figures 4-11 and 4-12 summarize the retro-reflected efficiencies for the 1st, 2nd, 5th, 10th, 15th, and 20th order TIR and echelle gratings plotted in figures 4-5 to 4-10. Results from the differential method for each of these grating orders, along with the Fresnel reflection component of the scalar wave approximation are plotted for the TIR grating in figure 4-11 and for the echelle grating in figure 4-12.

Looking at the plots as a function of refractive index for the TIR grating in figure 4-11 it can be seen that there is qualitative agreement between the differential method and scalar wave approximation for most grating orders plotted. There is an anomaly for the differential method results for 5th and 10th order gratings - they have an extra jog before leveling off. The sharply increasing part of the jog in each of these cases appears to correspond to the disappearance of two transmitted orders. There is, however, no corresponding jump in retro-reflection efficiency every time transmitted orders disappear.

The best agreement with the scalar wave approximation occurs for the 20th order grating followed by the 15th order grating. This might appear to indicate that agreement improves with increasing grating order, however, this is not always the case, as 1st and 2nd order gratings showed better agreement with the scalar wave approximation than the 5th and 10th order gratings.

As illustrated in figure 4-12, which shows the same plots for the echelle grating, there is again qualitative agreement between the differential method and scalar wave approximation for most grating orders that are plotted. The differential method curve for the 1st order grating does have a much sharper curve than the scalar wave approximation curve and higher grating order curves. As previously discussed, the reason for this is the sudden extinction of all transmitted orders. The 1st and 2nd order gratings' differential method results lie above the scalar wave approximation while higher plotted grating orders lie below the scalar wave approximation. For the grating orders plotted on the graph, it can easily be seen that agreement with the scalar wave approximation increases as the grating order increases.

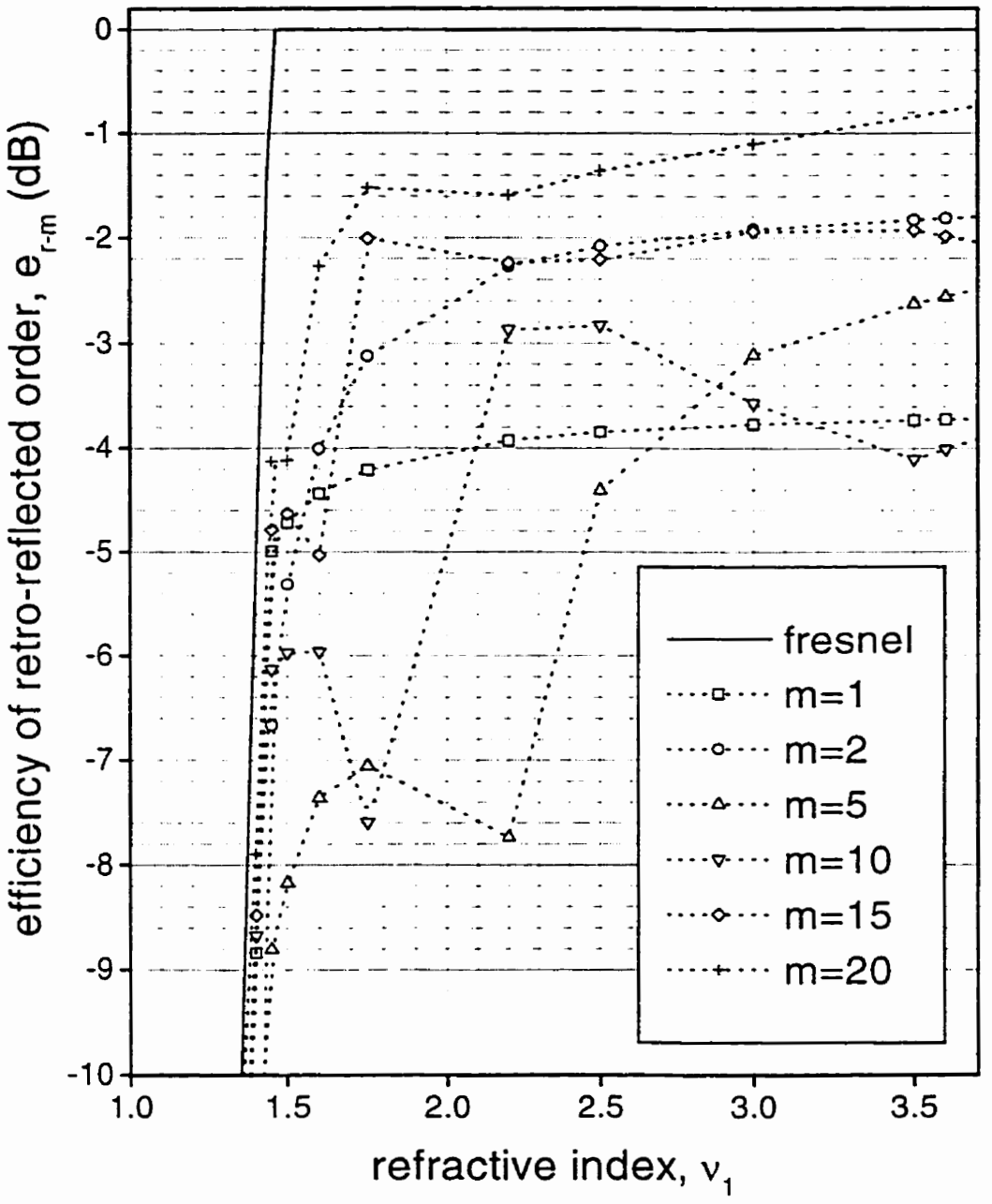

Figure 4-11: Plot of retro-reflected efficiencies along with scalar wave approximations as a function of refractive index for various TIR grating orders

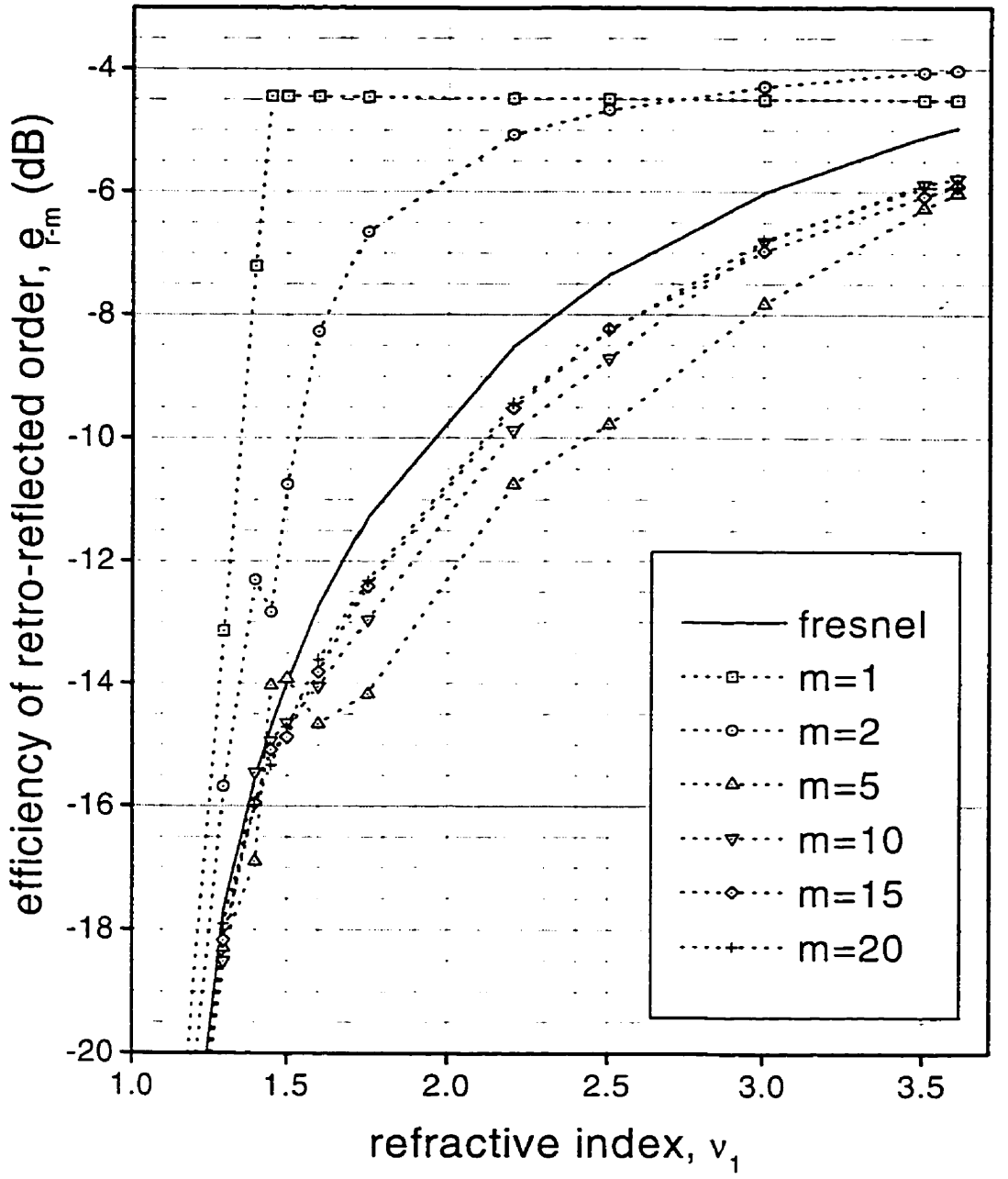

Figure 4-12: Plot of retro-reflected efficiencies along with scalar wave approximations as a function of refractive index for various echelle grating orders

4.3.2 Retro-Reflected Efficiencies as a Function of Grating Order

Figures 4-13 to 4-15 show plots of retro-reflected efficiencies as a function of grating order for both the echelle and TIR gratings. Plots of the scalar wave approximations as well as the differential method results are included on each of these graphs. Graphs for refractive index values v_1=1.45, 2.2, and 3.6 are given.

As illustrated in figures 4-13 to 4-14, for v_1=1.45 and v_1=2.2 grating orders higher than 5, the retro-reflected efficiency of the TIR grating is on average increasing slightly with grating order while that of the echelle grating is fairly constant. For v_1=3.6 it can be seen in figure 4-15 that the retro-reflected efficiency of the echelle grating is fairly constant after 5^{th} order, however, the retro-reflected efficiency of the TIR grating is only consistently increasing after 10^{th} order. Figure 4-13 shows that when the grating order is greater than six, a TIR grating with an index of refraction of 1.45 (SiO_2) is 8-12 dB more efficient than a similar echelle grating. The difference between the retro-reflected efficiencies of the echelle and TIR gratings is smaller than predicted by the scalar wave approximation.

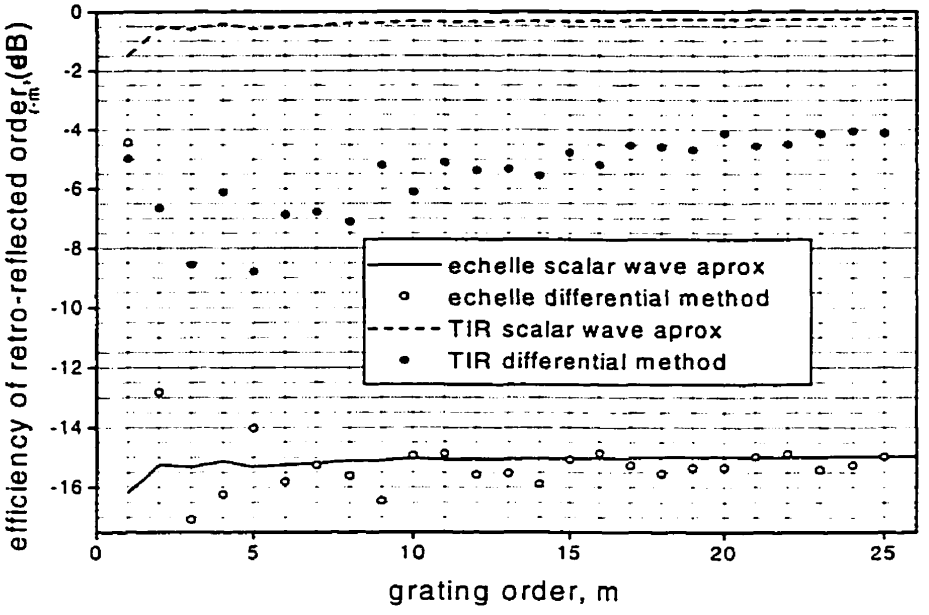

Figure 4-13: Plot of differential method results along with scalar wave approximations of retro-reflected efficiencies as a function of grating order for ν_1=1.45 echelle and TIR gratings

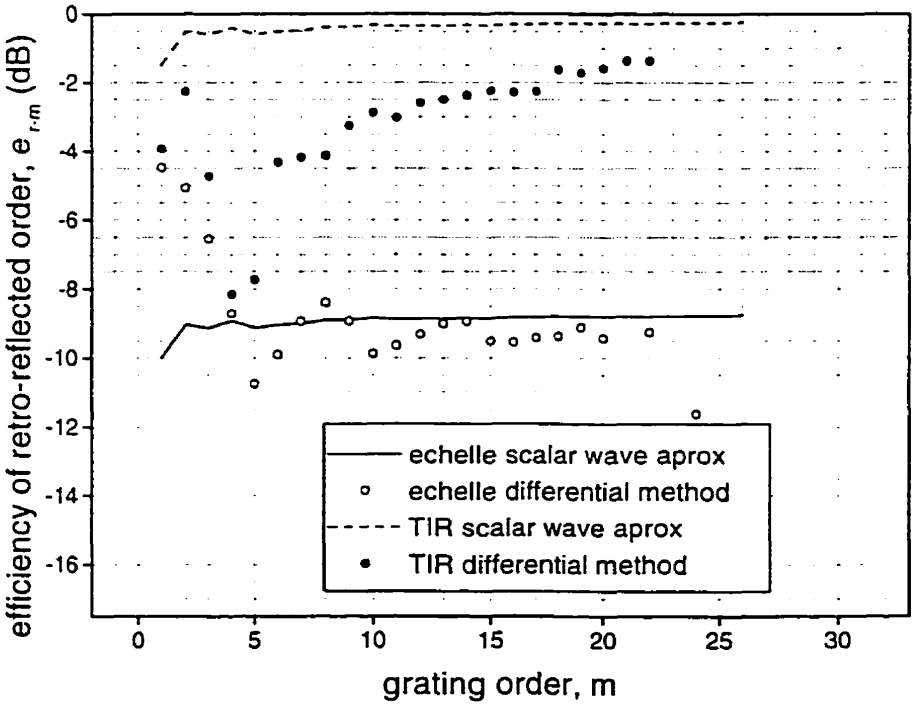

Figure 4-14: Plot of differential method results along with scalar wave approximations of retro-reflected efficiencies as a function of grating order for ν_1=2.2 echelle and TIR gratings

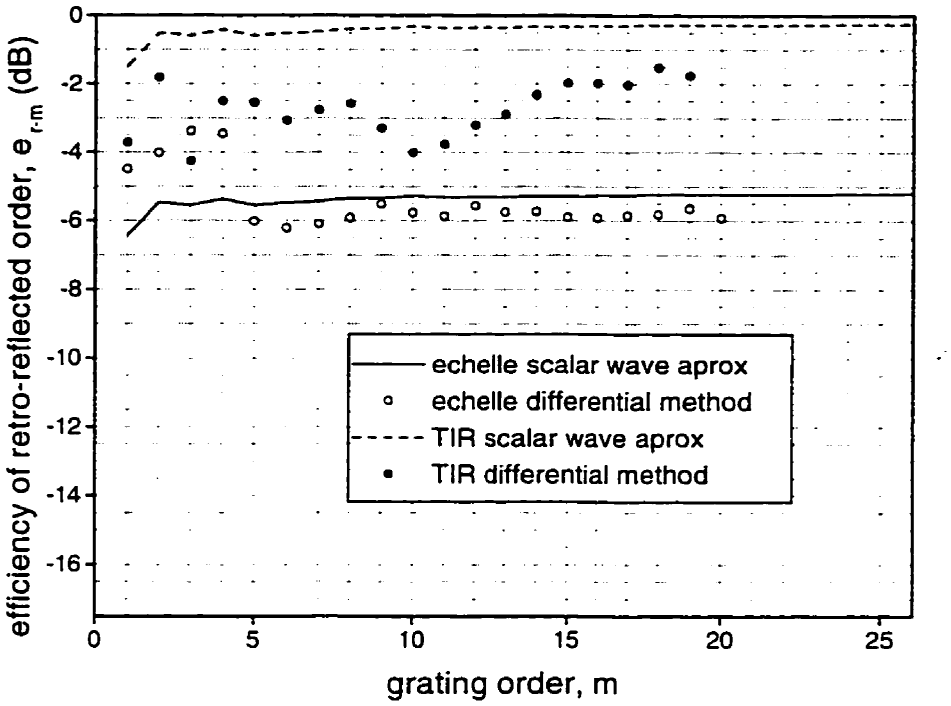

Figure 4-15: Plot of differential method results along with scalar wave approximations of retro-reflected efficiencies as a function of grating order for ν_1=3.6 echelle and TIR gratings

Figures 4-16 and 4-17 summarize the retro-reflected efficiencies for the ν_1=1.45, 2.2, and 3.6 TIR and echelle gratings plotted in figures 4-13 to 4-15. Differential method results for each of these grating orders, along with the scalar wave approximation are plotted for the TIR grating in figure 4-16 and for the echelle grating in figure 4-17. There is only one scalar wave approximation curve for the TIR grating because all the values of ν_1 plotted are greater than 1.414 so the Fresnel reflection coefficient is simply 1.

Figure 4-16 includes plots of retro-reflected efficiencies as a function of grating order for the TIR grating. In general it appears that as the grating order is increased and as the value of ν_1 is increased there is better agreement between the differential method and scalar wave approximation.

Figure 4-17, which includes plots as a function of grating order for the echelle grating, shows that above 5th order there is excellent agreement between the differential method and scalar wave approximation.

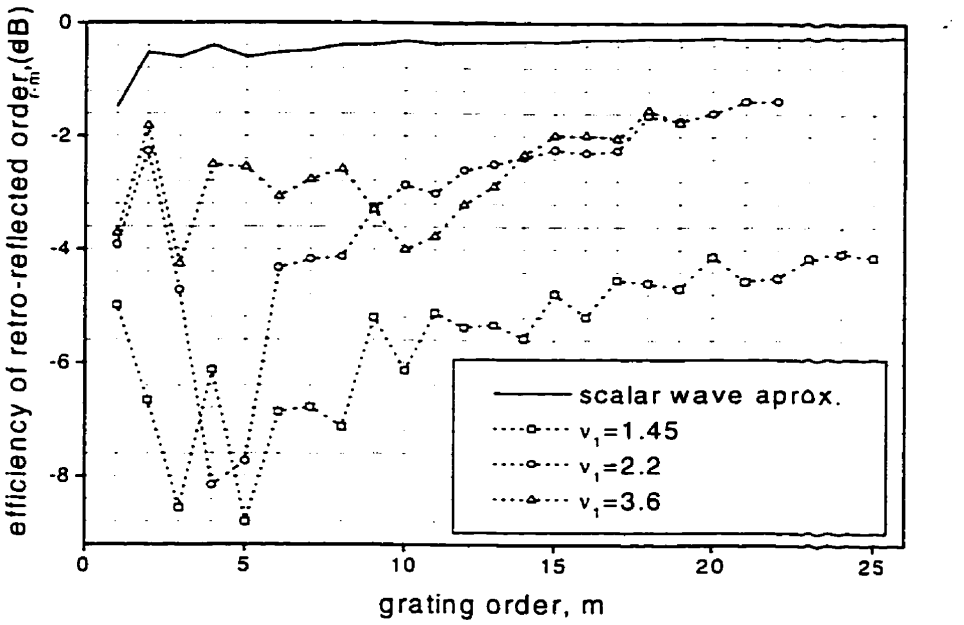

Figure 4-16: Plot of differential method results along with scalar wave approximations of retro-reflected efficiencies as a function of grating order for TIR gratings with various v_1 values

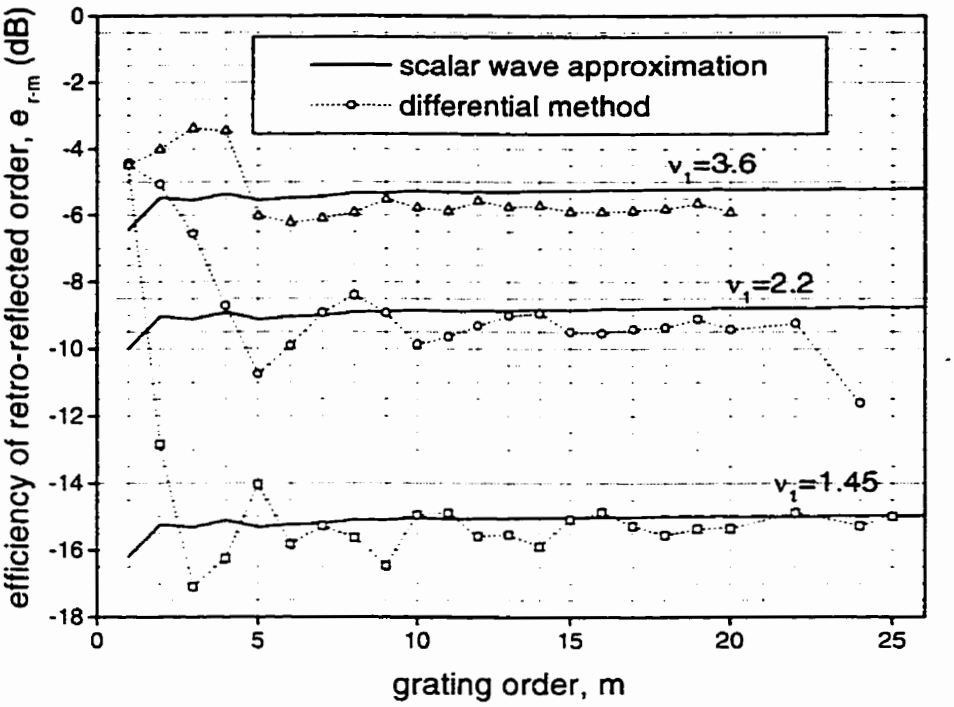

Figure 4-17: Plot of differential method results along with scalar wave approximations of retro-reflected efficiencies as a function of grating order for echelle gratings with various v_1 values

To summarize figures 4-5 to 4-17, there is often qualitative agreement between the differential method results and the scalar wave approximation, at least with the shape of the curves. For the results reported here, agreement with the scalar wave approximation generally improves with higher grating orders and higher refractive index values. The scalar wave approximation is unable to predict anomalies such as those in the 5th and 10th order TIR gratings and in the 1st order echelle grating. The scalar wave approximation does appear to be sufficient for predicting the improvement which total internal reflection facets provide over the echelle grating, though it generally predicts a greater difference between the two gratings than the differential method does.

4.4 RESULTS FOR THE TIR GRATING

4.4.1 TIR Grating Efficiencies as a Function of Refractive Index

Figures 4-18 to 4-23 show plots of different efficiencies as a function of the refractive index above the TIR grating. Each plot shows how the refractive index affects: the retro-reflected efficiency, the total of all reflected efficiencies, and the total of all transmitted efficiencies. Plots for grating orders 1, 2, 5, 10, 15, and 20 are presented.

In each of these plots it can be seen how the total reflected efficiencies and total transmitted efficiencies are related. To satisfy the energy balance criterion the sum of all diffracted efficiencies must be equal to 1. This means that as the sum of the reflected efficiencies increases, the sum of the transmitted efficiencies must decrease and vice versa.

In each of figures 4-18 to 4-23, it can be seen that as the refractive index is increased above the limiting case $\nu_1=1$, some of the light starts to end up in reflected orders. There is a sharp increase in the amount of reflected light between $\nu_1 \cong 1.3$ and $\nu_1 \cong 1.45$ for all grating orders as light starts to undergo total internal reflection at $\nu_1 > 1.414$. As ν_1 is further increased there is somewhat of a leveling off of the total reflected efficiencies, though this does not occur for all grating orders. It can be seen that the retro-reflected efficiency curve tends to follow the same general shape as the total reflected efficiencies curve.

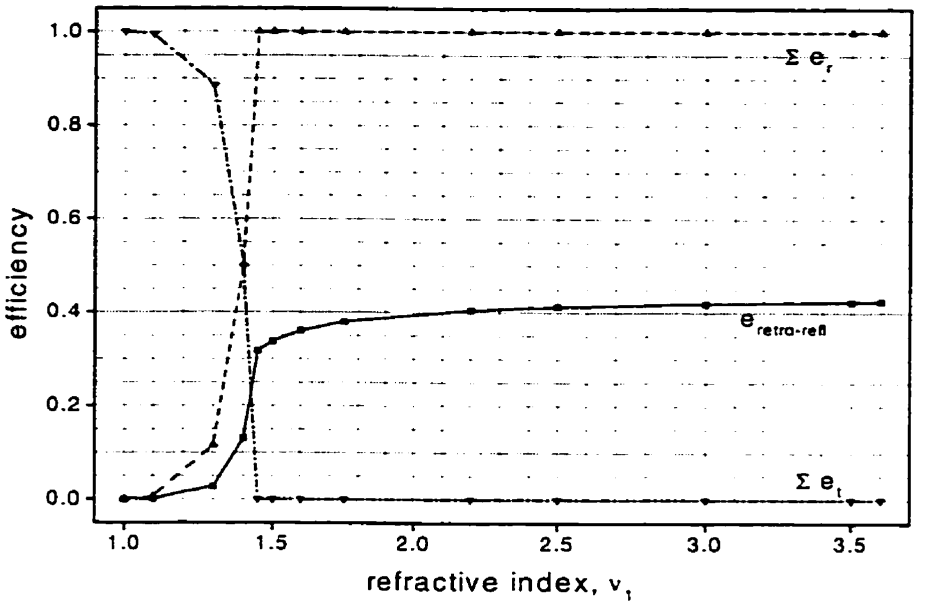

Figure 4-18: Plot of efficiencies as a function of refractive index for 1st order TIR grating

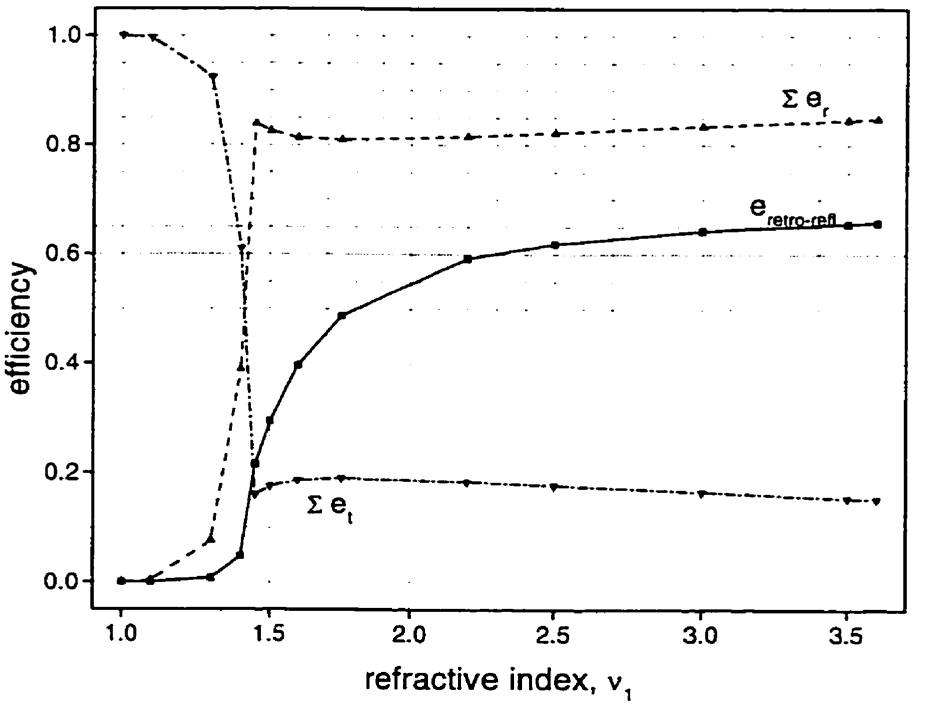

Figure 4-19: Plot of efficiencies as a function of refractive index for a 2nd order TIR grating

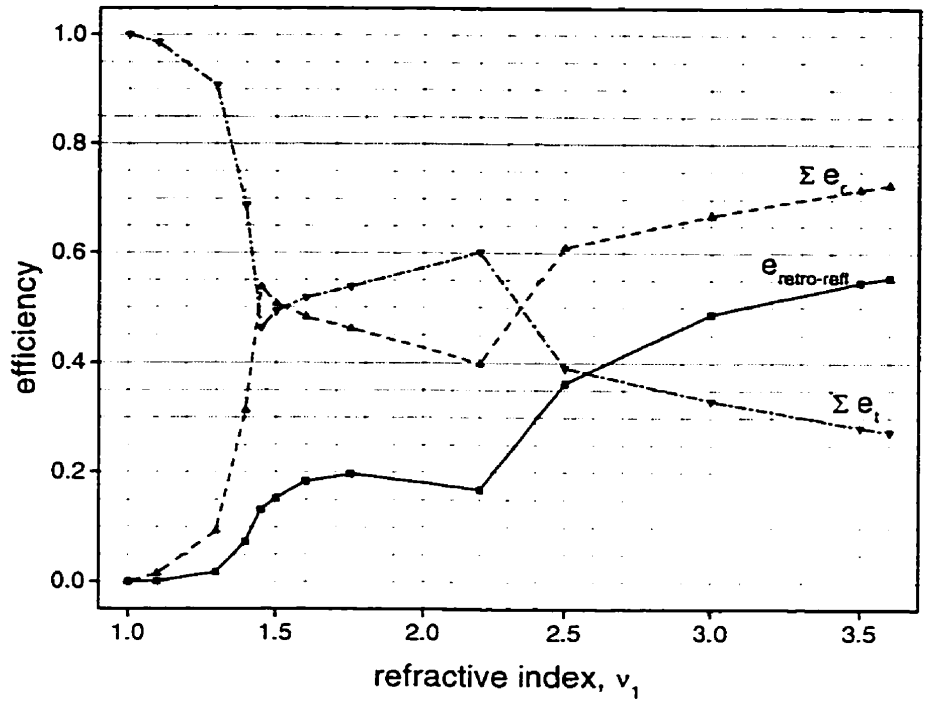

Figure 4-20: Plot of efficiencies as a function of refractive index for a 5th order TIR grating

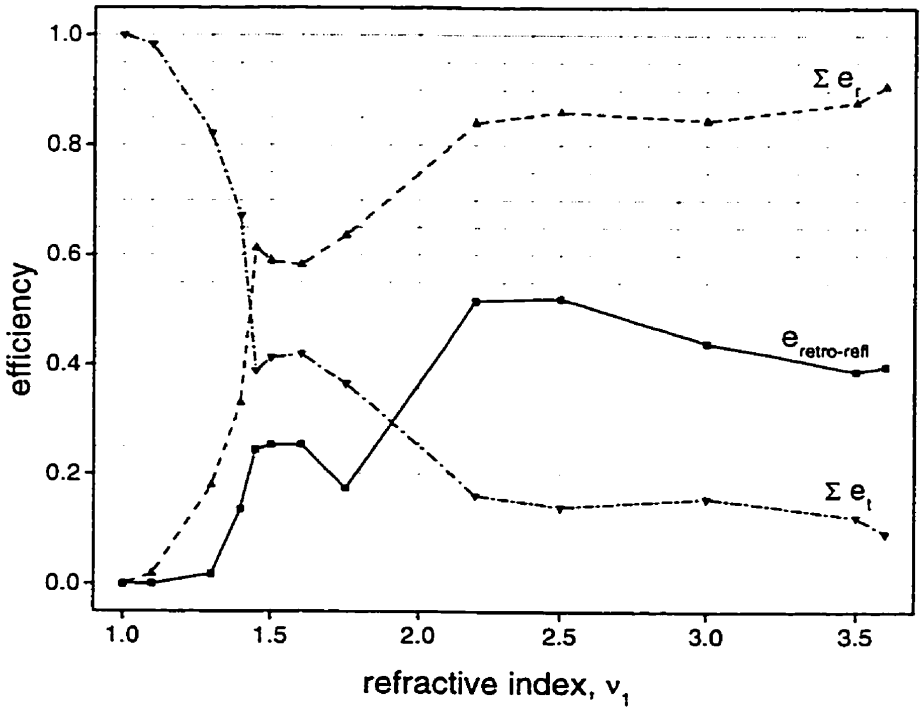

Figure 4-21: Plot of efficiencies as a function of refractive index for a 10th order TIR grating

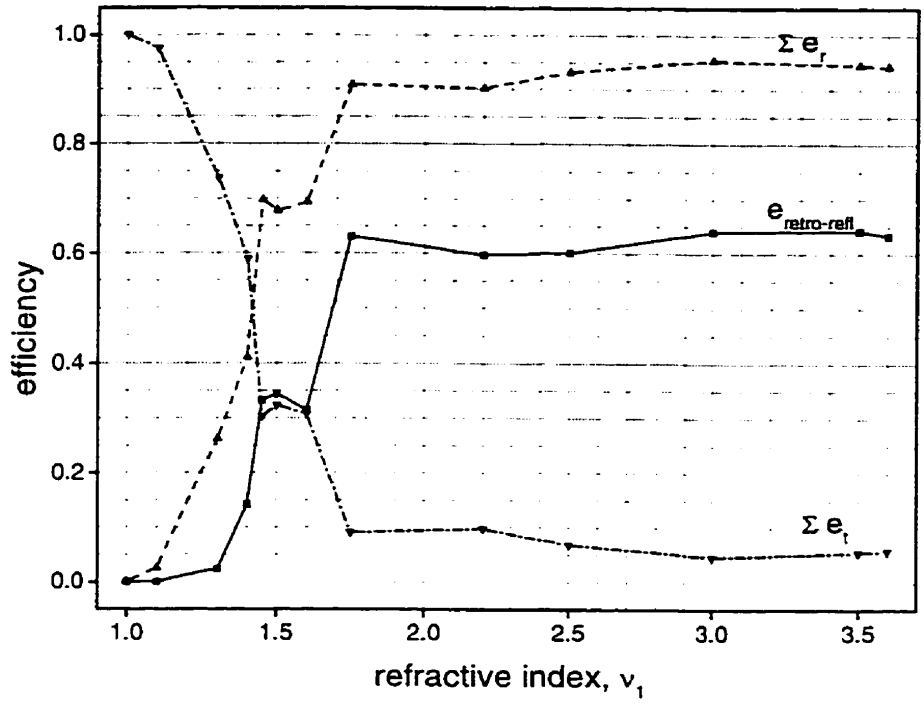

Figure 4-22: Plot of efficiencies as a function of refractive index for a 15th order TIR grating

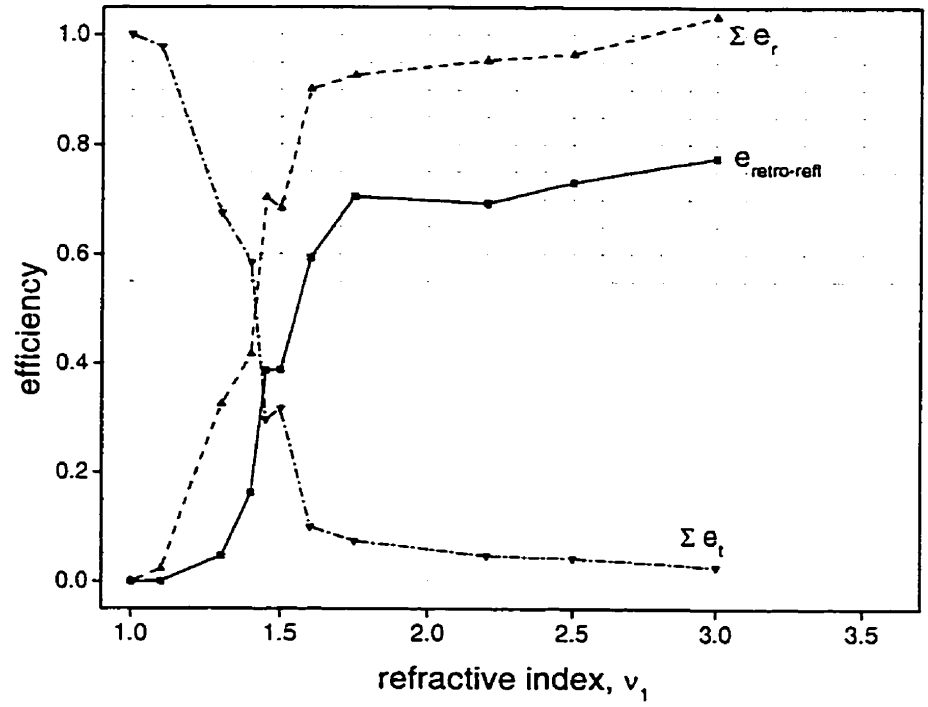

Figure 4-23: Plot of efficiencies as a function of refractive index for a 20th order TIR grating

4.4.2 TIR Grating Efficiencies as a Function of Grating Order

Figures 4-24 to 4-26 show plots of efficiencies for TIR gratings as a function of grating order. Each plot shows how the grating order affects: the retro-reflected efficiency, the total of all reflected efficiencies, and the total of all transmitted efficiencies. Plots for refractive index values v_1=1.45, 2.2, and 3.6 are presented.

Again, the shape of the retro-reflected efficiency curve roughly follows the shape of the total reflected efficiencies curve for all three graphs, although the discrepancy appears to be larger for the first few orders. For each of figures 4-24 to 4-26, these two curves generally drop as the grating order is increased from 1 to about 4. Each curve has a minimum total reflected (and retro-reflected) efficiency which occurs at m=5 for v_1=1.45, m=4 for v_1=2.2, and m=3 for v_1=3.6. As the order is further increased beyond the minimum, the curves generally rise with a shallower pitch than the fall. The curves for v_1=2.2 have the most distinct minimum. The curves for v_1=1.45 look the smoothest of the three and do not rise back up as high as the other two curves. The retro-reflection curve for v_1=3.6 has a second dip around m=10 which none of the other reflection curves have. We do not have a qualitative explanation for why these minimums occur.

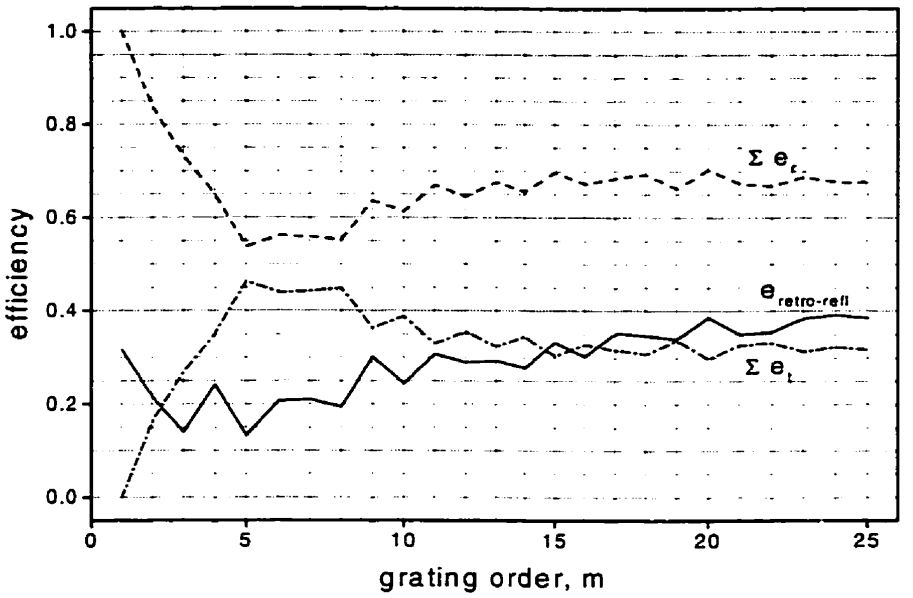

Figure 4-24: Plot of efficiencies as a function of grating order for ν_1=1.45 TIR gratings

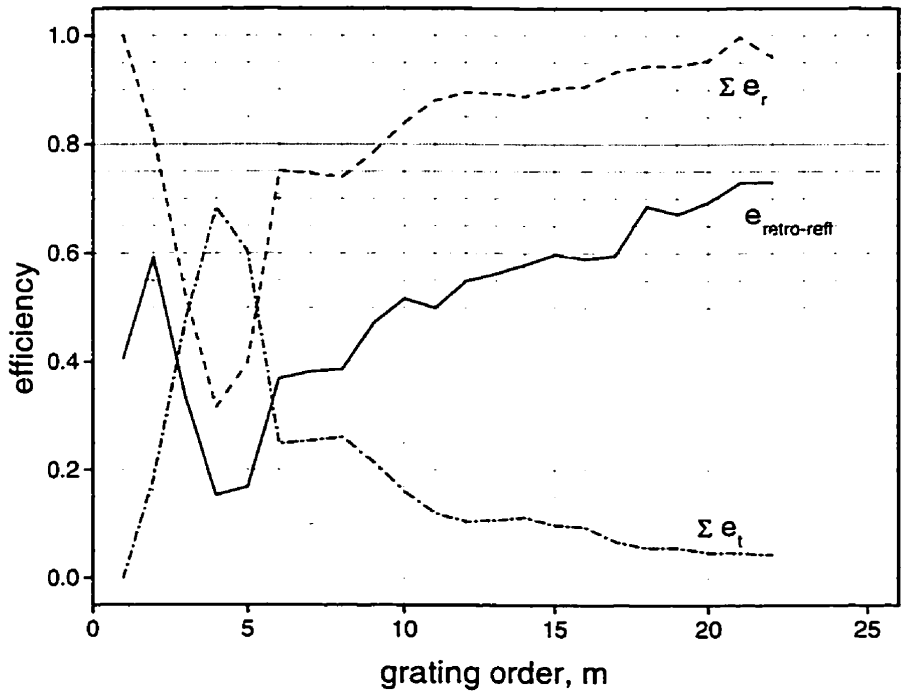

Figure 4-25: Plot of efficiencies as a function of grating order for ν_1=2.2 TIR gratings

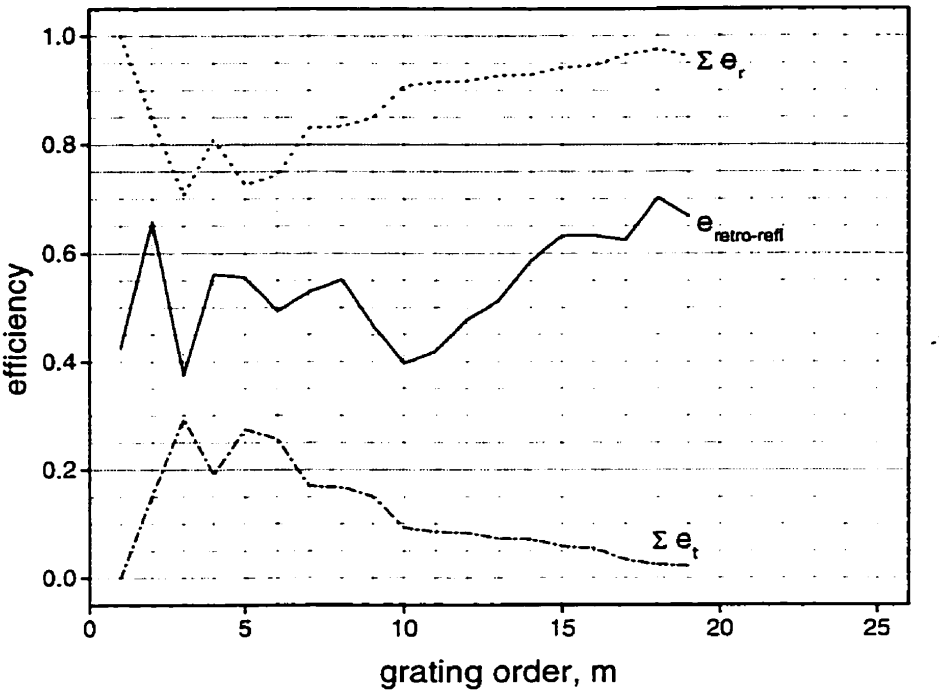

Figure 4-26: Plot of efficiencies as a function of grating order for ν_1=3.6 TIR gratings

4.5 RESULTS FOR THE ECHELLE GRATING

4.5.1 Echelle Grating Efficiencies as a Function of Refractive Index

Figures 4-27 to 4-32 show plots of different efficiencies as a function of the refractive index above the echelle grating. Each plot shows how the refractive index affects: the retro-reflected efficiency, the total of all reflected efficiencies, and the total of all transmitted efficiencies. Plots for grating orders 1, 2, 5, 10, 15, and 20 are presented.

The plot for m=1 looks very similar to that for the TIR grating. The plot for m=2 is also similar to that for the TIR grating, although a smaller percentage of the light is retro-reflected. For m=1, 2, and 5 there is a sharp increase in the total reflected efficiencies curve between $\nu_1 \cong 1.3$ and $\nu_1 \cong 1.45$. This increase, as discussed previously, corresponds to sudden loss of all transmitted orders.

Looking at the plot for the 5th order grating it can be seen that the shape of the retro-reflected efficiency curve does not follow the shape of the total reflected efficiencies curve. For grating orders larger than 5, it can be seen that the total reflected efficiencies curve follows a more or less linearly increasing path as does the retro-reflected efficiency curve.

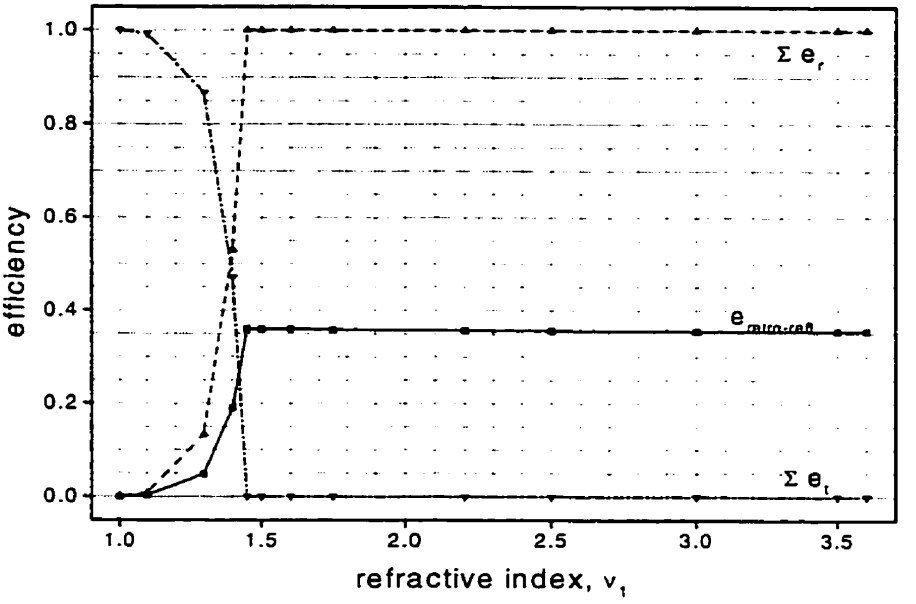

Figure 4-27: Plot of efficiencies as a function of refractive index for a 1st order echelle grating

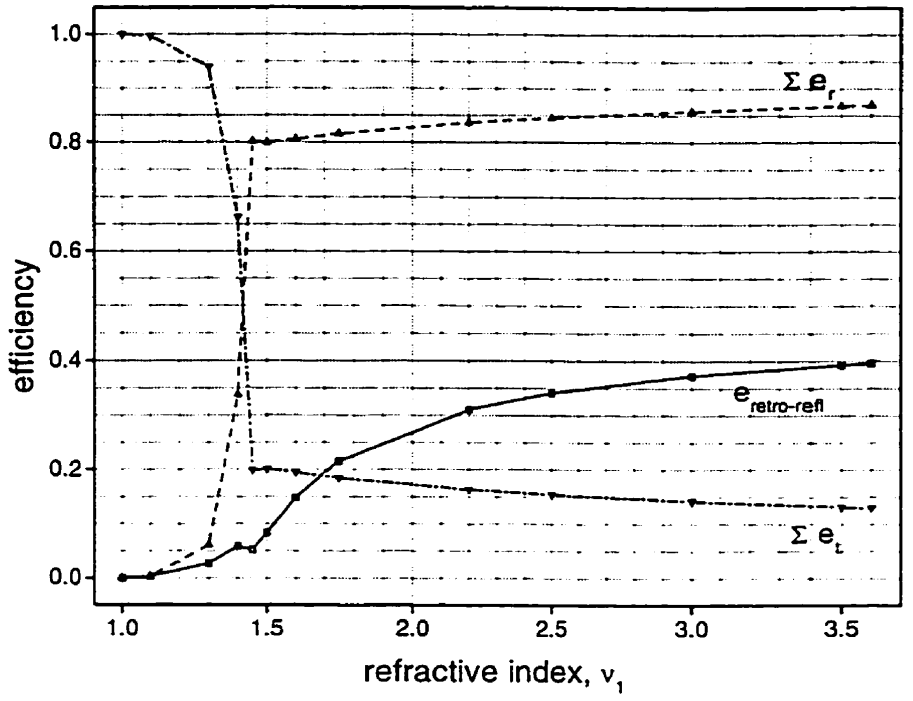

Figure 4-28: Plot of efficiencies as a function of refractive index for a 2nd order echelle grating

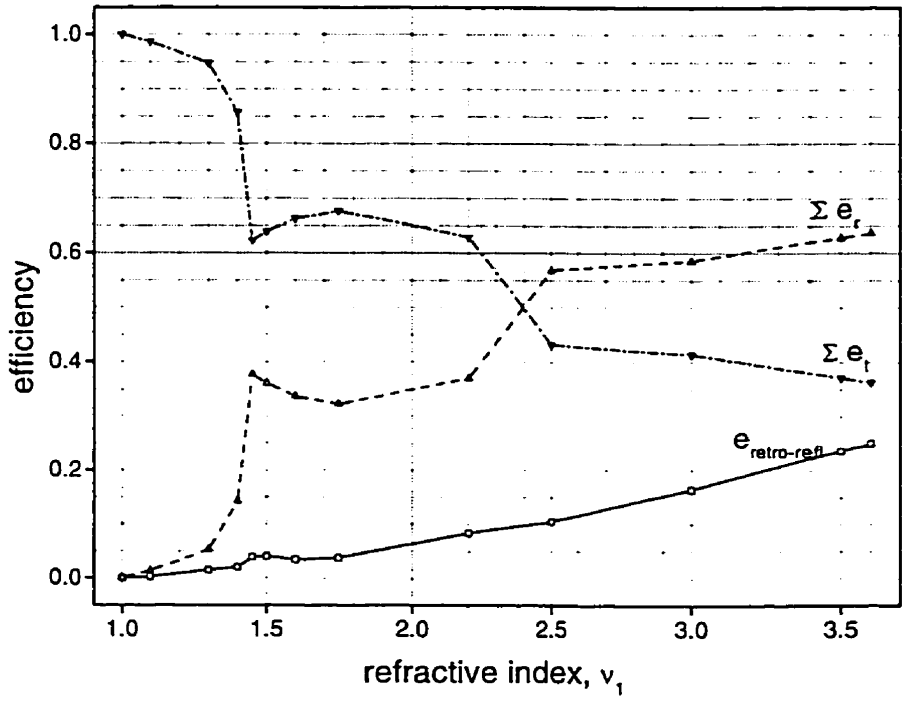

Figure 4-29: Plot of efficiencies as a function of refractive index for a 5th order echelle grating

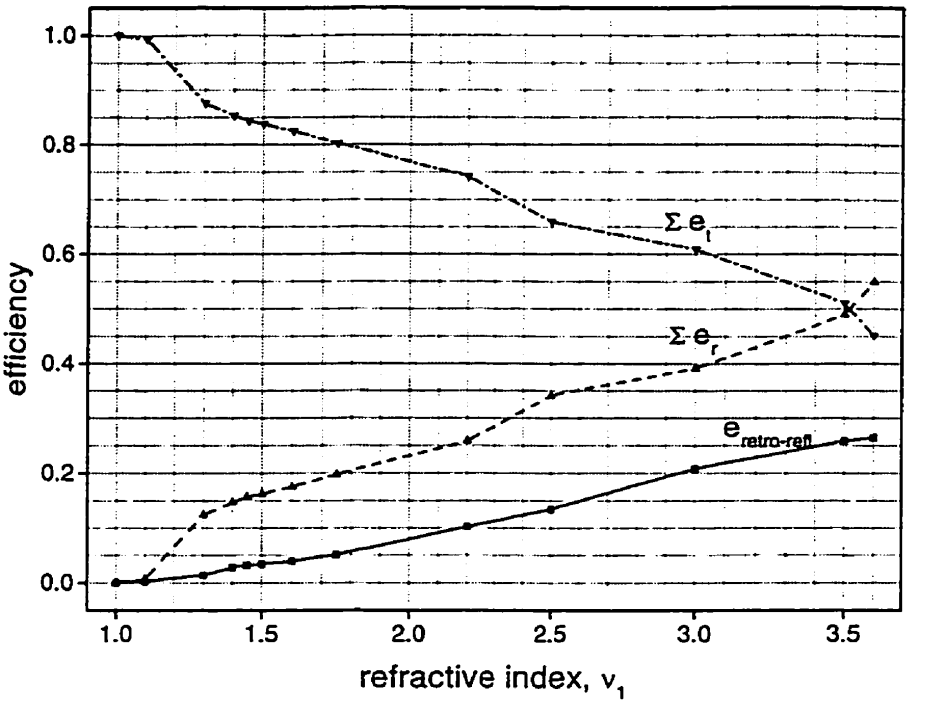

Figure 4-30: Plot of efficiencies as a function of refractive index for a 10th order echelle grating

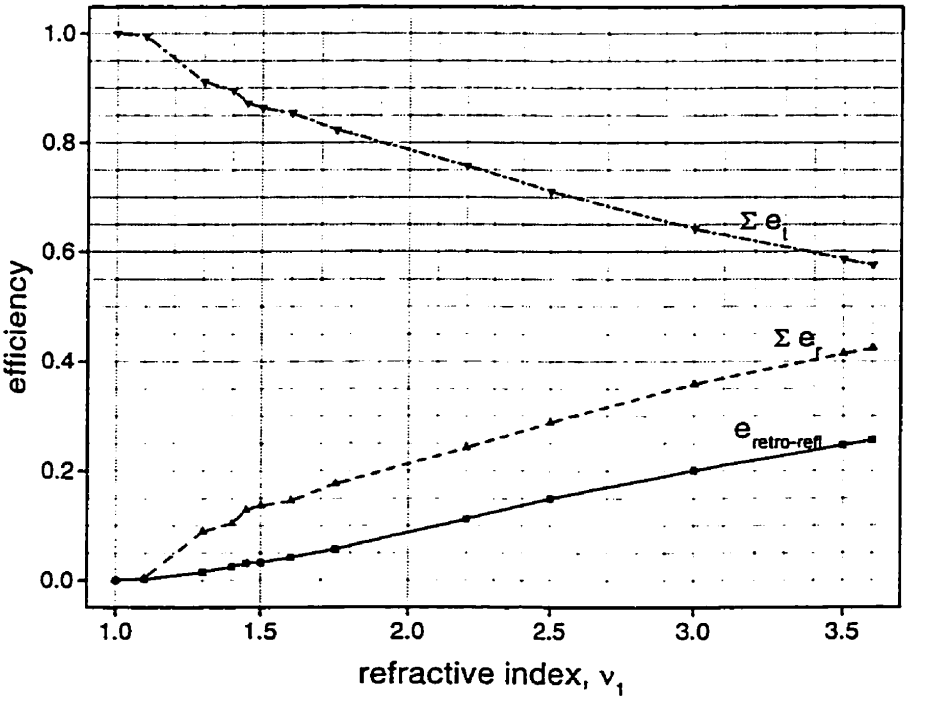

Figure 4-31: Plot of efficiencies as a function of refractive index for a 15th order echelle grating

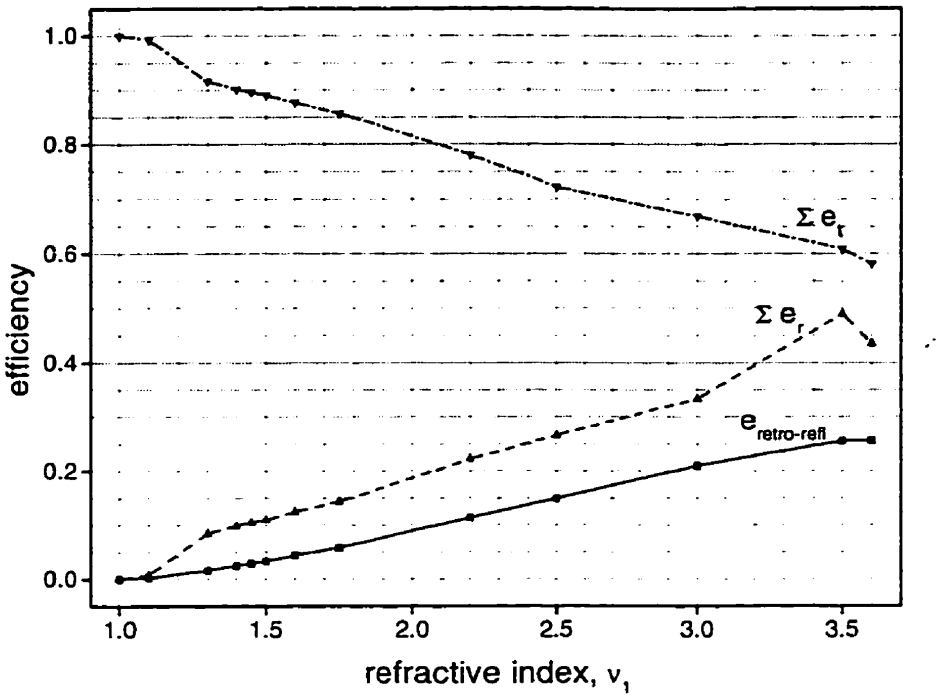

Figure 4-32: Plot of efficiencies as a function of refractive index for a 20th order echelle grating.

4.5.2 Echelle Grating Efficiencies as a Function of Grating Order

Figures 4-33 to 4-35 show plots of efficiencies for echelle gratings as a function of grating order. Each plot shows how the grating order affects: the retro-reflected efficiency, the total of all reflected efficiencies, and the total of all transmitted efficiencies. Plots for refractive index values v_1=1.45, 2.2, and 3.6 are presented.

The basic shape of the total reflection efficiencies curve for these graphs has it falling quite rapidly from unity for the first order grating to some value and then leveling off as the grating order is further increased. It can be seen that as the value of v_1 is increased the fall is more gradual and not as far. The smoothest curve occurs for v_1=1.45. The v_1=2.2 grating curve has a small peak around m=6 while the v_1=3.6 curve has 3 small peaks.

It can be seen that the shape of the retro-reflected efficiency curve follows that of the total reflected efficiencies curve quite closely for all graphs. The exceptions are the peaks mentioned previously and the first few grating orders of the v_l=3.6 plot.

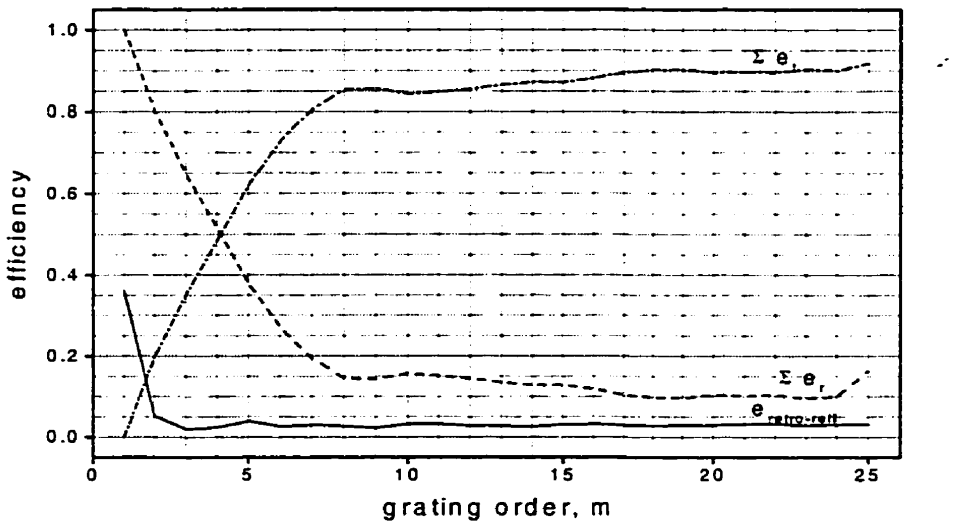

Figure 4-33: Plot of efficiencies as a function of grating order for v_l=1.45 echelle gratings

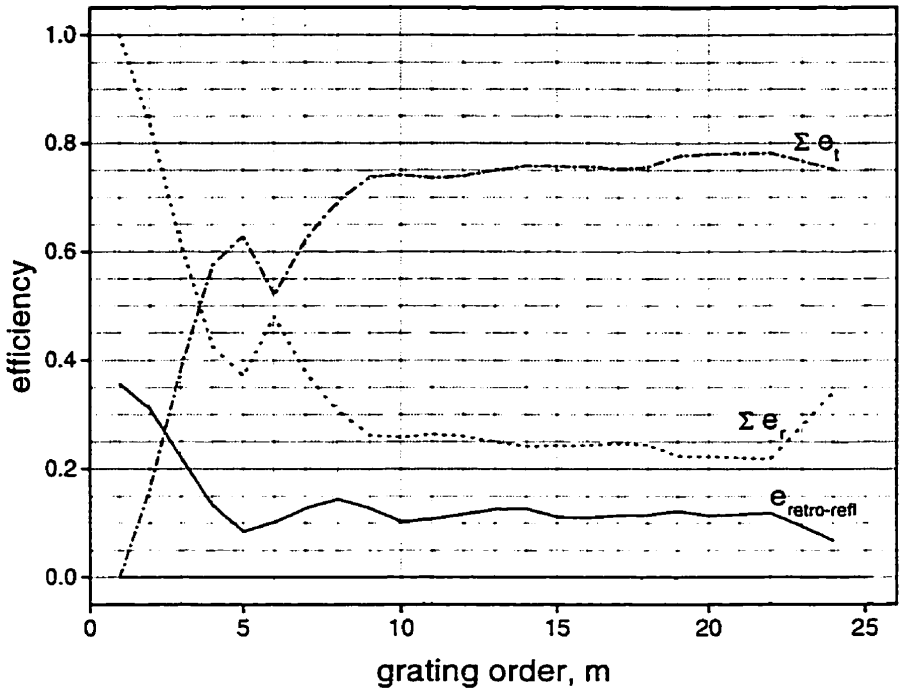

Figure 4-34: Plot of efficiencies as a function of grating order for v_1=2.2 echelle gratings

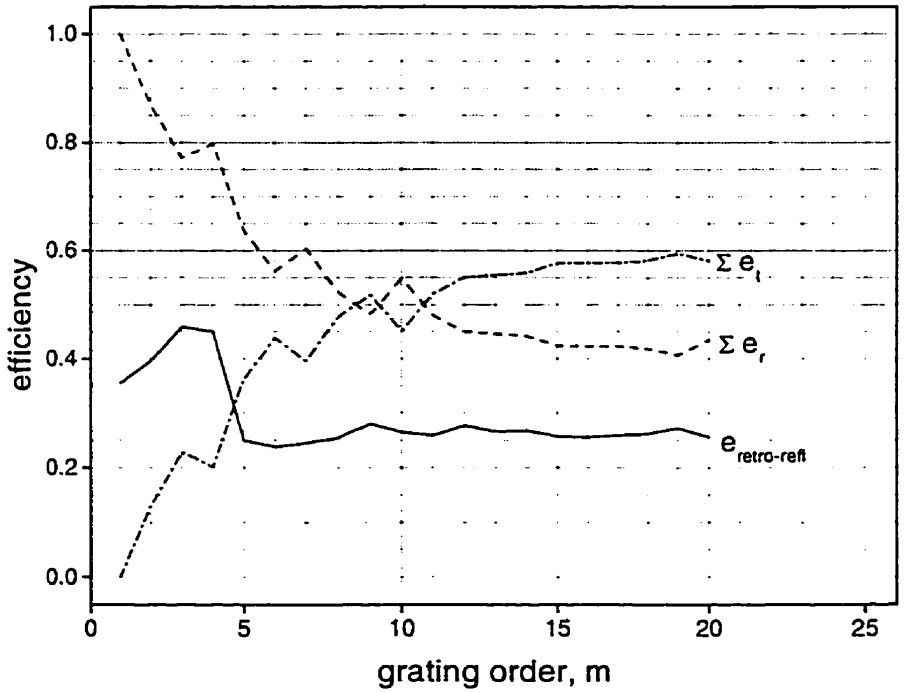

Figure 4-35: Plot of efficiencies as a function of grating order for v_1=3.6 echelle gratings

4.6 GRATING EFFICIENCIES FOR DIFFERENT REFLECTED ORDERS

4.6.1 TIR Grating Efficiencies as a Function of Reflected Order

Figures 4-36 to 4-39 illustrate how the reflected light is distributed among the different reflected orders for TIR gratings. Included are plots for 5th, 10th, 15th, and 20th order gratings (1st and 2nd order gratings were excluded since there are so few reflected orders). Each graph shows the efficiencies for ν_1=1.45, 2.2, and 3.6 (except for the 20th order plot where the validity criterion was not satisfied for ν_1=3.6 and it is replaced by ν_1=3.0). The scalar wave approximation is also included in the plots. The scalar wave approximation was calculated from equation (2.9) and interpolated for non-integer values of n by evaluating the numerator at the appropriate angles. The scalar wave approximation only has physical significance for integer values of n. The scalar wave approximation is the same for each value of ν_1 since they are in the range of total internal reflection.

For all but one of these plots the highest peak is around the retro-reflected order. This peak tends to be higher and wider for the ν_1=2.2 and ν_1=3.6 (or ν_1=3.0) curves than for the ν_1=1.45 curve. The ν_1=1.45 curve tends to have a second peak just below the zeroth reflected order which is nearly as large (or larger for the 5th order grating) as the peak around the retro-reflected order.

The scalar wave approximation predicts the highest peak will be at the retro-reflected order. For diffraction orders close to the retro-reflected order, differential method results show qualitative agreement with the scalar wave approximation. For reflected orders close to the zeroth, differential method results predict substantially more

diffracted optical power than the scalar wave approximation. Because of the power diffracted to orders close to the zeroth order, the efficiency of the retro-diffracted order is reduced from that predicted by the scalar wave approximation. The scalar wave approximation predicts that the distribution of the optical power among the diffraction orders is the same for all values of v_1. The differential method indicates that the distribution does depend on v_1.

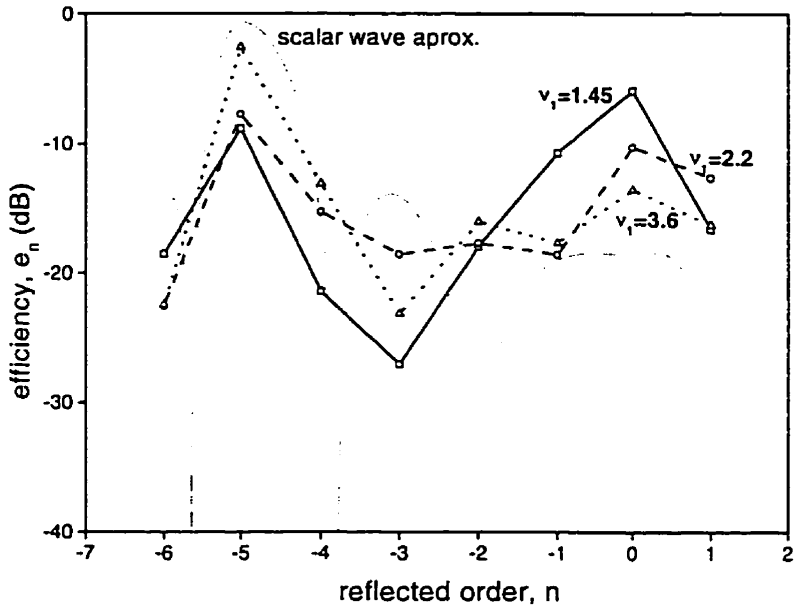

Figure 4-36: Plot of efficiencies along with scalar wave approximation as a function of reflected order for a 5th order TIR grating

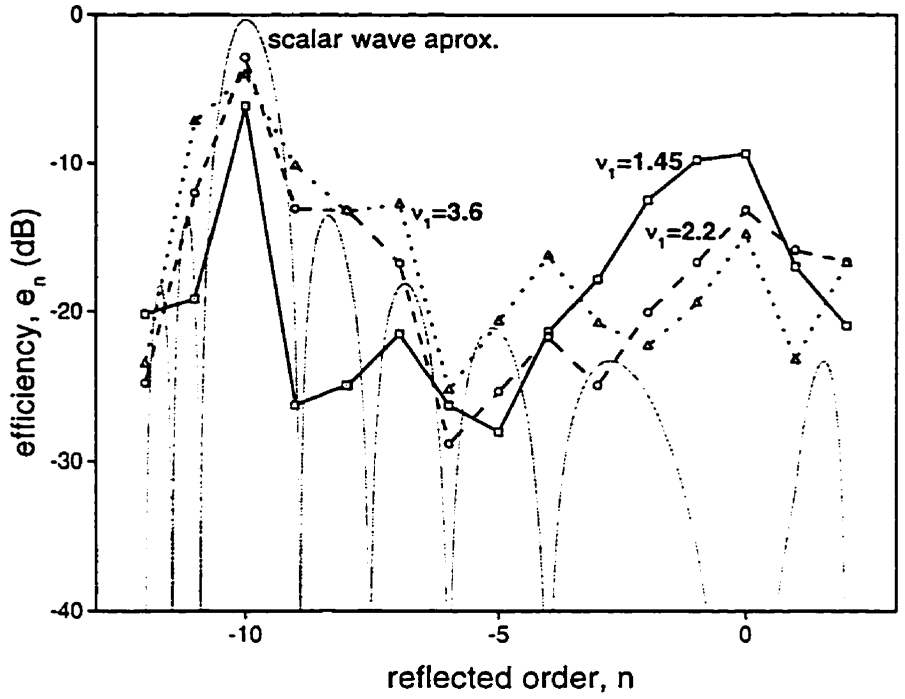

Figure 4-37: Plot of efficiencies along with scalar wave approximation as a function of reflected order for a 10^{th} order TIR grating

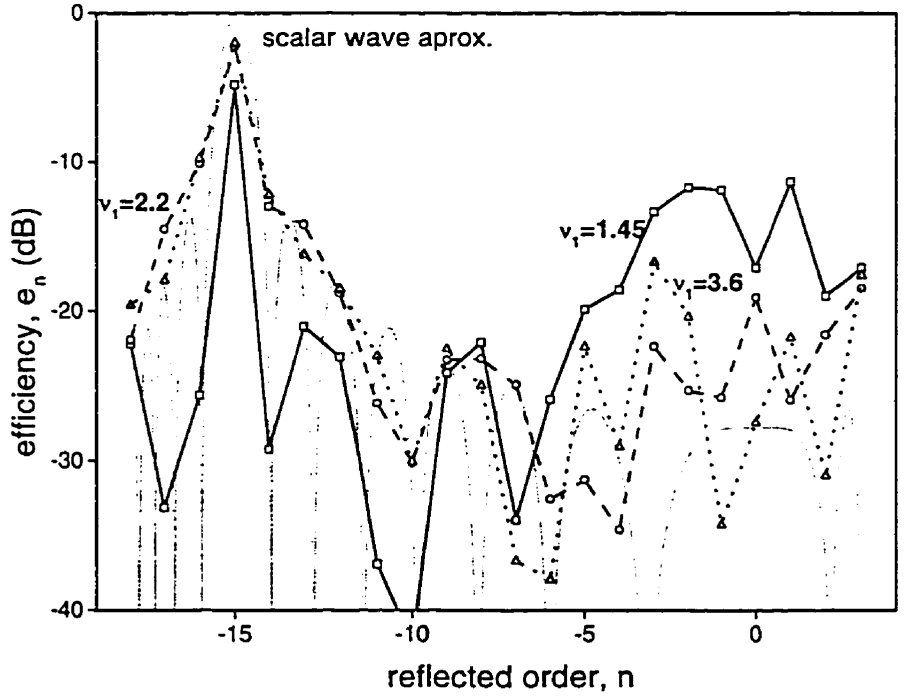

Figure 4-38: Plot of efficiencies along with scalar wave approximation as a function of reflected order for a 15^{th} order TIR grating

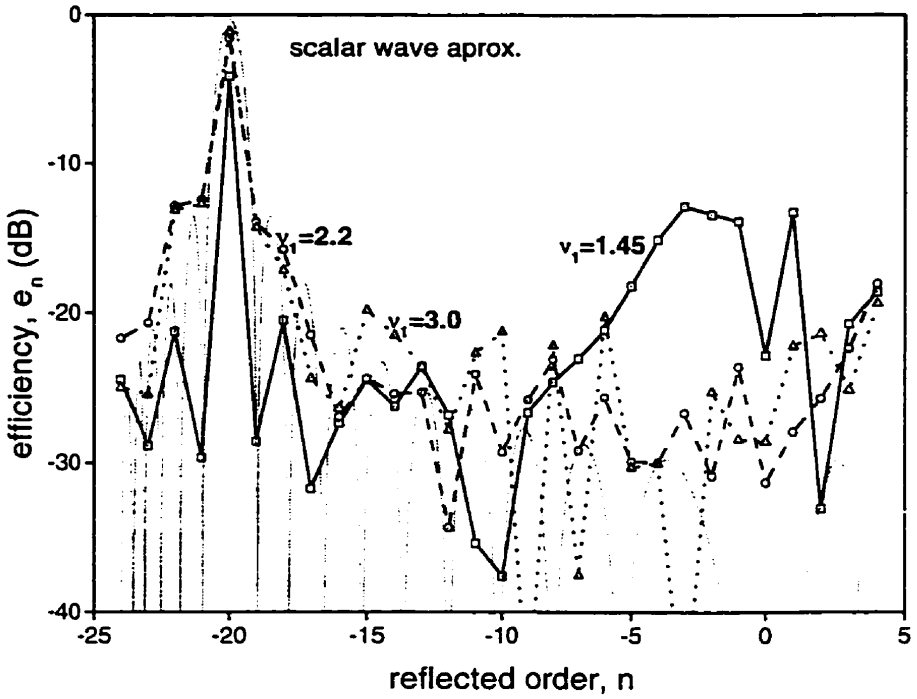

Figure 4-39: Plot of efficiencies along with scalar wave approximation as a function of reflected order for a 20th order TIR grating

4.6.2 Echelle Grating Efficiencies as a Function of Reflected Order

Figures 4-40 to 4-43 show how the reflected light is distributed among the different reflected orders for echelle gratings. Included are plots for 5th, 10th, 15th, and 20th order gratings (1st and 2nd order gratings were excluded since there are so few reflected orders). Each graph shows the efficiencies for v_1=1.45, 2.2, and 3.6. The scalar wave approximation for v_1=2.2 is also included in the plots. The scalar wave approximation was calculated from equation (2.9) and interpolated for non-integer values of *n* by evaluating the numerator at the appropriate angles. The scalar wave approximation only has physical significance for integer values of *n*. The shape of the plotted scalar wave approximation does not change with v_1 but is 6.2 dB lower for v_1=1.45, and 3.5 dB higher for v_1=3.6.

For all but one of these plots the highest peak is around the retro-reflected order. This peak tends to be higher and wider for the v_1=2.2 and v_1=3.6 (or v_1=3.0) curves than for the v_1=1.45 curves. The v_1=1.45 curve tends to have a second peak about halfway between the zeroth and retro-reflected orders which is nearly as high as (or higher than for the 5th order grating) and wider than the peak around the retro-reflected order. For all plots (except the v_1=2.2, m=5 plot) the v_1=2.2 and v_1=3.6 curves have a minimum value at approximately the same order as the second peak of the v_1=1.45 curve and then rise as they approach the highest reflected order.

The scalar wave approximation predicts the highest peak will be at the retro-reflected order. For diffraction orders close to the retro-reflected order, differential method results show qualitative agreement with the scalar wave approximation. The scalar wave approximation shows poor agreement with the differential method results for other diffraction orders. The scalar wave approximation predicts that the distribution of the optical power among the diffraction orders will have the same shape for all values of v_1. The differential method indicates that the shape of the distribution does depend on v_1.

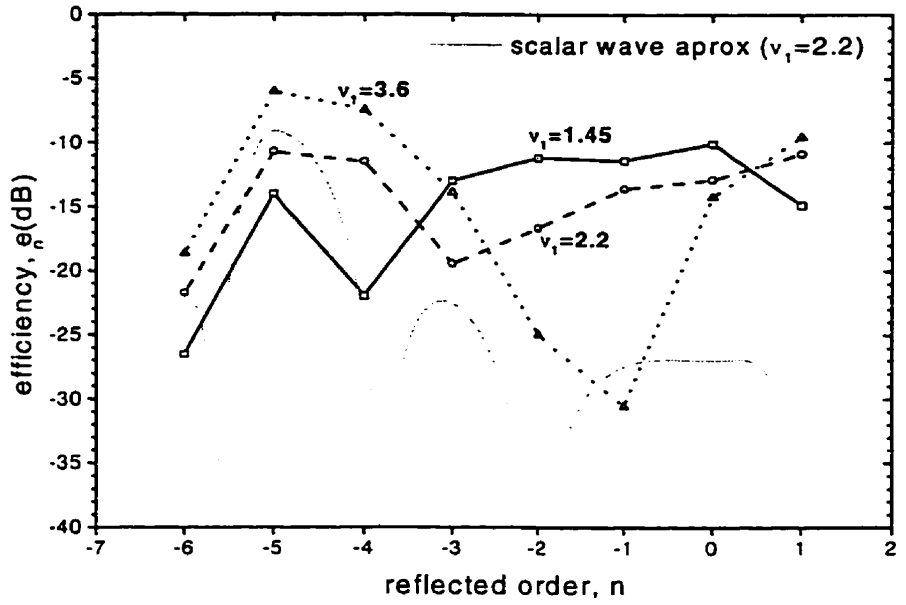

Figure 4-40: Plot of efficiencies along with scalar wave approximation as a function of reflected order for 5th order echelle grating.

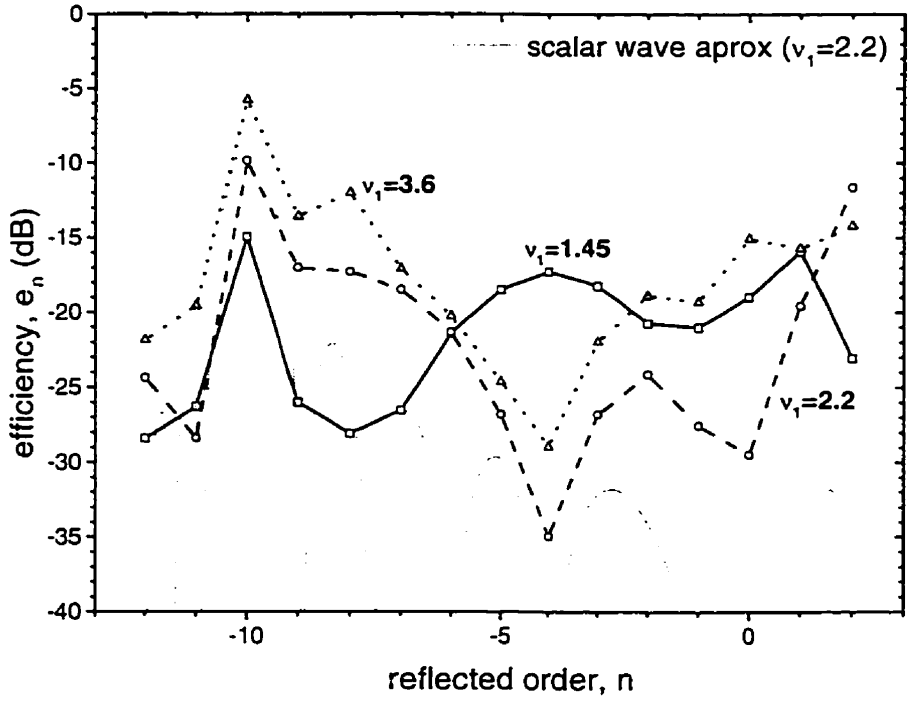

Figure 4-41: Plot of efficiencies along with scalar wave approximation as a function of reflected order for 10th order echelle grating.

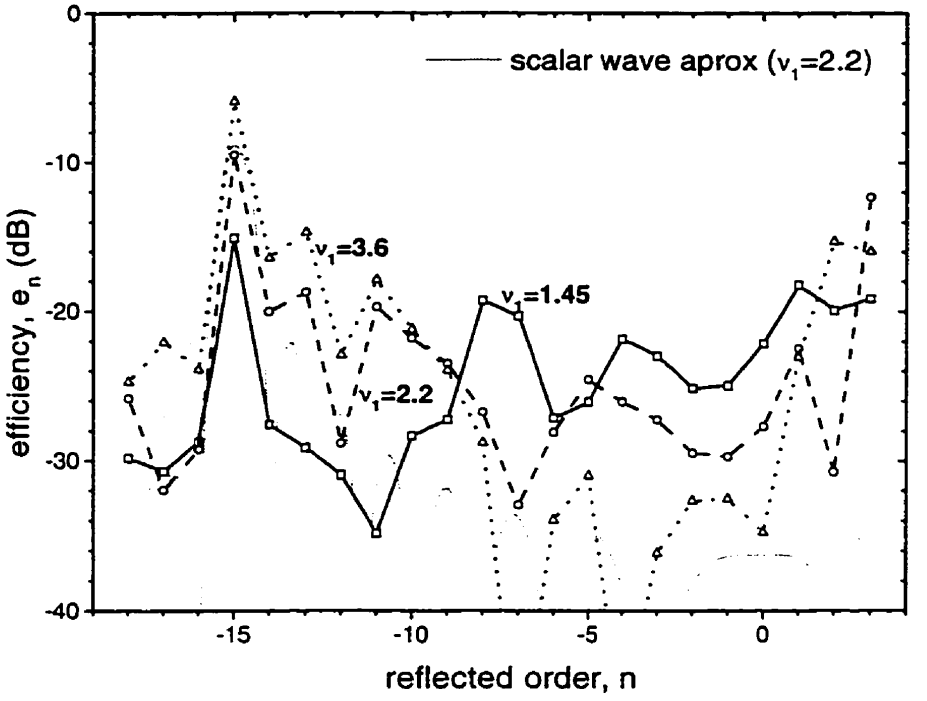

Figure 4-42: Plot of efficiencies along with scalar wave approximation as a function of reflected order for 15th order echelle grating.

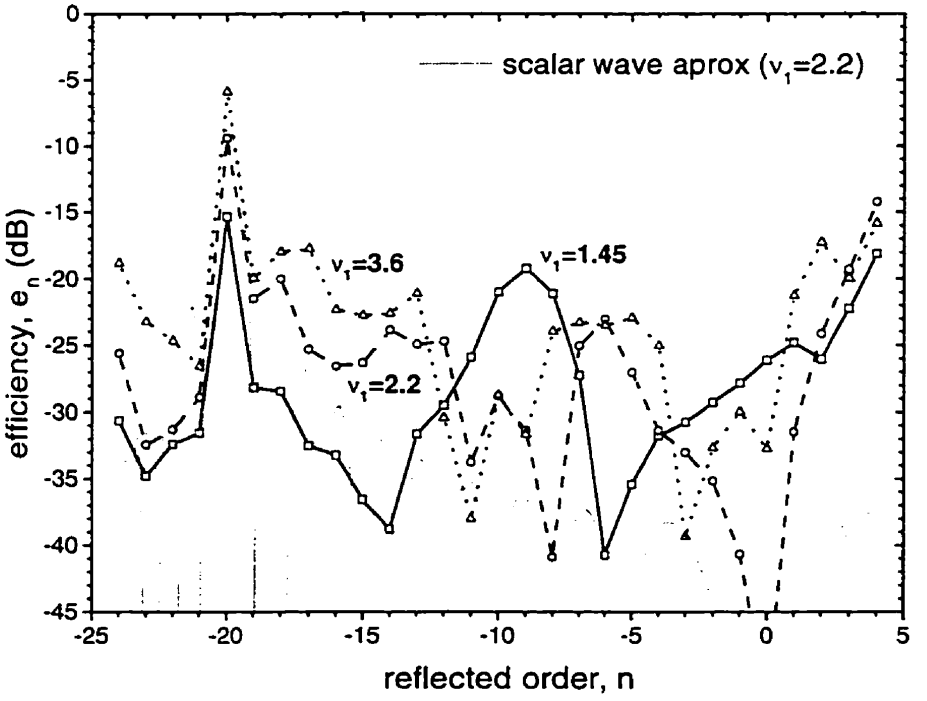

Figure 4-43: Plot of efficiencies along with scalar wave approximation as a function of reflected order for 20th order echelle grating.

4.7 WAVELENGTH DEPENDENCE OF RETRO-REFLECTED EFFICIENCY

Figures 4-44 to 4-53 show the wavelength dependence of the retro-reflected* efficiency for 15th and 20th order TIR and echelle gratings. Differential method results as well as the scalar wave approximation (according to equation (2.8)) are plotted in each graph. The gratings were designed for perfect retro-reflection at a wavelength of 1.550 μm and have refractive indices n_1=1.45, 2.2 and 3.6 (n_1=3.6 was not calculable for the 20th order grating). The −15th reflected order is plotted for the 15th order gratings and the −20th reflected order is plotted for the 20th order gratings.

It can be seen in figures 4-44 to 4-53 that the general shape of the wavelength dependence consists of a large central lobe around the design wavelength with lower, narrower side lobes somewhat symmetrically distributed around the central lobe. In all plotted cases there is a slight shift (~0.005-0.015 μm) in the peak of the central lobe to the lower wavelength side of the design wavelength 1.550 μm. This shift is seen in both the differential method and the scalar wave plots.

The shape of the central lobes of the echelle gratings agrees closely with the prediction from the scalar wave approximation. The shape of the side lobes agrees to varying degrees with the shape predicted by the scalar wave approximation. The side lobes appear to be shifted farther away from the central lobe than the scalar wave approximation predicts.

---

* Here "retro-reflected" refers to the reflected order closest to the angle of incidence. When $\lambda \neq \lambda_0$, perfect retro-reflection is not possible unless $\lambda = \lambda_0 \pm p\text{FSR}$ where p=1, 2, 3, ...

The shape of the central lobes of the TIR gratings agrees somewhat with the prediction from the scalar wave approximation. The central lobes for the v_t=1.45 gratings are more pointed than the scalar wave approximation. The side lobes for the TIR gratings are more distorted than the side lobes of the echelle grating. Distortion is more prevalent on the longer wavelength side. The position of the side lobes, when distinct, agree more closely with the scalar wave approximation for the TIR gratings than for the echelle gratings. The side lobes for all gratings are not as symmetric as predicted by the scalar wave approximation.

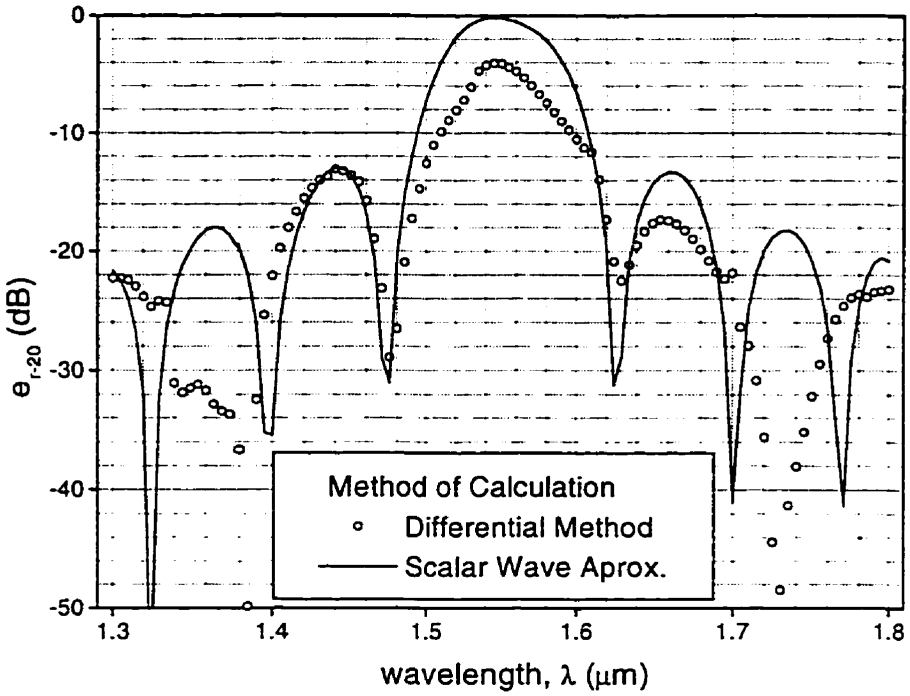

Figure 4-44: Plot of differential method results along with scalar wave predictions of the -20^{th} reflected order efficiencies as a function of wavelength for a 20^{th} order, v_1=1.45 TIR grating.

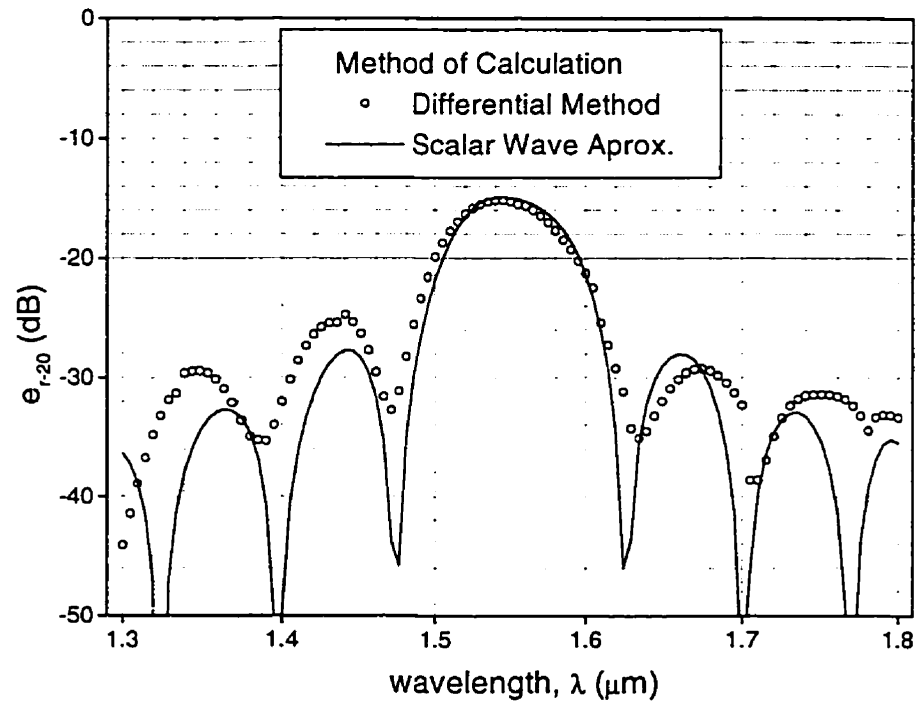

Figure 4-45: Plot of differential method results along with scalar wave predictions of the -20^{th} reflected order efficiencies as a function of wavelength for a 20^{th} order, v_1=1.45 echelle grating.

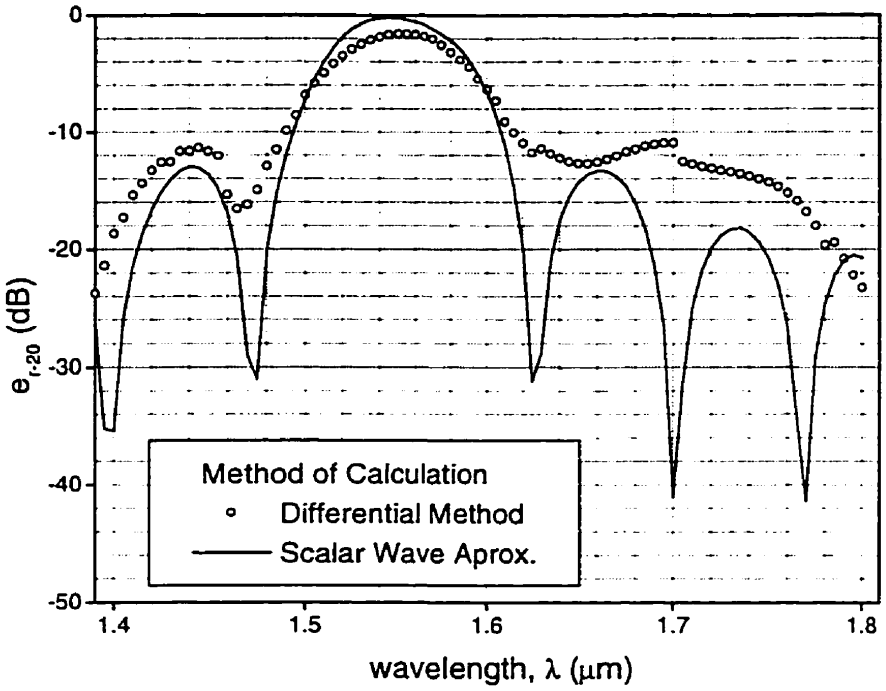

Figure 4-46: Plot of differential method results along with scalar wave predictions of the -20^{th} reflected order efficiencies as a function of wavelength for a 20^{th} order, ν_1=2.2 TIR grating.

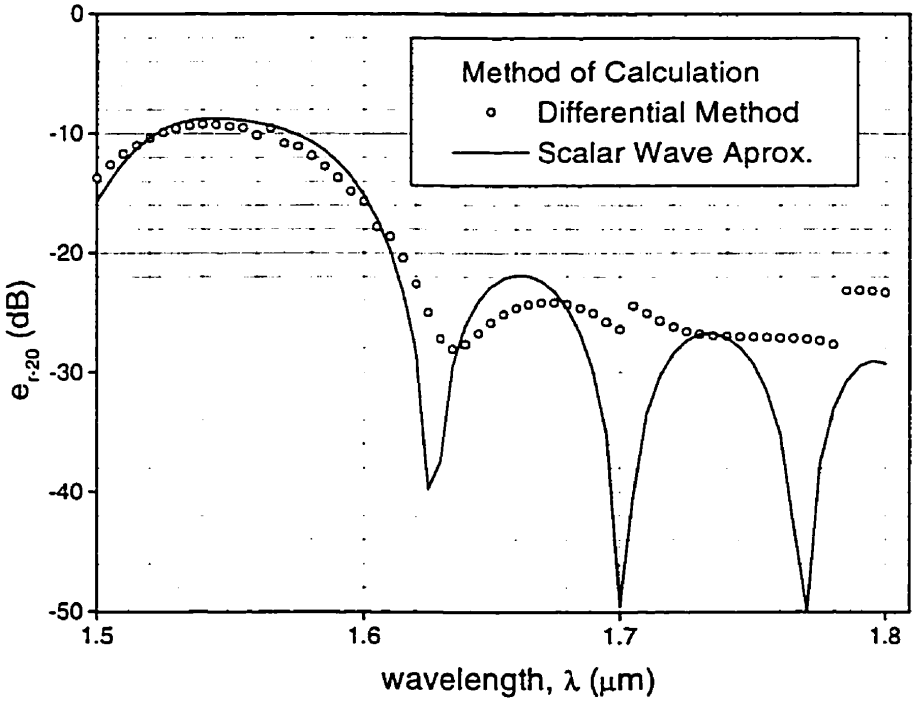

Figure 4-47: Plot of differential method results along with scalar wave predictions of the -20^{th} reflected order efficiencies as a function of wavelength for a 20^{th} order, ν_1=2.2 echelle grating.

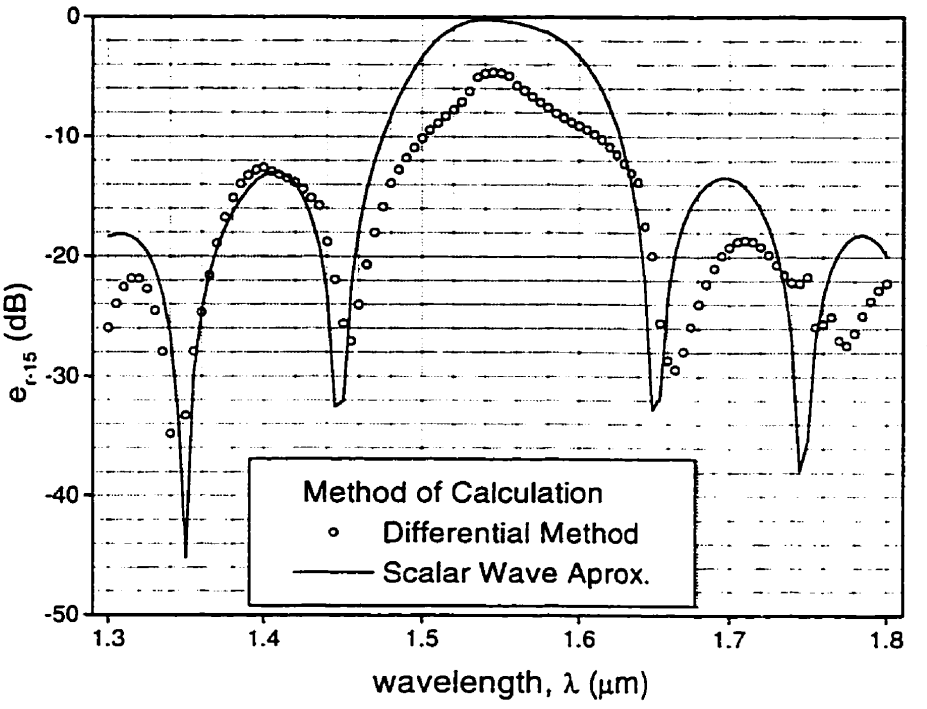

Figure 4-48: Plot of differential method results along with scalar wave predictions of the -15^{th} reflected order efficiencies as a function of wavelength for a 15^{th} order, ν_1=1.45 TIR grating.

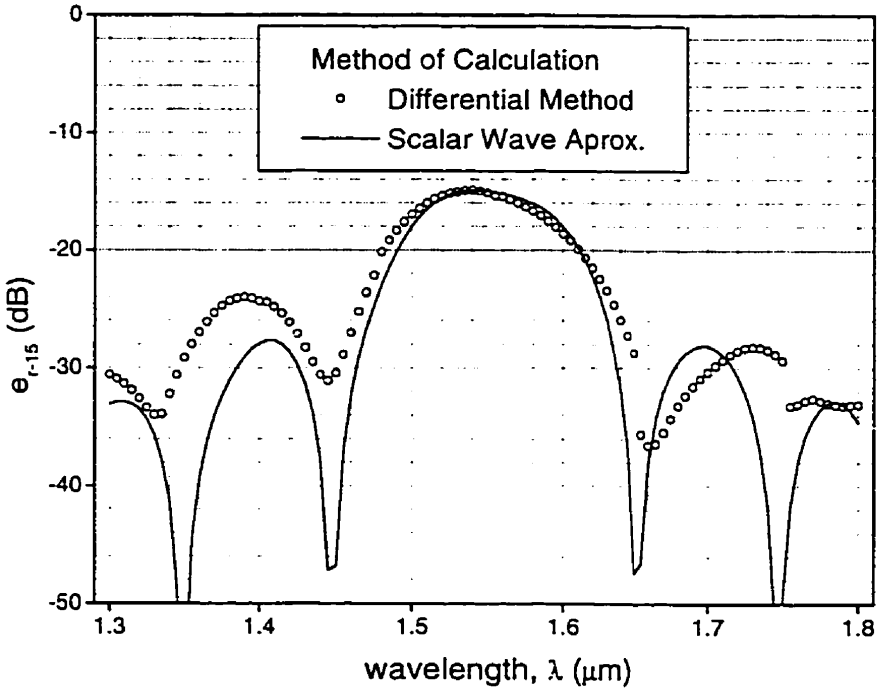

Figure 4-49: Plot of differential method results along with scalar wave predictions of the -15^{th} reflected order efficiencies as a function of wavelength for a 15^{th} order, ν_1=1.45 echelle grating.

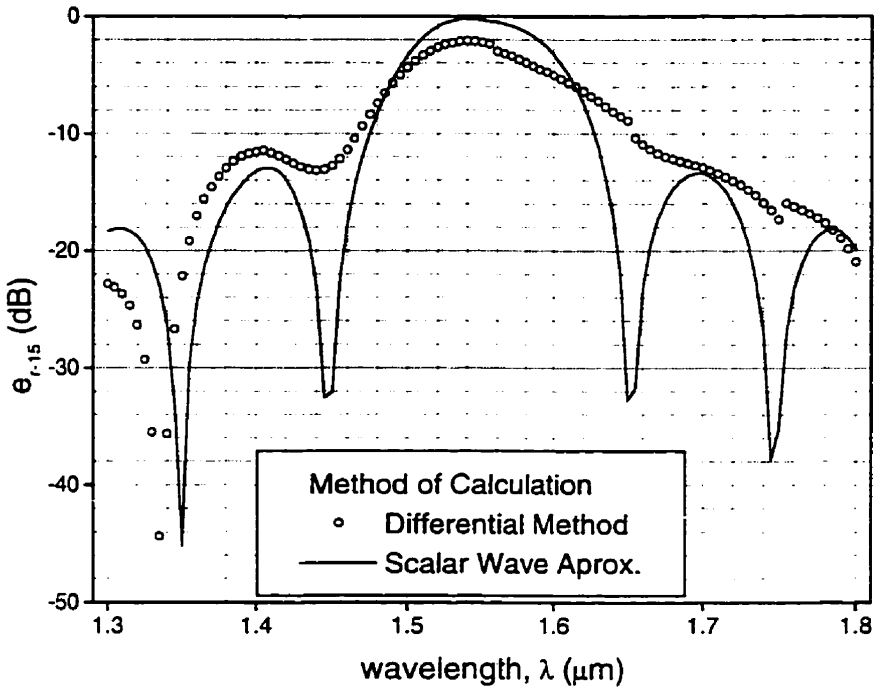

Figure 4-50: Plot of differential method results along with scalar wave predictions of the -15^{th} reflected order efficiencies as a function of wavelength for a 15^{th} order, ν_1=2.2 TIR grating.

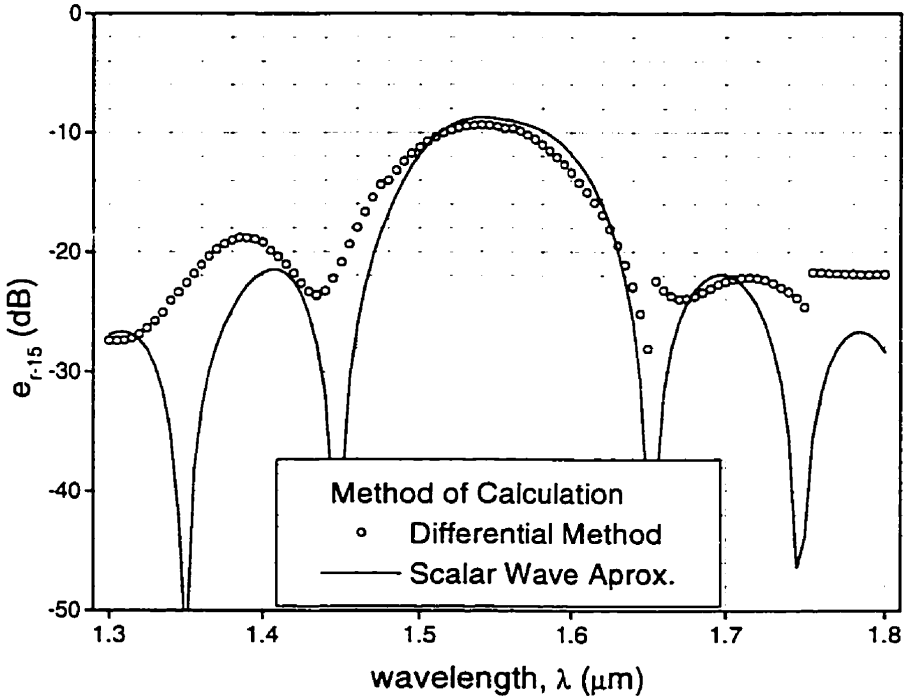

Figure 4-51: Plot of differential method results along with scalar wave predictions of the -15^{th} reflected order efficiencies as a function of wavelength for a 15^{th} order, ν_1=2.2 echelle grating.

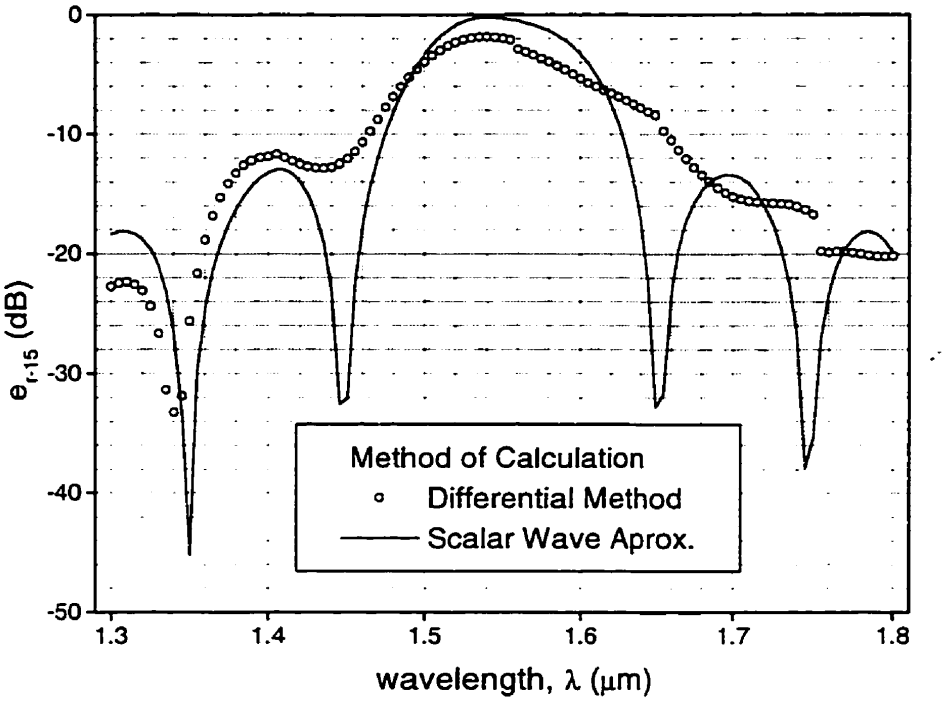

Figure 4-52: Plot of differential method results along with scalar wave predictions of the -15^{th} reflected order efficiencies as a function of wavelength for a 15^{th} order, ν_1=3.6 TIR grating.

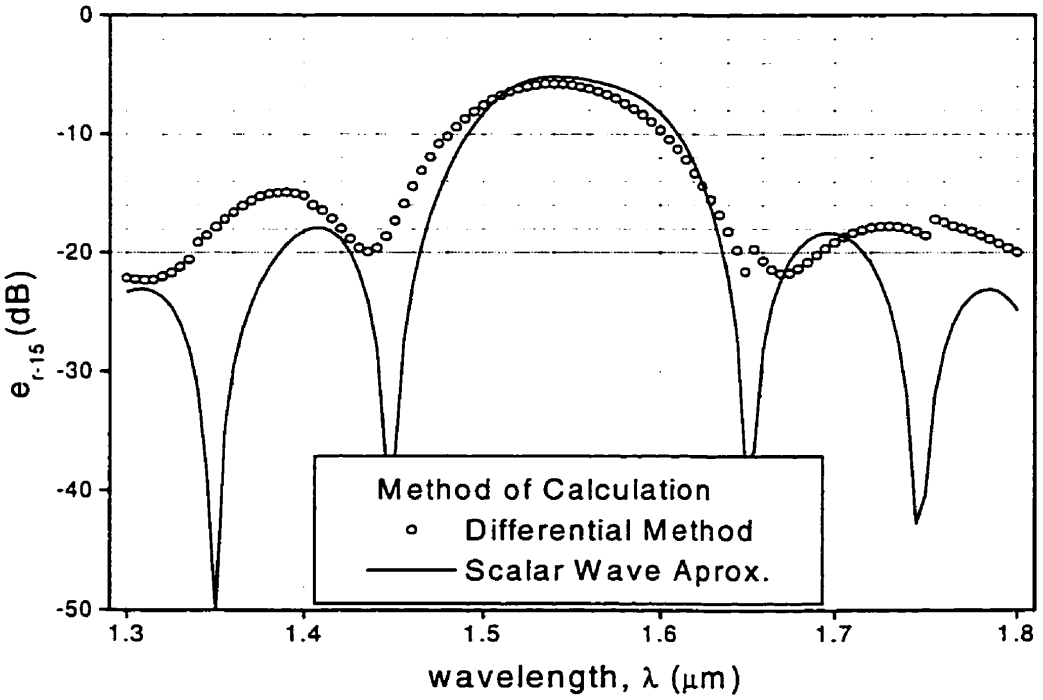

Figure 4-53: Plot of differential method results along with scalar wave predictions of the -15^{th} reflected order efficiencies as a function of wavelength for a 15^{th} order, ν_1=3.6 echelle grating.

4.8 COMPARISON WITH EXPERIMENTAL RESULTS

Sun and McGreer have designed and tested integrated concave gratings in the Eagle configuration with facets equivalent to those of bulk optic TIR gratings[12,13]. They achieved high diffraction efficiencies for 20th order gratings without facet metalization. Their results verify the principle of using total internal reflections to obtain highly efficient integrated optical gratings.

He et al[14] have built integrated optics wavelength demultiplexers based on concave gratings in the Eagle configuration utilizing facet configurations equivalent to both the echelle and TIR gratings. They report that a 24th order TIR grating with v_l=3.18 produced 4 dB greater response than a similar 12th order echelle grating with v_l=3.18. Using the differential method we were able to calculate that a 20th order bulk optic TIR grating with v_l=3.18 should theoretically produce 5.3 dB greater response than a 12th order bulk optic echelle grating with v_l=3.18. We could not extend the calculations higher than 20th order and still satisfy the validity criteria. Based on the stability of the retro-reflection curves for the TIR grating after 5th order (see figures 4-14 and 4-15) we do not expect that being able to extend the calculation to 24th order would significantly change the results. He, et al also report that their results indicate that loss from the TIR grating without metalized facets is approximately equivalent to that from an echelle grating with metalized facets, though with the advantage of having fewer production steps[14].

5 CONCLUSIONS AND RECOMMENDATIONS FOR FUTURE WORK

5.1 CONCLUSIONS

Results presented in this thesis indicate that treatment with the full theory of electromagnetic radiation validates the design principle of orienting grating facets to use total internal reflection for grating orders between 5 and 25 provided that $\nu_1>1.414$. Using $\nu_1=1.45$ (the index of refraction for silica glass), results indicate that a TIR grating used in the -20^{th} order Littrow mount (this is equivalent to one of the gratings used by Sun and McGreer[13]) is over 11 dB more efficient in TE mode than the corresponding echelle grating.

Results indicate that the scalar wave approximation is often a reasonable approximation for the retro-reflected efficiencies. For echelle gratings of order greater than 5 and less than 25, the scalar wave approximation agrees with the differential method to within 2 dB for most refractive indices. The scalar wave approximation is qualitatively not as accurate for the TIR gratings as for the echelle gratings. The scalar wave approximation generally predicts a greater difference between the TIR and echelle gratings than the differential method does.

Based on the agreement between the differential method results and the scalar wave approximation (which is polarization independent for $\nu_1>1.414$) it is expected that the TM mode results would also validate the design principle of the TIR grating.

The impressive results of Sun and McGreer help to verify experimentally the principle of using TIR to obtain highly efficient integrated optical gratings. Qualitative agreement between our theoretical results and experimental results reported by He et al

give initial indications that parallels between Littrow mount planar gratings and Eagle mount concave gratings are valid.

5.2 RECOMMENDATIONS FOR FUTURE WORK

Due to time constraints effort was concentrated on the most important objective which was obtaining results for 20th order (this was the design order used by Sun and McGreer[13]) gratings in the TE polarization. This goal was accomplished for the TE polarization; however, TM polarization results were only obtained for up to 3rd order gratings and were not considered reliable enough to present in this thesis. Effort could be made to try and extend the TM mode results to orders greater than the third.

Very little research went into choosing the numerical method used for integration of either of the polarizations. Perhaps a different numerical integration technique would be able to extend the TE polarization or TM polarization results to higher orders.

Results presented in this thesis are only for theoretical bulk-optic gratings. It may be useful to have a model to predict the output from integrated optic gratings. An attempt could be made to try and model the integrated optics gratings.

Experimental verification of results presented in this thesis is somewhat limited at this time. Further experimentation would verify more thoroughly the theoretical results presented in this thesis and their application to predicting efficiencies for integrated optic gratings.

All results presented in this thesis were calculated using the differential method. Perhaps in order to extend results to higher order gratings, deeper gratings, or ones with a larger refractive index difference a different approach would be more useful. One such approach is the integral method. Dr. Sergey Sadov is currently working on this method.

BIBLIOGRAPHY

[1] C. Palmer, E. Loewen, *Diffraction Grating Handbook 3rd ed.*, Richardson Grating Laboratory, Rochester (1996).
[2] S. P. Davis, Diffraction Grating Spectrographs, Holt Rinehart and Winston, New York (1970).
[3] M. C. Hutley, *Diffraction Gratings*, Academic Press, New York (1982).
[4] G. Winzer, H. F. Mahlein, A. Reichelt, "Single-mode and multimode all-fiber directional couplers for WDM," *Applied Optics*, **20**(18), 3128-3135 (1981).
[5] F. Bilodeau, D. C. Johnson, S. Thériault, B. Malo, J. Albert, K. O. Hill, "An All-Fiber Dense-Wavelength-Division Multiplexer/Demultiplexer Using Photoimprinted Bragg Gratings," *IEEE Photon. Techol. Lett.*, **7**(4), 388-390 (1995).
[6] Z. J. Sun, "Demultiplexer Based on Integrated Concave Grating", *Ph.D. Thesis*, University of Manitoba (1998).
[7] M. K. Smit, "New focusing and dispersive planar component based on an optical phased array," *Electron. Lett.*, **24**(7), 385-386 (1988).
[8] C. Cremer, G. Heise, R. Muller-Nawrath, L. Stoll, E. Veuhoff, H. Baumeister, "Grating Spectrograph in InGaAsP/InP," *Proceedings of ECOC '90*, 109-112 (1990).
[9] J. B. D. Soole, A. Scherer, H.P. LeBlanc, N.C. Andreadakis, R. Bhat, and M. A. Koza, "Monolithic InP-Based grating spectrometer for Wavelength-Division Multiplexed Systems at 1.5 μm," *Electron. Lett.* **27**(2), 132-134 (1991).
[10] C. Cremer, N. Emeis, M. Schier, G. Heise, G. Ebbinghaus, and L. Stoll, "Grating spectrograph integrated with photodiode array in InGaAsP/InGaAs/InP," *IEEE Photon. Techol. Lett.*, **4**(1), 108-110 (1992).
[11] K.A. McGreer, J. N. Broughton, H. J. Hnatiuk, Z. J. Sun, R. Cameron, "Advanced Grating Based WDM demultiplexer," Proc. SPIE Conf. Emerging Components and Technologies for All-optical Photonic Systems II, **2918**, 92-99 (1996).
[12] Z. J. Sun, K. A. McGreer, and J. N. Broughton, "Integrated concave grating WDM demultiplexer with 0.144 nm channel spacing," *Electron. Lett.*, **33**(13), 1140-1142 (1997).
[13] Z. J. Sun, K. A. McGreer, and J. N. Broughton, "Demultiplexer with 120 channels and 0.29-nm channel spacing," *IEEE Photon. Technol. Lett.*, **10**(1), 90-93 (1998).
[14] J-J He, B. Lamontagne, A. Delage, L. Erikson, M. Davies, E. S. Koteles, "Monolithic integrated wavelength demultiplexer based on a waveguide Rowland circle grating in InGaAsP/InP," *J. Lightwave Technol.*, **16**(4), 631-638 (1998).
[15] F. L. Pedrotti, L. S. Pedrotti, Introduction to Optics, Prentice-Hall, Englewood Cliffs (1987).
[16] B. E. A. Saleh, M.C. Teich, *Fundamentals of Photonics*, Wiley, New York (1991).
[17] E. Hecht, A. Zajac, *Optics*, Addison-Wesley, Reading (1974).
[18] M. N. O. Sadiku, *Elements of Electromagnetics 2nd ed.*, Saunders College Publishing, Fort Worth (1994).

[19] R. Petit, "A Tutorial Introduction," *Topics in Current Physics, Vol. 22: Electromagnetic Theory of Gratings* (ed.: R. Petit), Chap. 1, 1-40, Springer-Verlag, Berlin (1980).
[20] P. Vincent, "Differential Methods," *Topics in Current Physics, Vol. 22: Electromagnetic Theory of Gratings* (ed.: R. Petit), Chap. 4, 101-121, Springer-Verlag, Berlin (1980).
[21] M. A. Melkanoff, T. Swada, J. Raynal, "Nuclear Optical Model Calculations," *Methods in Computational Physics, Vol. 6: Nuclear Physics* (ed.: B. Alder, S. Fernback, M. Rotenberg), 2-79, Academic Press, New York (1966).
[22] M. G. Moharam, T. K. Gaylord, "Diffraction analysis of dielectric surface-relief gratings," *J. Opt. Soc. Am.*, **72**(10), 1385-1392 (1982).
[23] E. G. Loewen, M. Nevière, D. Maystre, "Grating efficiency theory as it applies to blazed and holographic gratings," *Applied Optics*, **16**(10), 2711-2721 (1977).
[24] E. G. Loewen, M. Nevière, "Simple selection rules for VUV and XUV diffraction gratings," *Applied Optics*, **17**(7), 1087-1092 (1978).
[25] D. Maystre, M. Neviere, R. Petit, "Experimental Verifications and Applications of the Theory," *Topics in Current Physics, Vol. 22: Electromagnetic Theory of Gratings* (ed.: R. Petit), Chap. 6, 159-225, Springer-Verlag, Berlin (1980).
[26] K. Knop, "Rigorous diffraction theory for transmission phase gratings with deep rectangular grooves," J. Opt. Soc. Am., **68**(9), 1206-1210 (1978)
[27] P. Vincent, "Integral equation computation of bump grating efficiencies in TE polarization," *J. Opt. Soc. Am. A*, **10**(3), 444-451 (1993).
[28] G. P. Agrawal, *Fiber-Optic Communication Systems*, ed: K. Chang, John Wiley & Sons, New York (1992).
[29] F. Bruno, M. del Guidice, R. Recca, F. Testa, "Plasma-enhanced chemical vapor deposition of low-loss SiON optical waveguides at 1.5μm wavelength," *Applied Optics*, **30**(31), 4560-4564 (1991).

APPENDIX

Tables of comparisons between different values of N_{hsteps} and N_{matrix}. Cases where the sum of efficiencies was not within 1% of 1 are not included in the results. N_{matrix} was chosen to be the minimum value for tables where different values of N_{hsteps} are compared. N_{hsteps} was chosen to be 500 for tables where different values of N_{matrix} are compared.

Table A-1: Average absolute percentage differences (%) between efficiencies for selected echelle grating orders calculated with N_{hsteps}=50 and N_{hsteps}=500.

order of grating	1	5	10	15	20	25	1-25
$n_1 = 1$	0.000	0.000	0.001	0.005	0.245	1.986	0.24
1.1	0.038	0.764	2.522	12.232	22.665	59.174	15.79
1.3	0.043	0.529	0.742	4.844	17.124	42.980	9.89
1.4	0.045	0.432	0.531	6.602	10.389	91.330	10.40
1.45	0.041	0.145	0.816	7.023	17.387	75.739	10.07
1.5	0.037	0.113	1.140	6.271	16.983		7.32
1.6	0.033	0.212	1.363	5.433	18.861		7.14
1.75	0.029	0.256	1.168	6.605	19.303		8.60
2.2	0.025	0.396	1.405	2.439	18.671		9.67
2.5	0.024	0.095	1.168	2.761	20.741		6.96
3	0.022	0.073	0.925	2.319	36.205		3.86
3.5	0.022	0.197	1.030	3.892	78.446		6.47
3.6	0.022	0.224	0.632	5.067	70.847		6.00
average	0.029	0.264	1.034	5.038	26.759	54.242	7.88

Table A-2: Average absolute percentage differences (%) between efficiencies for selected echelle grating orders calculated with N_{hsteps}=500 and N_{hsteps}=5000.

order of grating	1	5	10	15	20	25	1-25
$n_1 = 1$	0.00000	0.00000	0.00000	0.00000	0.00001	0.00003	0.00001
1.1	0.00068	0.00023	0.00958	0.00201	0.07045	0.03433	0.01472
1.3	0.00040	0.00482	0.00153	0.01370	0.00574	42.47614	1.77453
1.4	0.00038	0.00522	0.00097	0.03573	0.04973		0.37986
1.45	0.00039	0.00173	0.00061	0.02203	0.08652		1.01757
1.5	0.00035	0.00117	0.00058	0.01453	0.43307		3.44395
1.6	0.00033	0.00187	0.00098	0.04749	1.59329		6.64046
1.75	0.00028	0.00253	0.00382	0.24402	10.03300		5.07154
2.2	0.00024	0.00372	0.00182	0.64771			1.28998
2.5	0.00022	0.00103	0.00460	0.55784			3.37366
3	0.00022	0.00076	0.00574	3.49814			6.67269
3.5	0.00020	0.00171	0.01427	7.28892			2.75876
3.6	0.00020	0.00193	0.00306	6.69426			2.49028
average	0.00030	0.00205	0.00366	1.46664	1.53398	14.17017	2.68677

Table A-3: Average absolute percentage differences (%) between efficiencies for selected TIR grating orders calculated with N_{hsteps}=50 and N_{hsteps}=500.

order of grating	1	5	10	15	20	25	1-25
n_1 = 1	0.0000	0.0003	0.0012	0.0048	0.2453	1.9857	0.24
1.1	0.0199	0.2903	1.4012	8.5309	20.3102	42.2399	10.85
1.3	0.0119	0.1701	0.5824	3.0808	9.2121	19.5035	4.51
1.4	0.0062	0.1416	0.7102	2.8315	7.3771	14.7189	3.20
1.45	0.0108	0.1724	0.6336	2.8683	6.7831	17.2561	3.39
1.5	0.0117	0.1852	0.5420	2.1609	6.6787	33.0170	4.16
1.6	0.0124	0.1490	0.5190	2.6196	7.1887		3.30
1.75	0.0130	0.0995	0.6530	5.2259	9.9773		4.29
2.2	0.0133	0.1523	0.9459	3.4985	12.6976		5.75
2.5	0.0134	0.1307	0.8198	4.8597	14.3291		5.72
3	0.0134	0.1020	1.1374	3.6765	42.2141		4.21
3.5	0.0134	0.1298	0.9612	4.8601	68.7267		6.47
3.6	0.0134	0.1330	1.0069	4.3656	77.7530		6.22
Average	0.0118	0.1428	0.7626	3.7372	21.8071	21.4535	4.79

Table A-4: Average absolute percentage differences (%) between efficiencies for selected TIR grating orders calculated with N_{hsteps}=500 and N_{hsteps}=5000.

order of grating	1	5	10	15	20	25	1-25
n_1 = 1	0.00000	0.00000	0.00000	0.00000	0.00001	0.00003	0.00001
1.1	0.00079	0.01780	0.00316	0.00256	0.00144	0.00248	0.01222
1.3	0.00009	0.00156	0.00383	0.00304	0.00107	10.18969	0.41857
1.4	0.00007	0.00144	0.00474	0.00308	0.02091	47.80935	1.94766
1.45	0.00011	0.00170	0.00506	0.00472	0.06884		0.08452
1.5	0.00011	0.00237	0.00495	0.00997	0.12825		0.54721
1.6	0.00013	0.00128	0.00345	0.01643	0.37494		1.93724
1.75	0.00013	0.00088	0.00204	0.12803	4.91915		4.93699
2.2	0.00014	0.00153	0.00481	0.55197	54.76891		4.04147
2.5	0.00012	0.00153	0.00683	1.49074			3.67277
3	0.00012	0.00091	0.00571	6.02475			1.36317
3.5	0.00012	0.00125	0.00421	8.05192			2.93698
3.6	0.00012	0.00134	0.00459	8.59893			3.36759
Average	0.00016	0.00258	0.00410	1.91432	6.69817	14.50039	1.94357

Table A-5: Absolute percentage differences (%) between retro-reflected efficiencies for selected echelle grating orders calculated with N_{hsteps}=50 and N_{hsteps}=500.

order of grating	1	5	10	15	20	25	1-25
n_1 = 1.1	0.02	0.24	0.12	2.01	5.92	2.57	2.05
1.3	0.04	0.07	0.19	1.68	4.94	6.93	1.68
1.4	0.06	0.22	0.22	2.81	2.86	7.30	1.61
1.45	0.05	0.15	0.33	2.67	3.67	1.00	1.22
1.5	0.05	0.02	0.38	2.29	3.23		1.23
1.6	0.04	0.11	0.17	1.61	1.39		1.13
1.75	0.04	0.01	0.29	0.68	1.86		1.22
2.2	0.03	0.14	0.27	0.81	0.80		3.38
2.5	0.03	0.01	0.17	0.64	0.32		1.57
3	0.03	0.01	0.18	0.57	5.81		0.84
3.5	0.03	0.00	0.04	0.48	0.99		0.58
3.6	0.03	0.00	0.05	0.46	2.44		0.60
average	0.04	0.08	0.20	1.39	2.85	4.45	1.42

Table A-6: Absolute percentage differences (%) between retro-reflected efficiencies for selected echelle grating orders calculated with N_{hsteps}=500 and N_{hsteps}=5000.

order of grating	1	5	10	15	20	25	1-25
n_1 =1.1	0.000000	0.000000	0.004466	0.000000	0.000000	0.000000	0.000682
1.3	0.000412	0.000000	0.000668	0.000000	0.001229	2.691664	0.110014
1.4	0.000525	0.002456	0.000367	0.000795	0.005092		0.027128
1.45	0.000501	0.001527	0.000342	0.002637	0.007872		0.011181
1.5	0.000445	0.000000	0.000000	0.000615	0.018949		0.212337
1.6	0.000419	0.001274	0.000271	0.001683	0.104138		0.373308
1.75	0.000364	0.000000	0.000000	0.013609	0.878017		0.478420
2.2	0.000310	0.001192	0.000000	0.001162			0.096997
2.5	0.000282	0.000286	0.000829	0.100591			0.402833
3	0.000283	0.000000	0.000587	0.119585			1.582606
3.5	0.000255	0.000085	0.000355	0.197259			0.060081
3.6	0.000255	0.000080	0.000038	0.199832			0.082635
average	0.000338	0.000575	0.000660	0.053147	0.145042	1.345832	0.286519

Table A-7: Absolute percentage differences (%) between retro-reflected efficiencies for selected TIR grating orders calculated with N_{hsteps}=50 and N_{hsteps}=500.

order of grating	1	5	10	15	20	25	1-25
n_1 = 1.1	0.0517	0.0519	0.7920	7.55	39.36	7.26	8.23
1.3	0.0311	0.0202	0.2332	1.15	1.09	4.05	0.92
1.4	0.0173	0.0262	0.0252	0.99	1.40	2.30	0.39
1.45	0.0146	0.0456	0.1068	0.52	0.07	1.02	0.21
1.5	0.0153	0.0268	0.0266	0.49	0.71	5.55	0.57
1.6	0.0157	0.0075	0.0481	0.52	0.89		0.47
1.75	0.0158	0.0331	0.1790	0.26	1.34		0.40
2.2	0.0156	0.0398	0.1194	0.29	2.01		0.59
2.5	0.0155	0.0584	0.0328	0.53	0.47		0.35
3	0.0153	0.0099	0.0448	0.55	6.07		0.54
3.5	0.0152	0.0006	0.0010	0.64	9.11		0.81
3.6	0.0152	0.0017	0.0283	0.67	12.24		0.99
average	0.0199	0.0268	0.1364	1.18	6.23	4.04	1.21

Table A-8: Absolute percentage differences (%) between retro-reflected efficiencies for selected TIR grating orders calculated with N_{hsteps}=500 and N_{hsteps}=5000

order of grating	1	5	10	15	20	25	1-25
n_1 = 1.1	0.00000	0.00000	0.00000	0.00000	0.000	0.000	0.000
1.3	0.00036	0.00000	0.00210	0.00087	0.000	0.243	0.011
1.4	0.00022	0.00000	0.00023	0.00000	0.005	20.294	0.814
1.45	0.00015	0.00038	0.00156	0.00009	0.006		0.014
1.5	0.00014	0.00026	0.00130	0.00061	0.026		0.014
1.6	0.00016	0.00000	0.00087	0.00172	0.052		0.090
1.75	0.00015	0.00016	0.00050	0.00044	0.180		0.373
2.2	0.00017	0.00043	0.00008	0.09302	7.233		0.388
2.5	0.00014	0.00061	0.00095	0.10890			0.566
3	0.00014	0.00012	0.00088	0.28995			0.172
3.5	0.00014	0.00004	0.00055	0.49230			0.138
3.6	0.00014	0.00004	0.00051	0.57019			0.237
average	0.00016	0.00017	0.00079	0.12984	0.938	6.846	0.235

Table A-9: Average absolute percentage differences between efficiencies calculated with different matrix sizes (N_{matrix}), for first order echelle grating with N_{hsteps}=500.

Matrix sizes	3(min)-5	5-11	11-15	15-21	21-25	25-31	31-35
n_1 = 1	0.000000	0.000000	0.000000	0.000000	0.000000	0.00	0.00
1.1	0.007569	0.000000	0.000000	0.000000	0.000028	5.54	
1.3	0.047468	0.000490	0.000117	0.000003	0.000576	6.52	178.07
1.4	0.078403	0.000772	0.000100	0.000006	0.004126	7.62	161.18
1.45	0.009641	0.002106	0.000022	0.000022	0.006090	9.24	113.62
1.5	0.062199	0.003040	0.000000	0.000028	0.003066	4.85	
1.6	0.131871	0.004432	0.000022	0.000014	0.003417	5.39	99.00
1.75	0.204200	0.006046	0.000043	0.000014	0.004978	19.18	
2.2	0.330303	0.009263	0.000087	0.000030	0.005953		
2.5	0.378139	0.010601	0.000109	0.000101			
3	0.428049	0.012029	0.000131				
3.5	0.458072	0.012931	0.000153				
3.6	0.462620	0.013063	0.000131				
Average	0.199887	0.005752	0.000070	0.000022	0.003137	7.29	110.37

Table A-10: Absolute percentage differences between retro-reflected efficiencies calculated with different matrix sizes (N_{matrix}), for first order echelle grating with N_{hsteps}=500.

Matrix sizes	3(min)-5	5-11	11-15	15-21	21-25	25-31	31-35
n_1 = 1							
1.1	0.010011	0.000000	0.000000	0.000000	0.000000	18.45	
1.3	0.061972	0.000412	0.000000	0.000000	0.000206	19.34	180.31
1.4	0.101046	0.000158	0.000053	0.000000	0.009311	12.85	165.07
1.45	0.012349	0.002698	0.000028	0.000028	0.009901	14.19	183.60
1.5	0.079691	0.003894	0.000000	0.000056	0.005118	6.67	
1.6	0.169137	0.005682	0.000028	0.000028	0.003231	9.06	156.05
1.75	0.262316	0.007761	0.000056	0.000028	0.008180	25.48	
2.2	0.425614	0.011921	0.000112	0.000028	0.009902		
2.5	0.487828	0.013657	0.000140	0.000140			
3	0.552889	0.015513	0.000169				
3.5	0.592095	0.016686	0.000197				
3.6	0.598038	0.016858	0.000169				
Average	0.279415	0.007937	0.000079	0.000034	0.005731	15.15	171.26

Table A-11: Total efficiencies for different matrix sizes (N_{matrix}), for first order echelle grating with N_{hsteps}=500.

Matrix sizes	3(min)	5	11	15	21	25	31	35
n_1 = 1	1.000000	1.000000	1.000000	1.000000	1.000000	1.000000	1.000000	1.000000
1.1	1.000000	1.000000	1.000000	1.000000	1.000000	1.000001	0.996393	0.537302
1.3	1.000000	1.000000	1.000000	1.000000	1.000000	1.000011	0.999881	0.942944
1.4	1.000000	1.000000	1.000000	1.000000	1.000000	0.999988	0.959872	1.092505
1.45	1.000000	1.000000	1.000000	1.000000	1.000000	0.999979	1.028043	0.973797
1.5	1.000000	1.000000	1.000000	1.000000	1.000000	0.999988	0.957595	1.440645
1.6	1.000000	1.000000	1.000000	1.000000	1.000000	1.000011	1.023152	1.012993
1.75	1.000000	1.000000	1.000000	1.000000	1.000000	1.000018	1.027022	0.000000
2.2	1.000000	1.000000	1.000000	1.000000	1.000000	0.999978	0.000000	0.000000
2.5	1.000000	1.000000	1.000000	1.000000	1.000000	0.000000	0.000000	0.000000
3	1.000000	1.000000	1.000000	1.000000	0.000000	0.000000	0.000000	0.000000
3.5	1.000000	1.000000	1.000000	1.000000	0.000000	0.000000	1.525325	4.167400
3.6	1.000000	1.000000	1.000000	1.000000	0.000000	0.000000	0.655823	1.564048

Table A-12: Average absolute percentage differences between efficiencies calculated with different matrix sizes (N_{matrix}), for fifth order echelle grating with N_{hsteps}=500.

Matrix sizes	5-9(min)	9(min)-11	11-15	15-21	21-25	25-31	31-35
n_1 = 1	0.00	0.0000	0.0000	0.0000	0.0000	0.00	0.00
1.1	45.65	0.4591	0.1273	0.0549	0.2200	153.65	
1.3	53.49	1.3422	0.2163	0.0429	0.5993		
1.4	57.03	0.9436	0.2263	0.0450	0.3996		
1.45	48.62	1.3289	0.2415	0.0348	0.6824		
1.5	48.79	2.9614	0.4723	0.0666	0.5245		
1.6	65.29	2.6657	0.4924	0.0760	0.3785		
1.75	56.70	1.9629	0.4128	0.0712	0.4524		
2.2	75.16	1.9615	0.4419	0.0811	0.7506		
2.5	77.88	2.9697	0.5124	0.0704	1.1111		
3	88.29	3.0095	0.5185	0.1035	0.6068		
3.5	95.27	4.1327	0.6626	0.0882	2.5439		
3.6	97.36	4.1179	0.6445	0.0655	4.1797		
average	62.27	2.1427	0.3822	0.0616	0.9576	76.82	0.00

Table A-13: Absolute percentage differences between retro-reflected efficiencies calculated with different matrix sizes (N_{matrix}), for fifth order echelle grating with N_{hsteps}=500.

Matrix sizes	5-9(min)	9(min)-11	11-15	15-21	21-25	25-31	31-35
n_1 = 1							
1.1		0.1620	0.0710	0.0118	0.0829	21.44	
1.3		0.9434	0.2878	0.0398	0.0384		
1.4		0.3374	0.0162	0.0113	0.1240		
1.45		0.5531	0.0668	0.0058	0.0152		
1.5		4.7432	0.7672	0.0917	0.7861		
1.6		7.0749	1.2265	0.1564	0.0497		
1.75		3.5102	0.7247	0.1098	1.1256		
2.2		0.0482	0.2245	0.0531	0.1621		
2.5		0.1158	0.0272	0.0074	0.9718		
3		0.2787	0.0463	0.0088	0.0481		
3.5		0.2657	0.0590	0.0179	0.0912		
3.6		0.2905	0.0530	0.0120	0.2551		
average		1.5269	0.2975	0.0438	0.3125	21.44	

Table A-14: Total efficiencies for different matrix sizes (N_{matrix}), for fifth order echelle grating with N_{hsteps}=500.

Matrix sizes	5	9(min)	11	15	21	25	31	35
n_1 = 1	1.000000	1.000000	1.000000	1.000000	1.000000	1.000000	1.000000	1.000000
1.1	1.000000	1.000000	1.000000	1.000000	1.000000	1.000060	1.174131	1.366341
1.3	1.000000	1.000000	1.000000	1.000000	1.000001	1.000126	5.627084	1.503269
1.4	1.000000	1.000000	1.000000	1.000000	1.000004	0.998696	11.222791	0.965557
1.45	1.000000	1.000000	1.000000	1.000000	0.999998	1.000719	1.318001	1.024211
1.5	1.000000	1.000000	1.000000	1.000000	1.000005	1.000874	3.339687	1.081587
1.6	1.000000	1.000000	1.000000	1.000000	0.999998	1.000724	22.173488	1.257197
1.75	1.000000	1.000000	1.000000	1.000000	1.000005	0.998401	22.869961	1.212777
2.2	1.000000	1.000000	1.000000	1.000000	1.000013	0.996893	77.975491	0.992671
2.5	1.000000	1.000000	1.000000	1.000000	1.000015	0.998316	3.430840	1.635383
3	1.000000	1.000000	1.000000	1.000000	1.000009	1.001024	2.312066	1.128887
3.5	1.000000	1.000000	1.000000	1.000000	0.999995	1.000940	4.822470	1.517431
3.6	1.000000	1.000000	1.000000	1.000000	1.000013	0.991414	8.574895	1.942947

Table A-15: Average absolute percentage differences between efficiencies calculated with different matrix sizes (N_{matrix}), for tenth order echelle grating with N_{hsteps}=500.

Matrix sizes	5-11	11-15(min)	15(min)-21	21-25	25-31	31-35
n_i = 1		0.000	0.000	0.000	0.000	0.000
1.1		73.721	5.858	0.092	87.746	
1.3		111.340	15.999	0.352		
1.4		95.429	18.177	0.446		
1.45		69.145	14.747	0.451		
1.5		79.914	14.795	0.485		
1.6		73.715	14.591	1.058		
1.75		83.600	9.824	1.372		
2.2		82.656	12.606	0.819		
2.5		87.750	10.621	1.507		
3		91.345	11.522	2.706		
3.5		86.121	10.044	3.910		
3.6		70.492	7.955	3.752		
Average		77.325	11.288	1.304	43.873	0.000

Table A-16: Absolute percentage differences between retro-reflected efficiencies calculated with different matrix sizes (N_{matrix}), for tenth order echelle grating with N_{hsteps}=500.

Matrix sizes	5-11	11-15(min)	15(min)-21	21-25	25-31	31-35
n_i = 1						
1.1		5.554	0.004	0.027	58.940	
1.3		19.125	5.924	0.040		
1.4		27.502	4.169	0.199		
1.45		6.471	8.740	0.234		
1.5		17.291	8.915	0.475		
1.6		20.929	6.069	0.428		
1.75		10.935	2.851	0.372		
2.2		15.046	1.532	0.001		
2.5		6.605	1.526	0.011		
3		5.004	1.798	0.567		
3.5		4.301	1.979	0.158		
3.6		7.371	1.793	0.180		
Average		12.178	3.775	0.224	58.940	

Table A-17: Total efficiencies for different matrix sizes (N_{matrix}), for tenth order echelle grating with N_{hsteps}=500.

Matrix sizes	5	11	15(min)	21	25	31	35
n_i = 1	0.737210	1.000000	1.000000	1.000000	1.000000	1.0000	1.0000
1.1	0.737210	1.000000	1.000000	1.000000	0.999997	1.0555	451.5208
1.3	0.737210	1.000000	1.000000	1.000000	1.000006	6.7524	81.9537
1.4	0.737210	1.000000	1.000000	1.000000	1.000014	3.8861	5.6361
1.45	0.737210	1.000000	1.000000	1.000000	1.000023	7.8496	65.5008
1.5	0.737210	1.000000	1.000000	1.000000	1.000056	11.2183	30.6186
1.6	0.737210	1.000000	1.000000	1.000000	0.999943	73.1646	86.1606
1.75	0.737210	1.000000	1.000000	1.000001	0.999949	454.9122	35.4484
2.2	0.737210	1.000000	1.000000	0.999997	1.001090	30.2208	25.1250
2.5	0.737210	1.000000	1.000000	0.999996	1.000411	33.8558	11.4577
3	0.737210	1.000000	1.000000	0.999991	0.999055	32.0701	36.8897
3.5	0.737210	1.000000	1.000000	0.999999	1.002750	58.3363	94.5045
3.6	0.737210	1.000000	1.000000	1.000002	1.002164	12.6786	9.4261

Table A-18: Average absolute percentage differences between efficiencies calculated with different matrix sizes (N_{matrix}), for fifteenth order echelle grating with N_{hsteps}=500.

Matrix sizes	5-11	11-15	15-21	21-23(min)	23(min)-25	25-31	31-35
n_1 = 1			0	0	0	0	0
1.1		99.59	71.54	16.02	8.23	13.98	
1.3		122.66	117.77	20.53	6.89	44.63	
1.4		151.50	89.40	35.55	8.75	63.68	
1.45		140.51	81.61	34.14	6.10		
1.5		165.18	104.08	31.05	6.26		
1.6		159.89	92.56	22.31	7.47		
1.75		156.90	112.75	20.48	7.48		
2.2		123.52	81.20	18.94	6.30		
2.5		128.84	90.76	18.62	6.35		
3		132.80	131.51	27.64	9.36		
3.5		117.70	108.07	30.58	10.00		
3.6		116.94	112.41	30.87	10.78		
Average		134.67	91.82	23.59	7.23	30.57	0

Table A-19: Absolute percentage differences between retro-reflected efficiencies calculated with different matrix sizes (N_{matrix}), for fifteenth order echelle grating with N_{hsteps}=500.

Matrix sizes	5-11	11-15	15-21	21-23(min)	23(min)-25	25-31	31-35
n_1 = 1							
1.1				0.79	0.12	0.09	
1.3				8.00	2.87	3.97	
1.4				0.22	0.88	3.50	
1.45				1.67	2.17		
1.5				9.17	2.31		
1.6				11.06	1.45		
1.75				9.69	0.85		
2.2				4.69	0.60		
2.5				1.38	0.57		
3				0.02	0.85		
3.5				0.29	0.56		
3.6				0.26	0.32		
Average				3.94	1.13	2.52	

Table A-20: Total efficiencies for different matrix sizes (N_{matrix}), for fifteenth order echelle grating with N_{hsteps}=500.

Matrix sizes	5	11	15	21	23(min)	25	31	35
n_1 = 1	0.727607	0.826977	1.000000	1.000000	1.000000	1.000000	1.000000	1.000000
1.1	0.727607	0.826977	1.000000	1.000000	1.000000	1.000000	1.0015	25.3072
1.3	0.727607	0.826977	1.000000	1.000000	1.000000	1.000000	0.9993	4.5236
1.4	0.727607	0.826977	1.000000	1.000000	1.000000	0.999997	1.0112	2.5808
1.45	0.727607	0.826977	1.000000	1.000000	1.000000	1.000003	3.3239	11.3041
1.5	0.727607	0.826977	1.000000	1.000000	1.000000	1.000020	1.5002	37.9923
1.6	0.727607	0.826977	1.000000	1.000000	1.000001	1.000018	11.7925	72.3980
1.75	0.727607	0.826977	1.000000	1.000000	0.999996	1.000127	238.3846	60.8391
2.2	0.727607	0.826977	1.000000	1.000000	0.999985	0.999586	90.2666	17.9339
2.5	0.727607	0.826977	1.000000	1.000001	0.999983	0.998483	86.3062	18.7459
3	0.727607	0.826977	1.000000	0.999999	1.000112	1.001856	52.0966	13.7937
3.5	0.727607	0.826977	1.000000	1.000006	1.000163	1.000444	54.4595	10.2955
3.6	0.727607	0.826977	1.000000	0.999995	0.999852	1.002576	209.9843	128.7648

Table A-21: Average absolute percentage differences between efficiencies calculated with different matrix sizes (N_{matrix}), for twentieth order echelle grating with N_{hsteps}=500.

Matrix sizes	5-11	11-15	15-21	21-25	25-29(min)	29(min)-31	31-35
n_1 = 1				0.00	0.00	0.00	0.00
1.1			105.12	64.05	90.27	21.99	6.77
1.3			120.39	128.19	73.75	28.44	37.46
1.4			153.18	104.23	63.33	34.49	
1.45			147.71	74.67	83.87	22.32	
1.5			153.86	77.49	86.91	19.51	
1.6			149.84	91.87	87.75	16.56	
1.75			168.99	98.30	72.58	21.87	
2.2			126.96	92.76	88.73		
2.5			129.55	86.67	51.84		
3			134.52	91.16	82.32		
3.5			125.52	96.78	75.06		
3.6			115.77	94.15	75.97		
Average			135.95	84.64	71.72	20.65	14.74

Table A-22: Absolute percentage differences between retro-reflected efficiencies calculated with different matrix sizes (N_{matrix}), for twentieth order echelle grating with N_{hsteps}=500.

Matrix sizes	5-11	11-15	15-21	21-25	25-29(min)	29(min)-31	31-35
n_1 = 1							
1.1				8.59	3.97	0.45	0.23
1.3				18.62	16.12	0.41	5.88
1.4				17.17	14.75	1.39	
1.45				25.06	12.46	2.63	
1.5				26.40	5.96	2.40	
1.6				27.69	1.22	0.98	
1.75				23.84	9.87	0.46	
2.2				49.97	12.41		
2.5				50.03	12.51		
3				41.62	6.63		
3.5				34.22	3.94		
3.6				32.31	6.08		
Average				29.63	8.83	1.25	3.06

Table A-23: Total efficiencies for different matrix sizes (N_{matrix}), for twentieth order echelle grating with N_{hsteps}=500.

Matrix sizes	5	11	15	21	25	29(min)	31	35
n_1 = 1	0.714286	0.755929	0.813789	1.000000	1.000000	1.000000	1.000000	1.000000
1.1	0.714286	0.755929	0.813789	1.000000	1.000000	1.000000	1.000000	0.999982
1.3	0.714286	0.755929	0.813788	1.000000	1.000000	1.000000	0.999996	1.009893
1.4	0.714285	0.755929	0.813788	1.000000	1.000000	1.000000	1.000009	1.2648
1.45	0.714285	0.755929	0.813788	1.000000	1.000000	1.000001	0.999949	6.1278
1.5	0.714285	0.755929	0.813788	1.000000	1.000000	1.000004	0.999708	15.5170
1.6	0.714285	0.755929	0.813788	1.000000	1.000000	1.000016	1.001094	10.4830
1.75	0.714285	0.755929	0.813788	1.000000	1.000000	0.999967	1.002293	58.3012
2.2	0.714285	0.755929	0.813788	1.000000	1.000000	1.002676	1.3451	14.2129
2.5	0.714285	0.755929	0.813788	1.000000	0.999998	0.987346	2.2073	448.8772
3	0.714285	0.755929	0.813788	1.000000	1.000007	1.001637	15.6952	52.3298
3.5	0.714285	0.755929	0.813788	1.000000	0.999972	1.098107	84.6883	103.0861
3.6	0.714285	0.755929	0.813788	1.000000	1.000022	1.016807	397.7129	229.6802

IMAGE EVALUATION
TEST TARGET (QA-3)

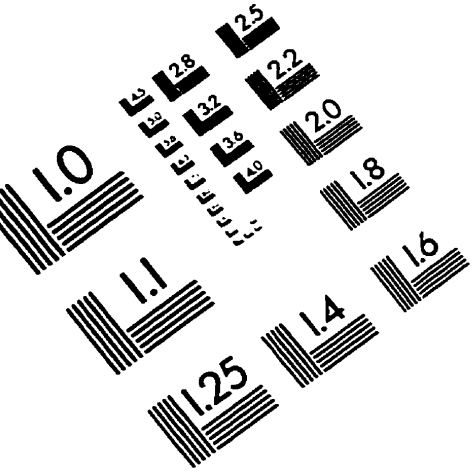

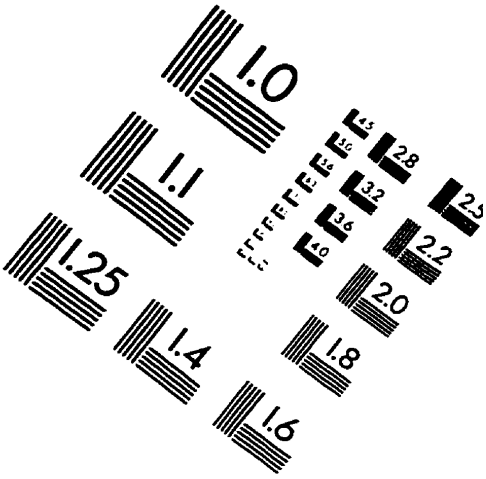

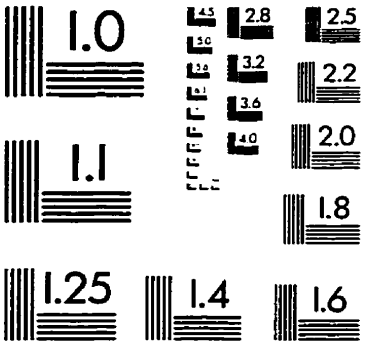

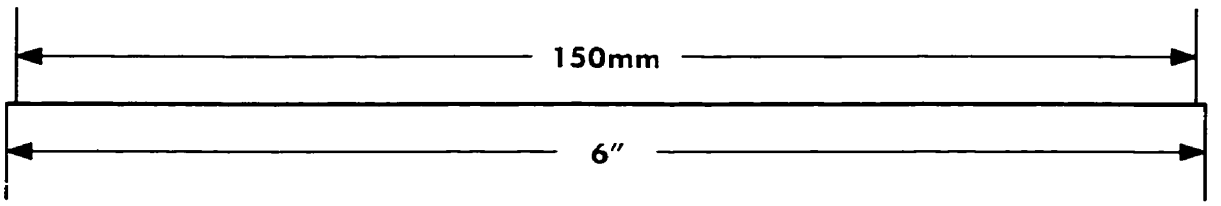

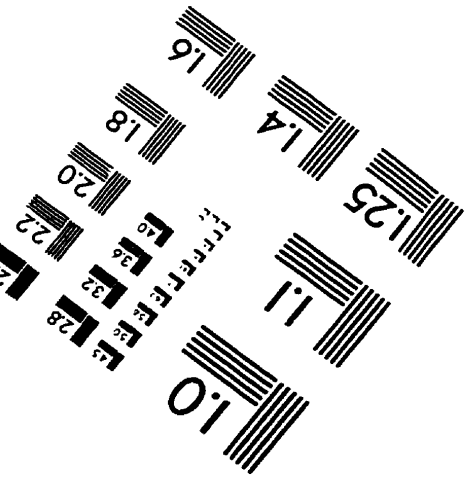

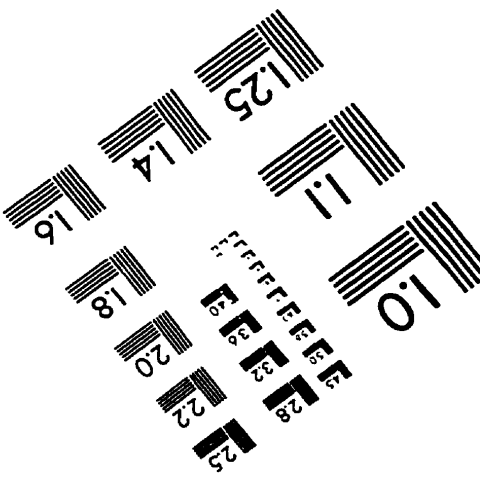

APPLIED IMAGE, Inc
1653 East Main Street
Rochester, NY 14609 USA
Phone: 716/482-0300
Fax: 716/288-5989